Diffusive Mass Transport Studies Using Biosensors

Zimei Rong

12 April 2013

School of Engineering and Materials Science

Thesis submitted for the degree of

Doctor of Philosophy of

Queen Mary University of London

Declaration

I hereby declare that whilst registered as a candidate for the degree of Doctor of Philosophy at Queen Mary University of London, I have not registered a candidate or enrolled student for any other award of the university, or academics, or professional organisation.

Signed

Zimei Rong

Acknowledgements

The researches for this thesis were carried out in the Interdisciplinary Research Centre in Biomedical Materials, Queen Mary University of London.

First of all, I would like to thank Prof Gelb Sukhorukov for proof reading my manuscript and helping me to complete my study. In addition, I also truly appreciate the advice and help given during the last stage of my PhD from Dr Asa Barber and Mr Jonathan Hill.

I would like to thank Prof Pankaj Vadgama for giving me this opportunity. I thank my colleagues Dr John Mitchell, Dr Yiling Lu, Dr Joseph Gargiuli, Dr Jaroslaw Wasikiewicz, Dr Nima Roohpour, Dr Anna-Maria Spehar-Deleze, Dr Salzitsa Anastasova-Lvanova, Dr Marjan Zahedi, Ms Greeshma Nair, Ms Suwimon Boonrngsiman and Ms Hong Chang for their help and friendship.

I thank the technical staff: Mr Chris Straw, Mr Chris Mole, Mr Tony Willis and Mr Mike Collins for their timely technical support.

I thank Mrs Catherine Jones for always displaying great patience and wisdom, and helping me greatly.

I wish to thank my family members in New Zealand and the Netherlands for their help and understanding. I thank my wife Zhihui for her support and my son Edward for checking the grammar of this manuscript.

I acknowledge the financial support from Queen Mary University of London for the student fees; and a grant from the BBSRC, Enterprise Fellowship from the Royal Society of Edinburgh and BBSRC, a Partnership Grant from Innovation China UK.

During this work, I appreciate the collaborations within the group and outside. The collagen gels for diffusion measurements in Chapter 2 and 3 were prepared by Dr Umber Cheema and Dr Burcak Alp of University College London, United Kingdom. Also in Chapter 3, the *in vivo* experimental work including electrodes fabrications and *in vitro* evaluations of lactate electrodes were conducted by Dr Eugenia Leitao and Dr Jonathan Popplewell. Experimental work in Chapter 11 was conducted by Prof Artur Terzyk and Dr Piotr Gauden of Nicolaus Copenicus University, Poland.

Finally I would like to thank Dr Panagiotis Kosmas (internal examiner) and Dr Danny O'Hare (external examiner) for their constructive comments.

This thesis is dedicated to my sister

Bifeng Rong

Abstract

Diffusive mass transport is fundamental for many scientific research areas including physics, chemistry, biology, pharmacy, medicine and geography. In tissue engineering and regenerative medicine, the diffusive mass transport property of artificial and natural biological materials is a key parameter for understanding 3D scaffolds towards designing vascular networks capable of mimicking natural tissues. The aim was to understand diffusion coefficient differences for biomedical materials of different geometrical shapes and matrix properties, including collagen gels and polymeric membranes.

Theoretical work involved producing analytical expressions for diffusion, variously in a planar sheet, a cylinder and a sphere for different initial and boundary conditions. Dynamic amperometric current responses at recessed, membrane covered planar and hanging mercury drop electrodes were also studied. Experimentally, glucose and lactate needle enzyme electrodes were fabricated and an experimental rig was designed to measure analyte concentrations within gels. The analyte diffusion coefficient in a collagen gel was obtained by fitting the simulated to the experimental concentration profiles. Also, a membrane covered planar electrode system was developed to measure the diffusion coefficient of electrochemically active solute through various polymeric barriers. Here, a fit of the simulated to the experimental amperometric current transients was made. Conventionally, a drug release curve is used to characterise drug release, which depends on drug concentration and substrate geometric size and shape. A more intrinsic property, the effective diffusion coefficient, independent of drug concentration or substrate, was determined by fitting calculated drug release to experimental curves. Finally, solute diffusion across dual

laminar flows in a microfluidic system was analysed and used to determine ammonia diffusion coefficient in aqueous solution.

The key novelty of this work was the construction of a series of accurate but simple expressions for mass transport in various geometric matrices which enabled the determination of diffusion coefficients by a specific analytical expression obtained from Fick's Laws and the best fit, avoiding extensive numerical computation such as finite element methods. For all the above, corresponding one point equations were also derived to give initial rapid estimates of diffusion coefficients.

Table of Contents

List of Figures

List of Tables

List of Abbreviations

D is the diffusion coefficient.

c is the solute concentration.

x, y and z are the Cartesian spatial coordinates.

r, θ and z are the cylindrical coordinates.

r, θ and ϕ are the spherical coordinates.

t is the time.

t_0 is the initial time.

$t_{0.5}$ is time when adsorption reaches half saturation.

n is the number of electrons transferred per molecule during the redox reaction.

F is the Faraday constant.

A is the working area of the working electrode.

L is the thickness of a membrane.

R is the radius of a cylinder.

T is the dimensionless time, Dt/L^2 for a planar sheet and Dt/R^2 for a cylinder.

C is dimensionless concentration c/c_0.

J_0 and J_1 are the zero order and first order of Bessel functions, respectively.

σ is the standard deviation.

I is the ameprometric current.

I_b is the baseline current.

I_s is the steady state current.

Pe is the Peclet number.

ω is the angular rotation rate of the electrode.

ν is the kinetic viscosity.

a_t is the adsorption at time t.

a_{max} is the saturated adsorption.

V is the volume of diffusion compartment.

RDE represents the rotating disc electrode.

SPEES|PES represents sulphonated polyether ether sulphone – polyether sulphone copolymer.

EMEM represents eagle minimum essential medium.

ATP represents adenosine triphosphate.

KGy is a radiation absorbed dose measurement unit. The kilogray is equal to one thousand gray (1000Gy), and the gray is defined as the absorption of one joule of ionizing radiation by one kilogram (1 J/kg) of matter, e.g. human tissue.

BSA represents bovine serum albumin.

MEMS represents the micro-electromechanical systems.

SECM represents scanning electrochemical microcopy.

UME represents ultramicroelectrode.

EEMA represents 2-ethoxyethyl methacrylate.

MAP represents mean artery pressure.

PAS represents photoacoustic spectroscopy.

ATR represents attenuated total reflectance.

ac represents acetanilide.

an represents aniline.

pa represents acetaminophen (paracetamol).

ph represents phenol.

nt represents neutral.

ac represents acidic.

Chapter 1 Introduction

In this chapter, the nature of diffusion, including the complexity of diffusion will be introduced, followed by the importance of diffusion, mainly for the life sciences, and subsequently, methods for diffusion rate measurement, mainly using electrochemical and optical techniques. A key component for such diffusion measurement, the electrochemical biosensor, will be briefly introduced. Finally, an introduction to the subsequent chapters will be given.

1.1 Nature of Diffusion

Diffusion is a time dependent process by which a substance moves from one location within a system to another as a result of random motion, e.g. the famous Brownian motion, towards a dynamic equilibrium in the system. The diffusing substance here will be limited to molecules. Macroscopically, overall molecular diffusion is driven by a concentration gradient to reach a homogenous phase. Fick was the first to describe diffusion mathematically following the way Fourier described heat conduction. The phenomenological analogue between heat conduction and mass diffusion is well known; naturally, both heat conduction and mass diffusion are due to random molecular motions. The mathematical expressions for Fourier's Laws and Fick's Laws are very similar. Fick's First Law defines a relationship between the concentration gradient dC/dx and substance flux, the substance transport per unit area of section during a time interval as [1]:

$$Flux = -Ddc/dx \tag{1.1}$$

where D is the diffusion coefficient, c is the concentration and x is the spatial coordinate. Here a one dimension model is addressed. The negative sign means that

diffusion occurs in the opposite direction to the concentration gradient, with increasing concentration.

The concentration *c* changes with time *t*, which is governed by Fick's Second Law. With the most commonly used, one dimensional Cartesian coordinate, Fick's Second Law is written as [1]:

$$\frac{\partial c}{\partial t} = D\frac{\partial^2 c}{\partial x^2} \qquad 1.2$$

More generally, Fick's Second Law in a three dimensional Cartesian coordinate system is given by [1]:

$$\frac{\partial c}{\partial t} = D\left(\frac{\partial^2 c}{\partial x^2} + \frac{\partial^2 c}{\partial y^2} + \frac{\partial^2 c}{\partial z^2}\right) \qquad 1.3$$

In this thesis, diffusion in cylinders or spheres is also used. For such geometrical matrices, Fick's Second Law is described in cylindrical or spherical coordinates, respectively, for convenience, as [1]:

$$\frac{\partial C}{\partial t} = \frac{D}{r}\left(\frac{\partial}{\partial r}(r\frac{\partial C}{\partial r}) + \frac{\partial}{\partial \theta}(\frac{1}{r}\frac{\partial C}{\partial \theta}) + \frac{\partial}{\partial z}(r\frac{\partial C}{\partial z})\right) \qquad 1.4$$

$$\frac{\partial C}{\partial t} = \frac{D}{r^2}\left(\frac{\partial}{\partial r}(r^2\frac{\partial C}{\partial r}) + \frac{1}{\sin\theta}\frac{\partial}{\partial \theta}(\sin\theta\frac{\partial C}{\partial \theta}) + \frac{1}{\sin^2\theta}(\frac{\partial^2 C}{\partial \phi^2})\right) \qquad 1.5$$

Equations 1.4 and 1.5 seem complex. In practice, a symmetrical design is often adopted to reduce the complexity, i.e., the number of dimensions in equation 1.4 and 1.5. In reality, diffusion phenomena are complex. The complexity can be expressed using a diffusion coefficient, which is not really a constant. For an inhomogeneous substrate, the diffusion coefficient is a function of the spatial coordinate i.e., $D(x,y,z)$.

For an anisotropic substrate, the diffusion coefficient is a tensor, represented by a 3×3 matrix. However, a transformation of the coordinate system can be used so that certain problems in anisotropic substrates can be reduced to corresponding problems in isotropic substrates. The further complexity in mass diffusion is that the diffusion coefficient itself is a function of diffusing substance concentration, $D(c)$, due to interactions between the diffusing substance-substance and substance-substrate. Moreover, even the complex, concentration-dependent Fick's Laws cannot explain some diffusion behaviours in polymers because of the interaction between a diffusing substance and the substrate. A non-Fickian diffusion model incorporating such interaction was suggested by Alfrey et al [1]. However, such non-Fickian diffusion will not be discussed further in this thesis. The following is an example regarding the nature of diffusion; the critical question here is how fast solute transport is.

Here, an example is used to illustrate diffusion speed. In a three dimension Cartesian coordinate system, $x = 0$ is an interface; the initial condition is $c(x < 0, t < 0) = c_0$; $c(x > 0, t < 0) = 0$. Because of the semi-infinite nature of the sample volume, the problem can be simplified to a one-dimension question. The concentration profile can be expressed as [1]:

$$c(x,t) = \frac{c_0}{2}\,\mathrm{erfc}\frac{x}{2\sqrt{Dt}} \qquad 1.6$$

where erfc is an error function [2]. Equation 1.6 expresses the spatial and temporal concentration profile. At a specified time t, equation 1.6 expresses the spatial concentration profiles as shown in Figure 1.1. It can be seen from equation 1.6 that when time t tends to infinity, the concentration c tends to $c_0/2$, the steady state concentration. One may consider the $c(x,t) = c_0/4$ position, the half saturation concentration point on the curve in Figure 1.1. For the value of erfc(0.4769) = 0.5, the

relationship between position and time is $x = 0.9538\sqrt{Dt}$. The rate of $c(x,t) = c_0/4$ point move is given by

$$dx/dt = 0.4769\sqrt{D/t} \qquad 1.7$$

Equation 1.7 shows that the $c(x,t) = c_0/4$ position moves at a time-dependent speed as the parameter t in the right side of the equation. More precisely, speed is inversely proportional to square root of time. If one looks at different concentration points, say, $c(x,t) = c_0/8$, the value of the error function erfc(0.8134) = 0.25, so the coefficient in equation 1.7 is 0.8134 instead of 0.4769. So, the rate of transport of the solute is seen to be different.

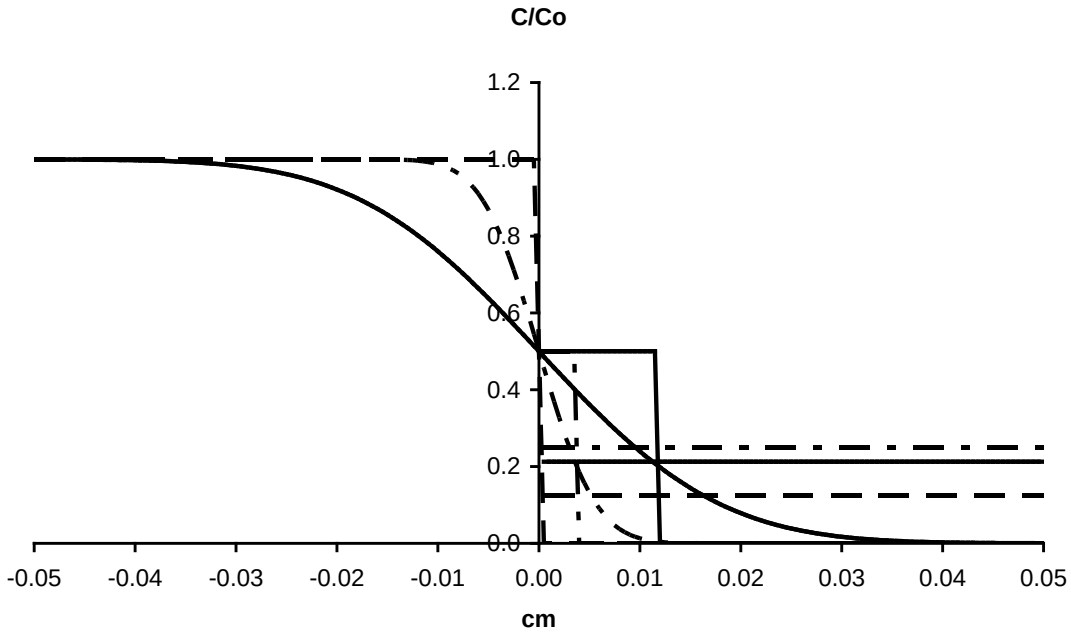

Figure 1.1 Solute concentration profiles for a semi-infinite system.

Solute concentration profiles for a semi-infinite system as shown in Figure 1.1 start with a normalised concentration of 1, in the left side in the figure, and a concentration of 0 in the right side, as shown by a dash line. The diffusion coefficient of this model (glucose in water) is 1×10^{-6} cm^2/s. After diffusion for 10 and 100 seconds, the

concentration profiles resemble a reverse sigmoid curve as shown in the dash-dot and solid line, respectively. The *x* axis, *y* axis, steady state concentration c = 0.5 and two vertical lines at x = 0.003568 (dash-dot) and 0.01128 (solid) form two rectangles, respectively. The rectangle with the dash-dot line has the same area as the right half of the dash-dot concentration profile with respect to the *x* axis. The rectangle with the solid line has the same area as the right half of the solid concentration profile. There are three parallel lines corresponding to normalised concentrations of 0.25 (dash-dot), 0.2124 (solid) and 0.125 (dash) respectively. For the time being, the concentration profile (right half) moves toward the right. However, different concentration positions at the concentration profile moves at different rates. The solid line moves at a general diffusion rate.

Because different concentration points move at different rates, a more general characterisation method is suggested. A general approach is defined with integration of concentration $c(x,t)$ in equation 1.6 from 0 to infinite, normalised by the equilibrium concentration $c_0/2$ as:

$$y = \int_0^\infty c(x,t)dx / c_0 / 2 = 2\sqrt{Dt/\pi} \qquad 1.8$$

The general position y is called the diffusion displacement and is an equivalent position where an equilibrium concentration $c_0/2$, solute diffuses through the interface x = 0 at time t. In Figure 1.1, the area under the right half of the concentration profile at time t = 10 seconds, 100 seconds, equals the area of the rectangle with the dash-dot line and the solid line, respectively; it can be seen that the steady state column (rectangle) expands.

The inverse function of equation 1.8 defines the time constant as

$$t_c = \pi y^2 / 4D \qquad 1.9$$

The physical meaning of the time constant t_c is the time required for the diffusion displacement y to move.

Differentiating equation 1.8 gives the general diffusion rate as:

$$\frac{dy}{dt} = \sqrt{\frac{D}{\pi t}} \qquad 1.10$$

Now, substituting equation 1.8 into equation 1.6, the value erfc($1/\sqrt{\pi}$=0.5642) = 0.4249, it is found that the diffusion displacement moves at a rate of the concentration curve at $0.2124c_0$ position, as shown in Figure 1.1. It can be seen from Figure 1.1 that the dash-dot sigmoid curve, the vertical dash-dot line and the solid horizontal line coincide; the solid sigmoid curve, the solid vertical line and the solid horizontal line coincide. This means that the general diffusion rate can be defined as the rate of the horizontal solid line moving forwards, alternatively, the rate of the rectangle expanding. For glucose diffusion in water, the diffusion coefficient is assumed to be $D = 1\times10^{-6}$ cm^2/s, at time t = 0.001, 1 and 1000 seconds, the diffusion rates are calculated to be 180, 5.6 and 0.18 μm/s respectively, according to equation 1.10. The diffusion rate slows down rapidly with time. The diffusion rate decrease can be seen from the diffusion driven force, i.e., concentration gradient. Differentiating equation 1.6 gives the concentration gradient as:

$$\frac{\partial c(x,t)}{\partial x} = \frac{c_0}{2\sqrt{\pi D t}} \exp(-\frac{x^2}{4Dt}) \qquad 1.11$$

Equation 1.11 shows that the concentration gradient decreases significantly with time.

Diffusion often occurs together with other phenomena such as chemical reactions. When diffusion is the slowest step in the overall process, it actually limits the rate of

the whole process. When studying chemical reaction kinetics in an undergraduate chemistry course, diffusion is often neglected because stirring is assumed. However, stirring is not always possible e.g. when studying cell activity in a biological system. In the following section, the subject areas where diffusion is important will be discussed.

1.2 Importance of Diffusion

Diffusive mass transport is of great importance in many scientific, clinical, industrial and environmental areas, e.g. some subject areas where diffusion is important are chemistry, biology, pathology, tissue engineering and regenerative medicine. This work stems from a tissue bioreactor science project so focus will be given to tissue engineering and regenerative medicine, then shift to biology and pharmacy. In the first part of this section, reasons will be given as to why diffusive mass transport is important for tissue engineering and regenerative medicine, for other life science areas, and, in the second part, briefly for other areas.

Starting with the importance of tissue engineering, the loss of tissue function due to congenital defects, disease or trauma is one of the most difficult, frequent and costly medical problems, particularly in an aging population. Current treatment methods, including autografts, allografts and artificial prostheses have limitations because of the shortage of donor tissue, immune rejection and pathogen transfer. Regenerative medicine provides an alternative.

The principle of tissue engineering therapy is that a small number of cells are initially isolated from a patient, expanded in culture and then implanted back into the patient.

Obviously this is a very complex process, which requires many scientists, engineers and clinicians to work together. At the moment, it is possible to grow a small piece, or more precisely, a thin layer (<0.5mm) of tissue. When a large piece or thick layer (>0.5mm) of a cellular construct is grown, viable tissue is limited to peripheral layers which is believed to be the result of an inadequate supply of nutrients, oxygen and the removal of waste products from deeper layers. Solute transport, even in vascular constructs, is limited beyond the vessels to the individual cells, mainly through diffusion. It has been realised that vascular networks are necessary as an analogue to natural tissue.

Some specific analogies can be imagined from the above. When a driver realises his or her car breaks down he or she will check the car to find the broken part. Then, he or she will buy a new part to replace the broken one. After the part replacement, the car can be driven straightaway. The key point here is that the driver buys the new part with the same specifications as the broken one. By comparison of this simple engineering model, work on tissue engineering and regenerative medicine can be considered to be where nature “manufactures” the original body but fails to provide the specifications. For living matter, one of the key parameters is diffusion coefficient in the natural as well as the replacement engineered tissue. For successful tissue engineering therapy, two aspects of work relevant to diffusion are needed. First, one needs to know the specifications of the natural tissue to be replaced. The importance of this is twofold. One can know what kind of scaffold to manufacture, not only the composition, but also the structure, such as pore size and porosity, and one can smoothly implant the artificial scaffold into the body. Secondly, during tissue scaffold fabrication, it is well known that size of the possible, viable avascular scaffold is

limited by nutrient delivery and waste product removal. So, to mimic natural vascular tissue, one needs to design artificial vascular systems for engineered scaffolds. The necessary parameters of metabolite transport and cell behaviours are needed for designing such structures.

However, quantitatively understanding transport properties of engineered and natural tissues is a challenge. Solute transport behaviour in constructs is practically complex to measure due to many reasons, for example, the transport of metabolites also regulates cell growth, and the cell density modifies the transport property of the construct. In this thesis, the main work is on acellular constructs and provides a foundation for the study of future cellular and vascular constructs.

The diffusive mass transport is a fundamental property of a material, which is not limited to materials used for tissue engineering but relevant to many other areas where a barrier material is in place. For the human body, the importance of diffusion is not limited to tissue engineering or regenerative medicine, but also links to a fundamental understanding of biological behaviour at a cellular level, pathologically understanding disease development, diagnostics and treatment etc. The first step of the nutrient pathway in the body is the stomach digesting the food into nutrients. The next step is absorption and the subsequent step is the delivery of nutrients through the body through the blood stream. However, at this stage, the nutrients are still inside the blood vessels whereas almost all cells live outside the blood vessels. So, the final step is nutrients transport from the blood vessels to individual cells via diffusion. It is well known that oxygen take-up is *via* lung respiration. However, the oxygen supply for the cornea comes mainly from the air through diffusion. Oxygen uptake through

diffusion from the air also significantly contributes to the oxygen supply of human dermis and epidermis [3]. Below are set out further examples of diffusion supply in the diseases, cancer and osteoarthritis.

Cancer causes more than 10% of all human deaths (around 13% of all deaths in 2004) [http://www.who.int/mediacentre/factsheets/fs297/en/index.html]. About 60% of cancers are in air-contacting skin and lung cancers, which is partially due to nitric oxide diffusion outwards into the air [4]. Pathologically, diffusion out of nitric oxide is likely to increase cancer survival [4]. The highest osteoarthritis rate is in the UK and causes a severe NHS burden. Due to the avascular nature of articular cartilage, oxygen and nutrient concentration in articular cartilage is already low and vulnerable to any environment change. Poor nutrient supply and inadequate waste product removal are believed to be a principal cause of the onset and progression of osteoarthritis [5]. A further example of tissue diffusion is used for diagnostics. Thus, the diffusive transport of water and its measurement *in vivo* has also emerged as a diagnostic and research approach for many intracranial disease processes including ischaemic stroke, demyelinating disorders, neoplasms and intracranial infections [6].

Medication is also a relevant area that depends upon the diffusion process. Most medicines are taken orally; the drug then diffuses out of its capsule or formulation and diffuses through the lining layer of the gut to the whole body via the blood stream. Oral drug delivery, however, has its shortcomings, e.g., the capsule cannot provide long-term dosages. As a drug is usually more or less toxic and sent to the whole body, and yet is not suitable for targeting specific localised tissues, different local toxicity problems arise. As an alternative delivery, transdermal patch use is increasing. The

knowledge of the diffusion coefficient of a drug through skin has been vital to the development and optimisation of such transdermal drug delivery vehicles [7].

The importance of diffusion from the life sciences to the environment is also a valuable topic to consider. Annually, approximate 11.2 billion kilograms of pesticides are used globally and eventually such amounts of toxic chemicals will diffuse into the general environment through the soil, water and air [8]. Also, as an environmentally related question, with the increasing usage of nuclear power, nuclear waste product processing becomes important, e.g., how deep below ground should the nuclear waste be buried? Solid nuclear waste diffuses in solids. Oxygen and moisture diffusion through packaging is the key parameter for packaging. Since diffusion is so important, in the following section, the question of how to measure diffusion rate will be addressed.

1.3 Methods for Diffusion Coefficient Measurements

The diffusion coefficient describes the diffusive motion speed of a diffusing substance in a substrate. As such, motion is temperature dependent; the value of the diffusion coefficient depends on temperature. When one describes diffusion coefficient one should always specify the diffusing substance, the substrate and the temperature. A general approach to diffusion coefficient measurements is to make an arrangement for generating a concentration gradient in a system, to cause a substance to diffuse and then to measure the concentration change rate, with respect to time. From the time dependent concentration profile, the diffusion coefficient can be determined. Various techniques have been developed to measure diffusion coefficient and can be classified in different ways. These include such features as concentration related signals used for

the calculation, the method to detect the substance, the shape of the substrate and the organization of the concentration gradient, which will be addressed below.

With respect to the concentration related signal for monitoring a substance to determine a *D* value, two categories of methods have been used; steady state and dynamic measurement. In the steady state method, only one experimental value at the steady state is used, but usually, many physical parameters are required to calculate the *D* value and errors accompany these parameter measurements and calculations, therefore, large measurement errors are introduced, a major disadvantage of this method. In dynamic methods, a range of concentration relevant signals corresponding to the concentration gradient from non-equilibrium towards equilibrium, are used for the *D* value calculation usually with a subsequent data fit to minimize the measurement errors. Because of such multipoint data, only relative signals may be used, therefore, measurement errors are reduced.

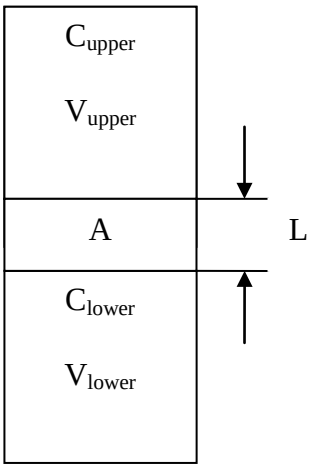

Figure 1.2 Schematic diagram of a two chamber diffusion system.

Diffusion coefficient values can be calculated from the time dependent concentration change or its derivative. Many types of apparatus have been designed for generating a

concentration gradient so that one can measure the concentration profile and calculate the coefficient. The Stokes diaphragm cell is probably the most common apparatus to measure diffusion coefficient of membrane shaped samples [9]. The schematic as shown in Figure 1.2 is similar to the capital letter **B**, consisting of two compartments separated by a membrane with a thickness L and diffusing area A. Initially, two compartments with volume V_{lower} and V_{upper} respectively are filled with solutions of different concentrations c_{lower} and c_{upper} respectively, and stirred. Assuming that the lower compartment has a higher concentration, the analyte diffuses into the upper compartment following Fick's Second Law. Although an exact solution to this process is available [10] it is never used because the solution is expressed in an infinite series. A pseudo-steady state approximation is assumed to simplify this system, i.e., a steady concentration profile in the membrane is assumed, therefore Fick's First Law can be employed to describe the diffusion process. After simple integration of concentration [9], the diffusion coefficient D can be expressed as

$$D = \frac{1}{\beta t} \frac{(c_{\text{lower}} - c_{\text{upper}})_{\text{initial}}}{(c_{\text{lower}} - c_{\text{upper}})_{\text{time t}}} \tag{1.12}$$

$$\text{where constant } \beta = \frac{A}{L}\left(\frac{1}{V_{\text{lower}}} + \frac{1}{V_{\text{upper}}}\right) \tag{1.13}$$

This pseudo-steady state approximation is valid with the following condition [11] as:

$$V_{\text{membrane}}\left(\frac{1}{V_{\text{lower}}} + \frac{1}{V_{\text{upper}}}\right) \succ 1 \tag{1.14}$$

This two chamber system for diffusion measurement is commercially available from PermeGear, Inc. (www.permegear.com), Mocon (www.mocon.com) and Labthink Instruments Co., Ltd (www.labthink.cn). In principle, any detection technique can be used for concentration measurement e.g. optical, electrochemical, radio, even nuclear magnetic resonance. The apparatus for concentration gradient formation varies with

the detection methods. Optical and electrochemical detection methods will be detailed here.

Optical detection based diffusion measurement methods can be divided into three categories. The first is based on measurement of the refractive index, which is proportional to the concentration. This technique can be accomplished by laser beam refraction [12] or interferometry [9]. The second category is based on spectroscopic measurement of substance concentration. Each kind of molecule has its own unique spectrum and the spectral intensity is proportional to the molecular concentration (Beer Lambert Law) so concentration can be readily obtained from intensity measurement. The third category is based on fluorescence measurement, which can be further divided into three types. The first is fluorescence intensity or lifetime, especially with ruthenium complex that is linked to oxygen concentration and used for oxygen measurement. The second is fluorescence recovery after photobleaching (FRAP) technique. Here when a high intensity laser beam targets an area of matrix containing fluorescent dye, the fluorescent dye molecules in the area are permanently bleached. Fluorescent dye molecules in surrounding areas then diffuse into the bleached areas. The diffusion coefficient of the dye can be calculated from the rate of the fluorescence recovery. The third is to measure fluorescence or fluorescence labeled tracer molecule diffusion coefficient to understand mass transport property of biological systems. Another kind of tracer method, the radiotracer method is used to measure radioactive isotope diffusion coefficient in solids.

Electrochemical detection operates in consumption mode, i.e., it reduces or oxidises the target molecules; this is the reason for which electrochemical systems have their intrinsic advantage for measurement of diffusion with a one compartment system. For

example, the analyte concentration remains at zero at the electrode surface under amperometric measurements, the amperometric currents is proportional to the analyte concentration gradient at the electrode surface and is a function of the diffusion coefficient of the surrounding environments where the concentration gradient forms. Therefore one can determine the diffusion coefficient by measuring the amperometric current. Electrochemical based diffusion measurement systems can be classified into five categories: bare electrodes, membrane-covered electrodes, rotating disc electrodes, membrane covered rotating disc electrodes and electrochemical biosensors.

Bare electrodes are used to measure solute diffusion coefficient in solution. In the case of large (mathematically infinite) planar electrodes, one-dimensional mass transport model is valid; diffusion coefficient can be calculated with the famous Cottrell equation

$$I = nFAc\sqrt{D/\pi t} \qquad 1.15$$

where n is the number of electrons transferred in the redox reaction; F is the Faraday Constant; A is the electrode area; c is the analyte concentration, D is the diffusion coefficient and t is the time. In practice, an electrode size is generally limited. In case of disc electrode, Mahon and Oldham [13] recently suggested an accurate but simple bipartite expression for disc electrodes. With the electrode size decreasing, microelectrodes can be used to measure diffusion coefficient in a localized scale. When an electrode downsized to ultramicroelectrode (UME), a new technique called scanning electrochemical microcopy (SECM) was developed, which can be used to measure the small molecules in tissues, and transport across and within bilayers and monolayers.

Membrane covered electrodes were probably first used by Bowers and Wilson [14] to measure electrochemically active solute diffusion coefficient in membranes, who presented analytical expressions for transient amperometric currents.

Another way to modify the disc electrode is the rotating disc electrode (RDE). Levich was the first to model diffusion and solution flow and provided an analytical expression for current (Levich current I_L) [15] as

$$I_L = 0.620158nFAD^{2/3}\omega^{1/2}\nu^{-1/6}c \qquad 1.16$$

where n is the number of electrons transferred in the redox reaction; F is the Faraday Constant; A is the electrode area; D is the diffusion coefficient; ω is the angular rotation rate of the electrode; ν is the kinetic viscosity; c is the analyte concentration. This equation can be used to determine analyte diffusion coefficient in solution. Gough and Leypoldt [16] formulated a model for solute diffusion through a membrane where the solute is consumed at the electrode surface, to evaluate diffusion coefficient in the membrane. Rotating disc electrodes are already commercial available (e.g., www.pineinst.com and www.metrohm-autolab.com).

In summary, a construct for diffusion measurement is designed and the boundary condition then arranged so that a simple analytical solution for the concentration or other relevant quantity is available. Diffusion performance can finally be characterised by comparing the calculated and experimental concentration relevant profiles. The present work started with the measurement of diffusion coefficients of glucose and lactate with corresponding biosensors, and so glucose and lactate biosensors will be briefly introduced.

1.4 Glucose and Lactate Biosensors

Glucose biosensors are of great importance in diabetes for continuous monitoring to reduce complications. Lactate monitoring in intensive care is used to assess oxygen debt. Because of its specificity, simplicity and low cost, glucose (lactate) enzyme needle electrodes are widely used in biotechnology, clinical practice and the food industry [17-21]. In this thesis, glucose needle electrodes were constructed to measure glucose at the centre of collagen gels, and glucose concentration profiles used to determine glucose diffusion coefficients in these collagen gels. Below is a brief history of glucose biosensors.

In 1962 Clark and Lyons [22] proposed that enzymes could be immobilized upon the electrochemical detectors to form enzyme electrodes. The term enzyme electrode was introduced by Updike and Hicks in 1967 [23]. Schichiri [24] was the first to report glucose needle electrodes with a platinum working electrode, with a silver reference electrode and an outer polyurethane membrane. The sensor had a response time of 16 seconds and a linear range up to 27 mM glucose. Vadgama [25] presented glucose needle electrodes with a platinum working electrode, a stainless steel reference electrode and an outer polyurethane membrane. The sensor had a response time of 60 seconds and a linear range up to 70 mM. Pfeiffer [26] constructed glucose needle electrodes with a response time of 100 seconds and a lifetime of 6 days. Wilson [27] proposed glucose needle electrodes in which the sensing element was located in the sensor body. An inner cellulose acetate membrane was used to reduce the response to biochemical interferents; the sensor had a lifetime of 10 days. Karube [28] presented glucose needle electrodes with lifetimes of 25 days, in which an inner Nafion membrane and outer cellulose acetate membrane were used to diminish the response

to interferents. Harrion [29] used Nafion as the outer membrane in their development of glucose needle electrodes, which were implanted subcutaneously in a dog, and had lifetimes of 14 days.

Understanding of the electrochemical theory around needle electrodes is essential for fabrication. The needle electrode consists of five functional components, i.e., platinum wire, a stainless steel tube, an inner membrane, an outer membrane and an enzyme layer.

Platinum wire is used as the working electrode and a stainless steel tube is a pseudo reference and counter electrode. Under polarising voltage of +0.65V *vs*. stainless steel, hydrogen peroxide is oxidised at the platinum electrode surface as:

$$H_2O_2 \rightarrow O_2 + 2H^+ + 2e^- \qquad 1.17$$

A negatively charged, inner membrane prevents negative charged, oxidisable compounds reaching the working electrode through Columbic repulsion and provides a surface for enzyme immobilisation. Glucose is oxidised at the enzyme layer as:

$$\beta\text{-D-glucose} + O_2 + H_2O \rightarrow \text{gluconic acid} + H_2O_2 \qquad 1.18$$

The outer membrane protects the enzyme layer and controls glucose as well as oxygen permeability. The membrane diffusion barrier can be manipulated through different pre-treatment conditions to control porosity, porous size and thickness. Polyurethane was used as the polymeric membrane because the pore size and porosity is a function of polyurethane concentration. The outer membrane also provides a barrier to macromolecules and is expected to be biocompatible for *in vivo* measurements.

The normal physiological glucose concentration within the human body is within the range from 4mM to 6 mM. A biologically meaningful range of glucose concentrations is from 1 mM to 20 mM. Therefore, this amperometric measurement range is preferred for needle electrodes. Glucose molecules pass through the outer membrane and are oxidised at the enzyme layer. If the glucose oxidation is much slower than the diffusion process through the membrane, the overall process is controlled by the glucose oxidation and the needle electrodes work in a kinetic (chemical reaction of glucose) limit mode. If the glucose oxidation is much faster than the diffusion through the outer membrane, the overall process is controlled by the glucose transport through the membrane and the needle electrodes work in a mass transfer limit mode. If the needle electrodes operate in a mass transfer limit mode, the current I through the needle electrodes is approximated by a membrane covered electrode system and is proportional to the glucose concentration in a one dimensional approximation as:

$$I \propto n F A D c / L \qquad 1.19$$

where n is the number of electrons transferred per molecule during the redox reaction; F is the Faraday constant; A is the working area of the working electrode; D is the glucose diffusion coefficient; c is the glucose concentration in the bulk solution; L is the thickness of the diffusion-controlling outer membrane.

The electrode response in current is proportional to the glucose concentration when the electrodes work in a glucose transport limit mode. Current signal versus glucose concentration will be non-linear due to Michaelis-Menten kinetics if the electrodes work in a kinetic limit mode. For greater linearity, a larger barrier, i.e., smaller diffusion coefficient (or thicker membrane, greater diffusion distance) is required.

From equation 1.19, increasing the barrier (L/D) leads to a signal decrease, which can be compensated by the working area A increasing to balance the reduction of the electrode sensitivity. The temperature coefficient of the amperometric current of enzyme electrode response is smaller when it operates in a mass transport limited mode compared with a kinetic limited mode. Detailed construction and related experimental work of glucose and lactate electrodes will be described in Chapter 2 and in Chapter 3, respectively.

1.5 Introduction of thesis

The main body of the thesis, individual chapters, will be described in a self contained format for publication. The outline of the thesis is as follows:

In Chapter 2, glucose needle enzyme electrodes were fabricated and used in a designed experimental rig to measure glucose concentration at the centre of cylindrical collagen gels. Theoretically, higher order expressions for the solution of Fick's Second Law for small dimensionless time were derived and an accurate but simple solution for the concentration evolution in a cylinder was constructed. The simulated to actual measured transient solute concentration profiles were obtained for glucose [30], lactate (Chapter 3) [31] and oxygen [32] diffusion coefficient measurements in collagen gels.

In Chapter 4, a series of expressions for solute transport within membranes under different initial and boundary conditions are presented and were used as theoretical support for studies on mass transport characterization of membranes including the correction of an error in the literature [33].

In Chapter 5, accurate but simple bipartite expressions for amperometric currents (concentration gradient) of recessed, membrane covered planar and hanging mercury drop electrodes are presented [34]. In Chapter 6, the order of magnitude of errors in previous diffusion coefficient determinations with membrane covered electrode systems will be analysed. Also, more accurate diffusion coefficients from the reported data have been obtained [35]. In Chapter 7, the diffusion coefficients of acetaminophen and catechol through mixed cellulose esters membrane have been determined by fitting simulated and experimental data [36]. In addition, bovine serum albumin biofouling of membranes has been quantitatively assessed [36]. In Chapter 8, the Yen and Shih approximation for amperometric currents for membrane-covered electrodes [37] are shown along with the correction of an error of two orders of magnitude in their reported diffusion coefficient values. Furthermore, acetaminophen diffusion coefficients through microporous polycarbonate membranes [37], oxygen and acetaminophen diffusion coefficients at collagen films [38], and hydrogen peroxide, acetaminophen and catechol at interfacing polymerised protein films [39], together with hydrogen peroxide and glucose diffusion coefficients in buffer within a recessed electrode [40].

In Chapter 9, accurate but simple expressions for solute transport across parallel laminar flows in a microfluidic system have been generated [41], which enabled direct simulation, analysis by best fit, of experimental profiles for the exact determination of dye diffusion coefficient in aqueous solution within a microfluidic system [42].

In Chapter 10, accurate but simple expressions for solute adsorption kinetics within porous adsorbents of defined geometry (infinite planar sheet, infinite cylinder, finite

cylinder and sphere) have been presented [43], and enabled rapid determination of effective diffusion coefficients by fitting calculated kinetic adsorption curves to experimental data for activated carbon in Chapter 11 [44].

In Chapter 12, I will summarise the work which has been done.

Chapter 2 Needle Enzyme Electrode Based Glucose Diffusive Transport Measurement in a Collagen Gel and Validation of a Simulation Model

Rapid response needle enzyme electrodes were fabricated to measure the glucose concentration at the centre of a cylindrical spiralled collagen gel, which is a relevant constituent for tissue engineering scaffolds. The experimental data were based on a low consumption glucose sensor which minimised the distorting effect of substrate degradation. As the measurement was carried out within a collagen gel, stirring independence was compulsory for the biosensor. Glucose concentration changes were derived from a model based on the solution to Fick's Second Law. This had two different expressions for different dimensionless time (T) domains. The expression for large T and a first order approximation for small T were known. The expression for high order approximation for small T was then derived. An analytical expression consisting of fast convergent parts of these two expressions was proposed, which operates for the entire time region. A computational model for glucose concentration evolution where an electrode is located was proposed to operate for extended time periods. The model was confirmed by agreement between the simulated and observed data. An experimental technique is developed here to determine the glucose diffusion coefficient by fitting the simulated concentration profile to the observed one. The glucose diffusion coefficient within the collagen gel was estimated to be 1.3×10^{-6} cm^2/s; higher accuracy is achieved here because errors due to noise, baseline and zero time determination are minimised with best fit.

2.1 Introduction

Nutrient transport in physiological systems is a key determinant of tissue metabolism. It is also central to the degree of cell loading and tolerable dimensions possible with avascular tissue engineering scaffolds [45, 46]. Efforts have been undertaken to understand glucose transport in natural tissue [47–49]; there is, for example, relevance to peripheral tissue metabolism in diabetes, 100 million people worldwide suffer from this condition. Determination of the glucose diffusion coefficient within a model collagen gel of the type used for tissue engineering was undertaken using a needle electrode biosensor based on the classical glucose oxidase H_2O_2 detection regimen [50]. A critical feature of the device was a rapid response to enable adequate glucose tracking and also a highly diffusive restricting membrane layer to minimise local glucose consumption to ensure reliable measurement.

Glucose diffusion coefficients in aqueous solutions were measured fifty years ago [51, 52]. Recently more extensive measurements of glucose diffusion coefficients in different media have been undertaken; these include water [53], poly-ether-sulphone and poly-sulphone [54], polyvinyl alcohol [55], calcium alginate [56–58], collagen gel [59, 60], agarose gel [61, 62], pancreatic islets [47], human dura mater [48] and Saccharomyces cerevisiae aggregates [49]. Glucose diffusion coefficients in water, aqueous solutions, calcium alginate and agarose gel are in the range of $6.1–9.2\times10^{-6}$ cm^2/s. Glucose diffusion coefficients within polymeric membranes decrease from polyether sulphone (5.7×10^{-6} cm^2/s) to polysulphone (2.8×10^{-6} cm^2/s) and polyvinyl alcohol (1.3×10^{-8} cm^2/s) [54, 55]. Reported glucose diffusion coefficients in collagen gels are in the range $1.4–1.9\times10^{-6}$ cm^2/s [59, 60]. For biological matrices, values range from 1.6×10^{-6} cm^2/s (human dura mater) [48], to 1.1×10^{-6} cm^2/s (Saccharomyces cerevisiae flocs) [49], and 3.8×10^{-7} cm^2/s (islet of Langerhans) [47].

Two main categories of methods have been used to measure diffusion coefficients [1]; steady state and dynamic. The steady state method has a major disadvantage: only one experimental value (steady state) is used, also, many physical parameters are required therefore, more measurement errors are introduced. Based on a dynamic response to a step change in the boundary condition, there are three approaches, a differential method, an integral method and a dynamic simulation method. The experimental quantity could be concentration itself, but an optical or electrochemical sensor can also be used. Here we use a glucose enzyme needle electrode because previous experience with membranes allows operation in non-liquid media [50].

In the differential method [63], a constant concentration (partial pressure for gas) difference is applied to both sides of a membrane, and permeate flux is measured. As concentration is considered to be a fundamental quantity and flux is linearly proportional to the concentration gradient, this method is referred to as a differential method. Flux here can be measured directly or indirectly. For electrochemically active species, flux can be measured using a direct electrochemical current. Under a mass transfer limiting mode, amperometric current is proportional to permeate flux, the electrochemical reaction being much faster than mass transfer.

In the integral method [1, 63, 64], a constant concentration (partial pressure for gas) difference is applied to both sides of a membrane, and the accumulation of the permeate flux is measured. As the flux, *i.e.*, concentration gradient, is integrated, this method is referred to as the integral method. The accumulated flux can be measured directly or indirectly, and could be measured as net charge transferred, *i.e.*, the integral of the amperometric current. The permeation process can be considered to

have a linear part and a nonlinear part. The nonlinear part can be represented by the "time lag" parameter, before the start of the "linear" process. The asymptotic line for the charge (*i.e.*, integrated current) intercept on the time axis is the time lag.

In the dynamic method, a transient concentration profile is measured. As optical refractive index is proportional to concentration [61], an optical method can be used to measure refractive index change, and thereby concentration change. Another type of dynamic method, the rotating disk electrode has been used to determine electrochemical active solute diffusion in membranes, using the relationship between the electrochemical current and the rotation rate [15, 16, 65].

For modelling of tissues, hydrated type I collagen gels are plastically compressed and rolled to form a spiral assembly, which is then clamped at either side in a bioreactor [66]. No published method is available to measure diffusion in this kind of cylindrical collagen gel. In this work, glucose enzyme needle electrodes were fabricated and used to directly measure transient glucose concentration at the centre of a cylindrical collagen gel to determine the glucose diffusion coefficient. A cylindrical acellular collagen gel without glucose was immersed in a glucose solution of concentration c_0. Glucose concentration at the centre of the collagen cylinder was then measured. Diffusion is governed by Fick's Laws, and the analytical solution to glucose diffusion in the cylindrical collagen gel has two different expressions. The convergence of these two expressions was thoroughly analysed, and an analytical solution function constructed by combining fast convergent parts of theses two expressions, then used to simulate glucose concentration evolution at the centre of the gel. As calculated concentration here is a function of the diffusion coefficient, the latter was then

obtained from a best fit of the simulated concentration profile of the observed data. Use of the dynamic simulation model and the best fit procedure are described to indicate how the initial parameters were obtained.

2.2 Experimental

2.2.1 Reagents and associated materials

The following reagents and associated materials were used in needle electrode construction and measurement.

2.2.1.1 Reagents

Phosphate buffer solution: The composition of the phosphate buffer was: di-sodium hydrogen phosphate (Na_2HPO_4) (BDH, Dorset, UK), 52.8 mM, 7.50 g/L; sodium di-hydrogen phosphate (NaH_2PO_4) (BDH, Dorset, UK), 15.6 mM, 1.87 g/L or ($NaH_2PO_4 \cdot 2H_2O$) 2.43 g/L; sodium chloride (NaCl) (Sigma, Dorset, UK), 5.1 mM, 2.98 g/L. These three chemicals were dissolved in 1 litre of distilled water with the pH adjusted to 7.4 by drop-wise addition of concentrated sodium hydroxide solution (5 M NaOH (BDH, Dorset, UK)). The buffer solution was stored at room temperature.

Sulphonated Polyether Ether Sulphone – Polyether Sulphone Copolymer Solution (SPEES|PES): 0.1 g SPEES|PES (kind gift from ICI Colloids and Polymer Group, Runcorn, UK) was dissolved in 1 ml dimethylsulphoxide (BDH, Dorset, UK) at 10 % (w/v) concentration and stored at room temperature.

Glucose oxidase enzyme solution: 6 mg glucose oxidase enzyme (157500 units/g Sigma, Dorset, UK), and 40 mg bovine serum albumin (Sigma, Dorset, UK) were dissolved in 200 µl phosphate buffer and stored at 4 °C.

Glutaraldehyde solution: 5 µl glutaraldehyde (25% (v/v) aqueous solution, Sigma, Dorset, UK) was mixed with 100 µl phosphate buffer solution and stored at 4 °C.

Polyurethane solution: Trixene SC7602 (kind gift from Baxenden Chemicals Ltd, Accrington, UK) was dissolved in tetrahydrofuran (BDH, Dorset, UK).

Glucose solution: 18 g D-glucose (Sigma, Dorset, UK) was dissolved in 100 ml buffer solution and left overnight to allow equilibrium between alpha and beta glucose. Glucose solutions were stored at 4 °C and used after rewarming to room temperature.

2.2.1.2 Materials

Superglue was from Loctite, Herts, UK. **Conductive Epoxy** was from ITW Chemtronics, Georgia, USA. **Platinum wire** (polyester insulated with diameter of 0.125 mm) and **stainless steel tubes** (with inner diameter of 0.38 mm and outer diameter of 0.50 mm) were bought from Goodfellow, Cambridge, UK.

2.2.2 Construction of Needle Electrodes

Construction of needle electrodes can be divided into two parts, the structural part and the chemical part [50]. The platinum wire and stainless steel tube were the structural components of the needle electrodes and were connected to a low noise co-axial cable. Platinum wire was inserted into the stainless steel tube, and platinum wire and conductive wire were soldered with tin, as standard, providing a connecting resistance of around 1.4 to 1.5 Ohms. However, soldering of stainless steel tube and conductive wire with tin was a problem in the present study and was solved by use of the conductive epoxy; the contact resistance between the stainless steel tube and conductive wire with the conductive epoxy varied from 5.3 Ohms to 15.5 Ohms. The

platinum wire was polyester insulated; at the sensing end of the platinum wire, 0.5 mm polyester insulation material was scraped off for enzyme and membrane application.

The method of application of enzyme and polymers to the electrodes can be found in previous work [50]. The bare tip of the platinum wire was cleaned with acetone and ethanol, and kept upright while drying in ambient air. The electrode tip was dip coated with 10% (w/v) SPEES|PES membrane solution and dried overnight at ambient room temperature. The electrode tip was drop coated with a mixture of 8 μl glucose oxidase enzyme solution and 4 μl 1.2% (v/v) glutaraldehyde solution. After 30 minutes, the electrode tip was washed with the buffer solution to remove excess glutaraldehyde. The electrode was left overnight for drying at room temperature. Multi-polyurethane membrane layers (20, 30, 40, 50% (v/v) Trixene SC7602) in tetrahydrofuran were dip coated on to the electrode tip at 30 minutes intervals between successive layers. Trixene is very viscous and so it is difficult to accurately measure its volume using a pipette, so instead its weight was measured. The density of Trixene is around 0.95–1.05 g/cm^3. The electrode was then dried out overnight at room temperature.

The polyurethane membranes were used as barrier layers to control the glucose diffusion into the enzyme layer so that the electrode could work in a mass transfer limiting mode. The SPEES|PES membrane prevents oxidisable compounds reaching the working electrode due to electrical repulsion. The glucose is oxidised at the enzyme layer to produce hydrogen peroxide. Under a polarising voltage of +0.65 V *vs*. the pseudo reference, the hydrogen peroxide is oxidised at the working electrode to

produce an amperometric current. Because our electrodes were operated in a mass transfer limiting mode, the responses of electrode sub-components were not considered further.

2.2.3 Preparation of Acellular Collagen Gel

Acellular type I rat tail collagen gels were made as previously described [66, 67]. The collagen gel was prepared by mixing 4 ml of 2.16 mg/ml protein in 0.6% acetic acid solution of native acid soluble type I rat tail collagen (First Link (UK) Ltd, West Midlands, UK) with 1 ml of 10× concentration Eagle Minimum Essential Medium (EMEM) (Gibco Chemical, Invitrogen, Scotland, UK). The mixture was neutralised by dropwise addition of 5 M NaOH and 1 M NaOH. This mixture was then poured into a mould ($33\times20\times10$ mm^3). The gel was then compressed with 125 grams for 5 minutes. Finally, the gel was rolled with a surgical blade to form a cylinder. The end cylindrical collagen gel was 2.3 mm in diameter and 26.8 mm in length.

2.2.4 Calibration and Measurement

An AUTOLAB PGSTAT10 potentiostat instrument (Eco Chemie, Utrecht, Netherlands) was used for amperometric measurements. Before measuring glucose concentration, needle electrodes were conditioned in phosphate buffer solution for 4 hours to give a stable baseline response and then tested by stepwise addition of 1 M glucose solution with the increasing glucose concentration in a series of 1-2-5-10-15-20-25-30-35-40 mM as shown in Figure 2.1. The glucose solution was stirred for 2 seconds for proper mixing before measurement without stirring. The needle electrodes functioned stir-independently for concentrations up to 20 mM. The calibration for the needle electrode is not necessary as long as the measurement is

within a liner range as the normalised concentration is used in the calculation. The schematic experimental setup for measurement is shown in Figure 2.2 with the collagen gel arrangement used.

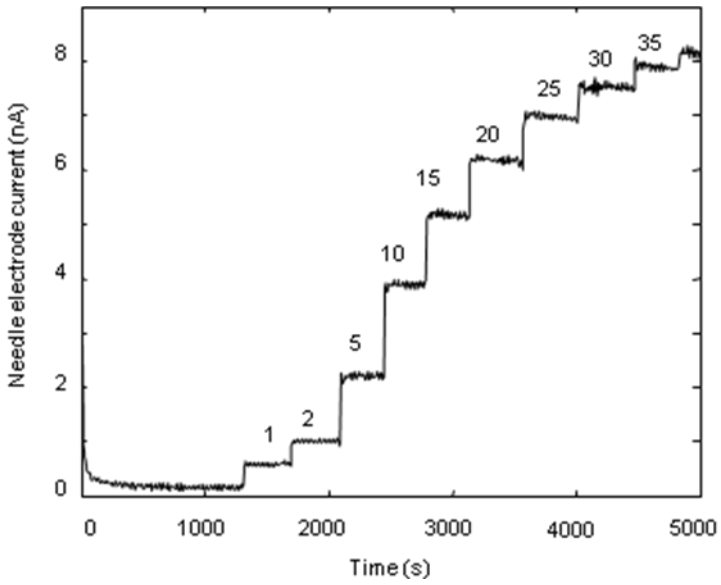

Figure 2.1 Glucose needle electrodes response with a stepwise addition of glucose in 1-2-5-10-15-20-25-30-35-40 mM series [30].

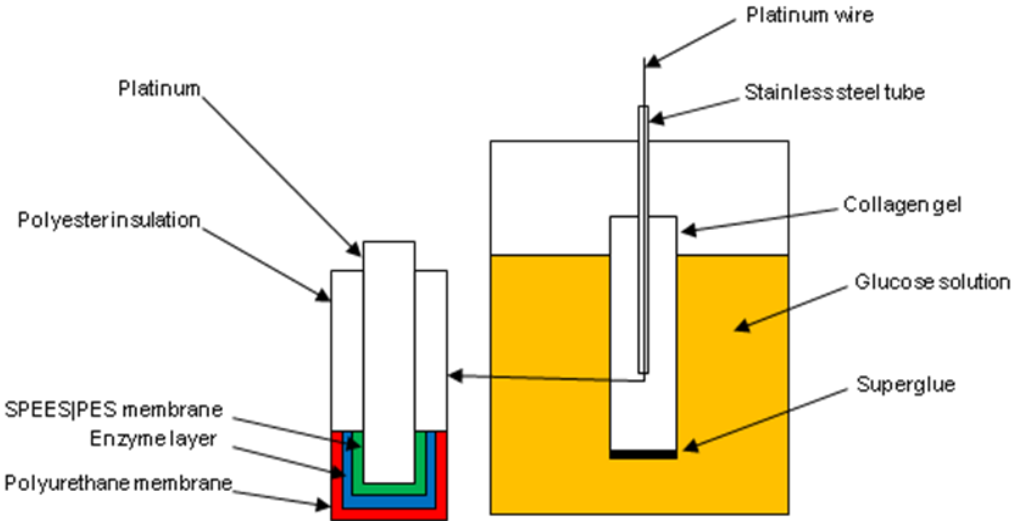

Figure 2.2 Schematic diagram of experiment setup to determine the glucose diffusion coefficient within a cylindrical collagen gel [30].

The electrode was axially inserted into the radial centre of the collagen gel one third to half way from the bottom, so the needle tip was in the centre of the gel segment immersed in the solution. The top of the collagen gel was kept above the solution surface and the bottom was sealed with superglue, as shown in Figure 2.2, so that no solution entered axially. Needle tip position was determined by a balance between the following two requirements. The needle tip was in the middle of the collagen gel below the solution so that any marginal effect was minimised through symmetry and an infinite cylinder was approximated. The reference electrode area to working electrode area ratio was required to be greater than 50:1 for a good signal to noise ratio, which required the needle electrode to be inserted more than 1 cm into the gel. Needle electrodes were retested following collagen contact; gels had no effect on electrode sensitivity, typical response curves are shown in Figure 2.3.

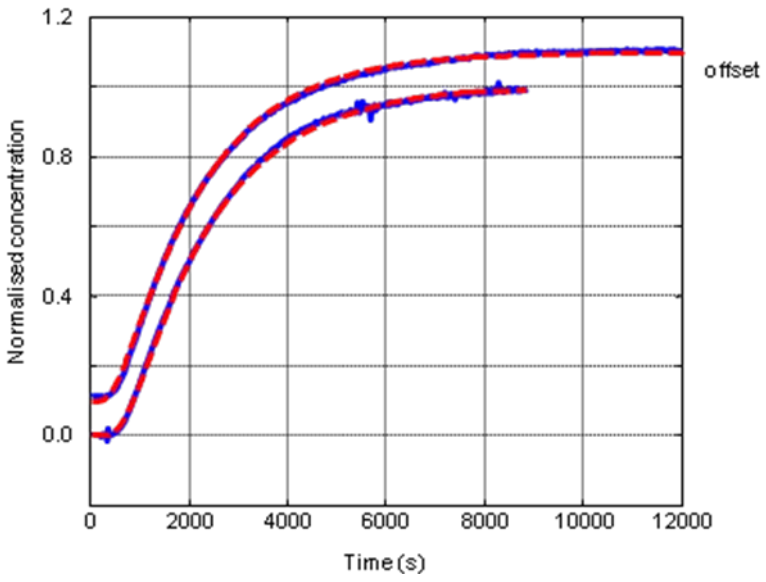

Figure 2.3 The normalised observed (-) and simulated (--) concentration evolution with time. The observed curve and simulated curve virtually overlap. The lower curves are for experiment a and the upper curves are for experiment b. The experimental and simulated curves for experiment b are shifted up 0.1 for clarity [30].

2.3 Mathematical Model of Mass Transfer within a Cylinder

The model envisages a cylindrical collagen gel with a radius of R without glucose immersed into a glucose solution with concentration c_0. Glucose diffuses into the gel and the concentration c follows Fick's Second Law and is a function of radial distance r and time t:

$$\frac{\partial c}{\partial t} = D\frac{\partial^2 c}{\partial r^2} + D\frac{\partial c}{r\partial r} \qquad 2.1$$

where D is the diffusion coefficient and the initial and boundary condition are: $c(r, t < 0) = 0$; $c\ (r = R, t \geq 0) = c_0$.

The analytical solution for diffusion within a cylinder has the same mathematical expression as heat conduction within a cylinder, known for a long time [1, 68, 69]. For convenience, the dimensionless time $T = Dt/R^2$ and concentration $C = c/c_0$, is introduced. The solution to equation 2.1 is given as [1, 68, 69]:

$$C = 1 - 2\sum_{n=1}^{\infty} \frac{J_0(\alpha_n r / R)}{\alpha_n J_1(\alpha_n)} \exp(-\alpha_n^2 T) \qquad 2.2$$

where n is an integer, and J_0 and J_1 are the zero order and first order of Bessel functions, respectively, with $J_0(\alpha_n) = 0$. As the needle electrode is located at the centre of the collagen cylinder, *i.e.*, $r = 0$, we have $J_0(0) = 1$ and equation 2.2 is simplified further. Equation 2.2 is a summation of an infinite series of exponential functions, which is not convenient for numerical simulation, therefore further analysis is necessary.

The terms of equation 2.2 corresponding to n equal to 1, 2, 3 and 4, respectively, are shown in Figure 2.4a. It can be seen that absolute values for the terms with n larger

than 1 are very small for $T > 0.18$ and decreases with T or n increasing, respectively. This tendency is true for $n > 4$. Hence, for $T > 0.18$, the higher order ($n > 1$) terms are negligible. Equation 2.2 with n limited to 1, 2, 3 and 4 is represented in Figure 2.4b for comparison. It can be seen that convergence of equation 2.2 is rapid for large T and slow for small T. For $T > 0.18$, the four curves with different approximations are virtually identical; therefore, the first term represents the whole solution well. However, equation 2.2 converges slowly for small T hence it is not practical for numerical simulations. An alternative solution for small T is therefore required.

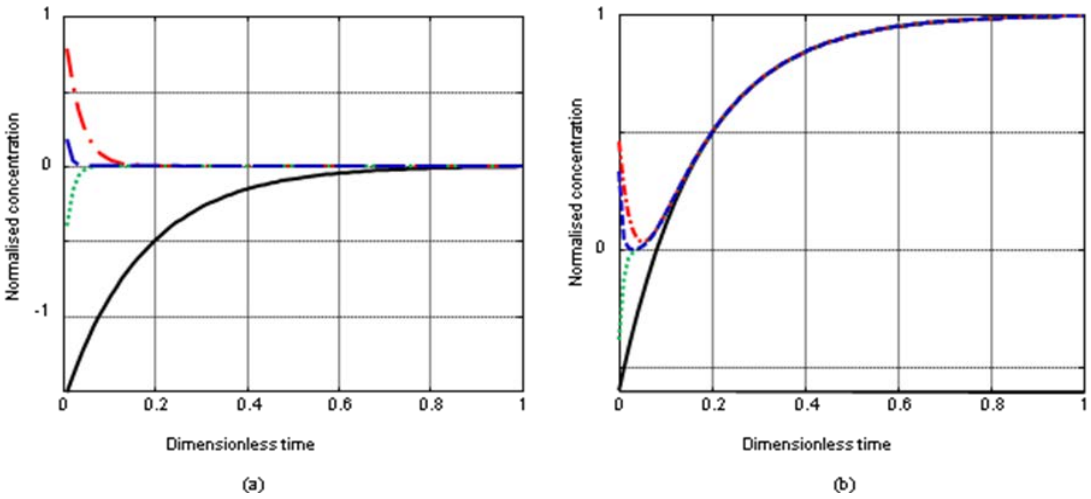

Figure 2.4 (a) The terms corresponding to n equals 1 (-), 2 (-·), 3 (··) and 4 (--) of equation 2.2, respectively. (b) Normalised concentration as equation 2.2 with n limited to 1 (-), 2 (-·), 3 (··) and 4 (--), respectively [30].

For small T, the expressions for the solution to equation 2.1 are different for r equals zero and nonzero [1, 68, 69]. Because the needle electrode is located at the centre of the cylinder, $r = 0$ is of interest. The first order approximation of the solution was derived using the Laplace transform method [70]. The first four terms of the solution are obtained with the Laplace transform method as:

$$C = \frac{1}{\sqrt{\pi T}} \exp(\frac{-1}{8T}) \left[K_{\frac{1}{4}}(\frac{1}{8T}) - \frac{T}{4} K_{\frac{3}{4}}(\frac{1}{8T}) - \frac{7T^2}{32} K_{\frac{5}{4}}(\frac{1}{8T}) - \frac{59T^3}{128} K_{\frac{7}{4}}(\frac{1}{8T}) \right] \qquad 2.3$$

where $K_{1/4}$, $K_{3/4}$, $K_{5/4}$ and $K_{7/4}$ are the fractional modified Bessel functions [2].

The first, second, third and fourth terms of equation 2.3 are shown in Figure 2.5a, respectively. It can be seen that absolute values of the second, third and fourth terms are very small for T < 0.08, and these values increase with T increasing. The first term, and accumulative terms up to the fourth for equation 2.3 are shown in Figure 2.5b for comparison. It can be seen that convergence of equation 2.3 is rapid for small T but slow for large T. For T < 0.08, the four curves with different approximations are virtually identical; therefore, the first term represents the whole solution well.

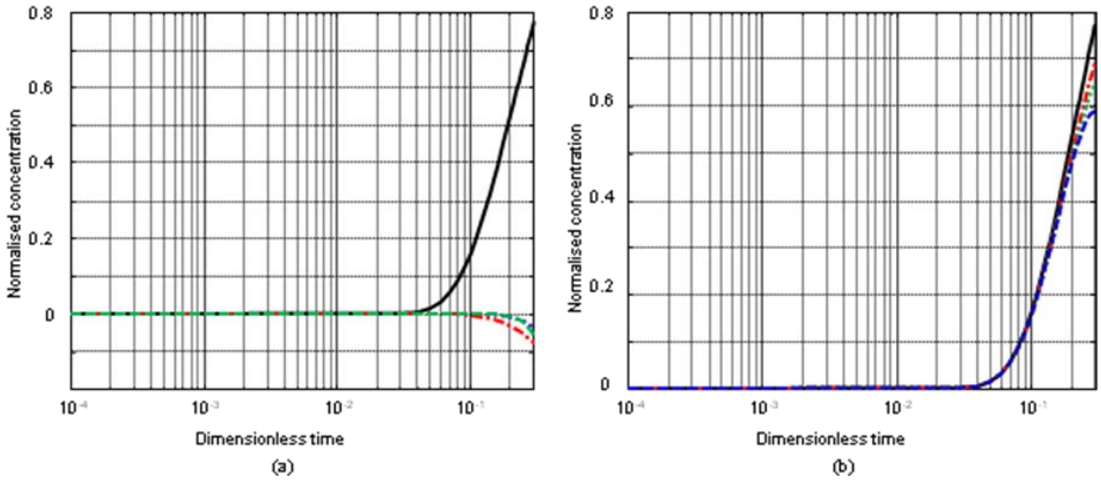

Figure 2.5 (a) The first (-), second (-·), third (··) and fourth (--) terms of equation 2.3, respectively. (b) The first term (-), first two term (-·), the first three terms (··) and all four terms (--) of equation 2.3 are compared [30].

An effort was thus made to construct a solution function by combining the rapidly convergent parts of equation 2.2 and 2.3. For a smooth connection, the two function

curves are required to intersect and to have the same value or close values for first derivatives at the intersection point. However, the curves for equation 2.2 with n limited to 1 and the first term of equation 2.3 do not intersect. The minimum difference between these two curves is 0.021. Therefore, more terms are required in the construction of an applicable solution function. Different combinations of equation 2.2 with different n up to 4 and equation 2.3 with different terms were tested. After a balance between complexity and accuracy, I constructed a normalised concentration function $C = c/c_0$ as follows:

$$C = 1 - 2\sum_{n=1}^{3} \frac{\exp(-\alpha_n^2 T)}{\alpha_n J_1(\alpha_n)} \text{ for } T > 0.063, \qquad 2.4a$$

$$C = \frac{1}{\sqrt{\pi T}} \exp(\frac{-1}{8T}) \left[K_{\frac{1}{4}}(\frac{1}{8T}) - \frac{T}{4} K_{\frac{3}{4}}(\frac{1}{8T}) \right] \text{for } T < 0.063. \qquad 2.4b$$

When $T = 0.06301$, equation 2.4a and equation 2.4b give the same value 0.0358. In fact, when T varies from 0.059 to 0.067, the difference between equation 2.4a and 2.4b is less than 0.0001. In other words, equation 2.4a and 2.4b overlap over the range: $0.059 < T < 0.067$ with functional value difference less than 0.0001, which satisfies practical requirements.

The expressions of suitable solutions for the same differential equation are different for large and small T. The fast convergent parts of these two expressions overlap and form a practical function for an entire time range. From Figure 2.4a it can be seen that the absolute values of terms, corresponding to n equals to 1, 2, 3 and 4 of equation 2.2 decreases with T increasing and n increasing, respectively. At the joint point ($T = 0.06301$), the absolute values of terms corresponding to n equals to 1, 2, 3 and 4, are 1.11, 0.156, 7.60×10^{-3} and 1.15×10^{-4}, respectively. This tendency is true for $n > 4$. Therefore, the terms with $n > 3$ are negligible for $T > 0.06301$. From

Figure 2.5a it can be seen that the values of the first, second, third and fourth terms, the absolute value of the term of equation 2.3 decrease with the term order number increasing and increase with *T*. At the joint point ($T = 0.06301$) the absolute values of the first four terms values are 3.64×10^{-2}, 6.35×10^{-4}, 4.30×10^{-5} and 7.71×10^{-6}, respectively. The terms with term order number > 2 are negligible for $T < 0.06301$. Therefore, it is reasonable that only the first three terms of equation 2.2 and the first two terms of equation 2.3 are used to construct the solution function, *i.e.*, equation 2.4.

2.4 Simulation and Best Fit

The use of simulation and best fit allowed manipulation of the calculated concentration and its comparison with experimental data. Because calculated concentration *C* is normalised, it needs to be multiplied using a factor (*N*) to be compared with experimental data. Simulated concentration also needs to be added on to the baseline current (*B*), which always exists experimentally. Therefore, the simulated concentration c_s is expressed as:

$$c_s = NC((t - t_0)D / R^2) + B \qquad 2.5$$

where t_0 is the time that the collagen gel was immersed into the glucose solution.

Mathematically, *N* stretches or compresses the simulated curve vertically; *B* shifts the overall simulated curve vertically; t_0 shifts the curve horizontally; D/R^2 stretches or compresses the curve horizontally. In principle, a complete set of four parameters *N*, *B*, t_0 and D/R^2 can be variously adjusted to fit the simulated curve to the experimental data. In practice, it is more convenient and meaningful to scale the experimental concentration and to manipulate the normalised simulated concentration at the same

time. Two parameters, the maximum concentration c_m and the baseline c_b are used to manipulate the experimental data, *i.e.*, to stretch and to shift the experimental curves vertically. The experimental concentration c_e is divided by the maximum concentration c_m to be normalised with subtraction of the baseline c_b as

$$C_{en} = \frac{c_e - c_b}{c_m - c_b} \qquad 2.6$$

where c_m and c_b are adjustable parameters. c_m and c_b are estimated at the first stage of manipulation, but can then be established by a best fit. Two parameters, the initial time t_0 and the diffusion related parameter D/R^2, are used to manipulate the normalised simulated data, *i.e.*, to stretch and shift the theoretical curves horizontally. Equation 2.4 can be rewritten as

$$C_{sn} = C((t - t_0)D / R^2) \qquad 2.7$$

where t_0 and D/R^2 are adjustable parameters. Agreement between equation 2.6 and 2.7 can be improved by adjusting parameters c_m, c_b, t_0 and D/R^2.

The initial parameters for these four parameters, c_m, c_b, t_0 and D/R^2 can be obtained in the following way. c_m and c_b are obtained from the maximum and minimum values of the experimental concentrations, respectively; t_0 is estimated from when the experiment starts; since the C_{sn} is 0.9951 when $T = Dt_1/R^2 = 1$, $D/R^2 = 1/t_1$ can be estimated from the time t_1 when the normalised concentration reaches 0.9951. The initial parameters are shown in Table 2.1. The four parameters c_m, c_b, t_0 and D/R^2 can be readjusted by comparison of the normalised simulated curve and the experimental data. Finally, D/R^2 is obtained from a best fit of equation 2.6 to 2.7 with optimization of the parameter c_m, c_b, t_0 and D/R^2. The best fit procedure is to minimise the standard deviation value of the normalised concentration:

$$\sigma = \sqrt{\frac{1}{m-1}\sum (C_{en} - C_{sn})} \qquad 2.8$$

where m is the experimental point number with summation over all the experimental points. The standard deviation characterises the agreement between simulation and experiment. The experimental concentration value is different from one experiment to another. Therefore, the standard deviation of absolute concentration is not generally comparable, whereas that for normalised current is generally comparable.

Table 2.1 Parameters for the dynamic model simulating glucose diffusion within a cylindrical collagen gel

parameter	Unit	experiment a		experiment b	
		initial	optimised	initial	optimised
c_m	mM	13.79	13.65	10.28	10.25
c_b	mM	-0.20	-0.02	0.02	-0.06
t_0	S	20	33.83	20	45.13
$D/R^2 \times 10^4$	s^{-1}	1.129	1.004	1.129	1.015
σ		0.038	0.0050	0.030	0.0066

2.5 Results and Discussion

Figure 2.1 shows the response of the needle electrode to stepwise increase of glucose concentration in the series of up to 40 mM. The response time was < 10 s, so it was ready to monitor glucose concentration evolution within the gels. It can be seen that stir independence is up to 20 mM. Also it can been seen that the amperometric current is up to 6 nA in our measurement (15 mM), therefore net glucose consumption is negligible (~10^{-14} mol/s). Calibration was carried out for every experiment.

Enzyme degradation of glucose here results in production of gluconic acid. However, the effect of gluconic acid on the sensor response due to potential pH change, close to the sensor tip has no significant effect on response for the following reasons. The needle electrode operated in low consumption mode, the amount of gluconic acid produced is small (~10^{-14} mol/s) on the basis of the assessed electrode current and therefore the glucose conversion rate. Proton diffusion away from the enzyme layer through the membranes will also have been relatively less hindered than that of glucose and gluconate ion transfer. Most significantly, however, the buffer concentration used would have eliminated any impact of local enzymatic generation of H^+; enzyme electrodes of the type used here have allowed reliable measurement of glucose without any evidence on adverse effect on transduction [50].

The time lag method solved the problem of slow convergence of the expression at small dimensionless time *T* with an integral of the expression. Because of mathematical simplicity and straightforward applicability, it has been used as a flexible, frequently used method for the characterisation of membrane mass transport. However, careful construction of the experimental setup is needed to avoid leakage [63, 64] and large upstream and downstream volume effects [64]. The method fails when permeability is high or flux is high, and for large *T*, and diffusion coefficients are overestimated [63]. The simultaneous concentration simulation method, adapted to measure concentration evolution after the boundary condition is changed, provides a reliable alternative. Furthermore, the time lag method is limited to membranes; therefore, a dynamic simulation method is necessary for the cylindrical collagen gel.

The constructed bipartite expression for concentration evolution at the centre of a cylinder for an entire time region as equation 2.4 has been verified by comparison of simulated and experimental curves in Figure 2.3. For the initial parameters, listed in Table 2.1, a Microsoft Excel spreadsheet was used to obtain the best fit. The corresponding best fitted parameters c_m, c_b, t_0 and D/R^2 are also shown in Table 2.1. Good agreement between the simulated curve with the best fitted parameters and the experimental curve was observed in Figure 2.3. It can be seen from Table 2.1 that the standard deviations decrease from 0.038 to 0.0050 for experiment a and from 0.030 to 0.0066 for experiment b, respectively. Through best fitting, the D/R^2 value changes from 1.129×10^{-4} s^{-1} to 1.004×10^{-4} s^{-1} for experiment a and from 1.129×10^{-4} s^{-1} to 1.015×10^{-4} s^{-1} for experiment b, respectively. It is also clear that even initial parameters from normalisation of the transient response operate well and differ only 10% from the optimised parameters, offering a simple method for approximating diffusion coefficients.

Once D/R^2 is obtained from a best fit, the diffusion coefficient can be calculated by $(D/R^2)\times R^2$. The diameter of the collagen gel was 2.3 mm and the estimated diffusion coefficients of glucose within the collagen gel of 1.33×10^{-6} cm^2/s and 1.34×10^{-6} cm^2/s (after 7 hours) shows excellent repeatability. Glucose diffusion for a 5% (w/v) collagen gel prepared from bovine Achilles tendon and cross-linked in glutaraldehyde has been measured by stop flow, and gave the result $D = 1.6\times10^{-7}$ cm^2/s [59], and for rat tail collagen by time lag was 1.441×10^{-6} cm^2/s [60]. Apparent glucose diffusion coefficient decreases with cell density [60], but otherwise our measured coefficients are comparable to published values.

The significance of this work is that it provides a simple practical method to characterise the solute diffusive phenomena through soft matter. Such measurements are relevant to the analysis of reaction rates in polymeric or biopolymeric phases where steric hindrance to diffusion can become significant, if not dominant further. A particular example is where a biorecognition process takes place at a sensor surface, and its dynamic behaviour becomes modified by limited diffusion, as might occur if the sensor is operating in a tissue matrix or a tissue engineered scaffold. Further development of this work should allow independent characterisation of reactive processes in such matrices by accurate uncoupling of mass transport. The cylindrical geometry and electrode combination adopted here facilitates access to mass transfer measurement.

Because of the reliability of the multi-parameter fit, the primary source of error is simply the measurement of gel dimension; the percentage error in the radius measurement $\Delta R/R$ contributes to a percentage error of $2\Delta R/R$ in the diffusion coefficient. Whilst the diameter of the collagen gel was measured here with a vernier clipper, some inaccuracy could occur because of soft matter indentation or possible dimensional changes over time in solution.

Because only normalised concentration is needed in the dynamic simulation method to obtain the glucose diffusion coefficients, provided the measuring range is within the linear range, no calibration is needed. This is an important simplification allowed by the present dynamic model.

For the time lag method, only noise is minimised during the lag time fitting. The time lag from curve fitting is reasonably accurate; indeed it was reported that a perfect fit can be observed [71]. It can also be seen that the errors are observed between the experimental current and simulated one [71]. Compared to indirect fitting to experiment currents for the time lag method, for the dynamic simulation method, a simulated curve directly fits the experimental concentration profile with minimization of theoretical and experimental errors due to noise, baseline, and zero time determination. Compared to the motor and regulator used in the rotating disk electrode method [15, 16, 65], the advantage of this method is simplicity and allows *in situ* monitoring, needed for further progress in the research of gels for tissue engineering.

2.6 Conclusions

Rapid response glucose needle electrodes have been fabricated and experiments were carried out to measure glucose concentration evolution at the centre of a cylindrical collagen gel, which mimicked glucose diffusion into an infinite gel cylinder as a route to diffusion coefficient determination. The needle electrodes worked in low analyte consumption mode and stirring independence.

Two different expressions were used to account for glucose concentration evolution depending on the dimensionless time domain. High order terms of the expression for small dimensionless time have been derived. After thorough investigation of the expressions, a practical solution function combined rapidly convergent parts of these two expressions, functions for the entire time range, and was verified by experiment.

Through analysing model parameters I have developed insight into diffusion dynamics and the numerical sensitivity of the model parameters. Compared to other established techniques, higher accuracy has been achieved because theoretical and experimental errors due to noise, baseline and zero time determination have been minimised through directly fitting. Finally, the actual best fitted parameter is D/L^2, therefore, accuracy of the diffusion coefficient largely depends on the accuracy of the radius measurement of the collagen cylinder.

Chapter 3 Needle Enzyme Electrode for Lactate Measurement *In Vivo*

Electrochemical lactate needle enzyme electrodes were fabricated based on lactate oxidase with a conventional hydrogen peroxide detection regimen with a linear range up to 7 mM, response time ~ 3 min and sensitivity ~1 nA/mM. A negatively charged inner (SPEES|PES) membrane was applied for ensuring selectivity by limiting oxidisable anion diffusion to the platinum working electrode; polyurethane outer membrane layers were dip coated over the enzyme layer to limit substrate diffusion to the enzyme layer to achieve (i) stir independence and (ii) a low oxygen requirement. Lactate was monitored subcutaneously in rats during controlled haemorrhage and hypovolaemic shock. Tissue lactate showed agreement with blood lactate before haemorrhage and for limited haemorrhage (up to 2 ml blood withdrawal from 16 ml total blood volume) but with blood loss above 3 ml the tissue lactate rise was less pronounced than in blood. Loss of intercompartmental equilibrium due to diffusion limitation is suggested as a factor in causing this difference. An experimental *in vitro* model was developed which employed the needle lactate electrode within a cylindrical collagen gel to monitor inward diffusion of lactate as a basis for determining the lactate diffusion coefficient. The high precision measurement gave a diffusion coefficient consistent with report values, 3.54×10^{-6} cm^2/s. The simplified experimental approach could allow lactate transport studies across tissue analogues.

3.1 Introduction

Under aerobic conditions, 32 adenosine triphosphate (ATP) molecules along with CO_2 and water are generated from one molecule of glucose. Alternatively, under

anaerobic conditions, lactate is produced with the generation of only two molecules of ATP [72]; this is a marked contrast in the energy economy of the cell. As a fundamental analysis of metabolism, a measurement of the molar ratio of glucose consumption rate to lactate production indicates the proportion of glucose undergoing aerobic *vs*. anaerobic metabolism and thereby the level of tissue available oxygen *viz*. a measure of the hypoxic state. For example, lactate levels in the brains of freely moving rats were measured during sleep and waking states to observe aerobic to anaerobic metabolic shifts [73]. Also, as a fundamental study of biology, lactate concentrations in skeletal muscle and liver have been measured to demonstrate the net transport of lactate across skeletal muscle and liver under hypoxic conditions [74, 75].

In the chemical context, lactate concentration in blood is an indicator of the overall oxygenation state of the organism, and reflects the general availability of oxygen for tissue respiration. Tissue deprivation of oxygen in a critically ill patient is the root cause of many adverse outcomes in hospitals [76]. Lactate level is regarded by many as the optimum indicator of oxygen debt and a measure of the severity of shock in human subjects [77–79]. However, blood lactate concentrations in the critically ill do not always provide a valid assessment of perfusion state adequate splanchnic and lung perfusion may for example be associated with high lactate output which may still swamp the liver's capacity to clear it [80]. Eventually, it could be more valuable to assess lactate in particular tissues rather than to make traditional assessments based on "body averaged" values because of tissue specific differences in lactate production – moreover there may be blood-tissue differences due to lactate transfer barriers between the two compartments. Current techniques for the assessment of shock states, e.g., measurement of cardiac / respiratory activity, blood pressure and blood

gases, are expensive and provide inadequate predictive information to help shock management or effective resuscitation. Patients in shock states generally appear to have a better prognosis if lactate levels are tightly controlled. It has been demonstrated that the ability to clear lactate down to normal values is one of the most important variables in predicting survival after injury. Moreover, continuous monitoring would not only allow for trend monitoring, but could better aid therapy with improved patient outcomes. This could also produce financial savings with respect to the cost of therapy.

In sport, anaerobic metabolism is often enhanced because of increased tissue oxygen demand due to extreme exercise, and blood lactate a useful measure to assess the degree of this anaerobic respiration and its possible underlying physiological mechanisms. As an example, lactate levels have provided an index of aerobic *vs*. anaerobic metabolism linked to muscle performance and with this an individual response to specific training; from a target ratio of anaerobic to aerobic metabolism, a coach can determine optimal training parameters [81]. The endurance of athletes has also been found to be related to anaerobic threshold [82].

Various approaches to *in vivo* lactate measurement have been advanced; nearly all exploit lactate oxidase coupled with electrochemical detection. Thus, lactate concentration in rats was measured voltammetrically with carbon electrodes incorporating lactate oxidase [73]; subcutaneous lactate in rats was monitored by microdialysis sampling with an active carbon electrode for electrochemical detection [83]. Lactate levels in rat brain have been measured using ceramic enzyme loaded microelectrodes [84] and also *via* microdialysis integrated microelectrodes [85], both

utilising lactate oxidase. Lactate concentrations in rat skeletal muscle and liver have been measured with an enzyme electrode *via* microdialysis [74, 75]. A needle enzyme electrode has been developed for muscle implantation and used in mice [86]. Accumulated lactate levels were measured in the ischemic myocardium of rabbits, using a conducting salt / lactate oxidase combination [87]. An amperometric catheter has allowed real time lactate monitoring in dogs; here, a venous lactate of 0.7 mM rose to 2 mM after a 30 min running exercise, returning to the baseline in 30 min [88]. Alternative studies have utilised near infrared diffusive spectroscopy [89] and open-flow microperfusion used to extract tissue fluid [90]. In future, for human studies, microfabricated biochips could well be used for monitoring [91]. The current study adopted the previous glucose electrode design based on a needle electrode construction however, because *in situ* perfusion of fluid into the tissue around the electrode tip stabilised performance [92], the Open Microflow approach was tested for the lactate needle electrode. This report, it is believed, is the first description of the Open Microflow technique used with a lactate electrode. Open Microflow utilises the negative hydrostatic pressure of subcutaneous tissue to induce fluid uptake from an external reservoir. The outcome is (i) tissue hydration and therefore enhanced solute transport (increased effective connective tissue) between the capillary bed and the sensor (ii) a fluid protective film between the sensor tip and tissue, reducing surface fouling and therefore electrode drift.

The measurement of the diffusion coefficient of a metabolite is a valuable basis for evaluating the local tissue microenvironment and the impact of tissue natural barriers in creating concentration heterogeneities. The apparent diffusion coefficient of a solute *in vivo* is a complex function of cell density, cell activity, and the interaction

between cells and their surroundings in the interstitial space; as such it can provide useful quantitative information for understanding the structural organization of tissues or organs utilising diffusion / reaction models. Here it provides an assessment of the possible barrier to lactate transport. Lactate diffusion has been measured *in vivo* by NMR which has provided an estimate of lactate displacement, in turn influenced by local tissue factors, *viz*. temperature, motion and intercompartment active and passive transport [93]. Here, a value for a xenograft tumour of $D = 2.1\times10^{-6}$ cm^2/s [93] was obtained and in a rat glioma tumour the value was 1.3×10^{-6} cm^2/s [94]. Importantly, these are significantly lower than for the lactate diffusion coefficient in simple aqueous solution, which in one report was measured to be 5.62×10^{-6} cm^2/s by a three-chamber diffusion cell [95].

In our previous work, a lactate enzyme electrode was devised with a linear range extending well above enzyme Km (1 mM) by using a polyvinyl chloride based surfactant bearing layer to restrict lactate diffusion to the enzyme layer for physiological measurement (up to 5 mM) [96]. The membrane had the effect of dropping the lactate concentration in the enzyme layer and so allowing the enzyme to operate within its kinetic range (well below Km). The membrane had low fouling in blood, an outcome which was also reflected in parallel observations for glucose sensors. Glucose enzyme electrodes with polyurethane membranes were used by us *in vivo* [92]. A dual approach was tested; in one approach the sensor was retained in an open ended cannula whilst implanted in subcutaneous tissue with the sensing tip perfused with buffer during measurements (Open Microflow), and in the second approach, a non-ionic surfactant was integrated into the outer protective polyurethane

membrane for enhanced biocompatibility. In the present work, lactate needle enzyme electrodes were similarly fabricated and evaluated for lactate both *in vitro*.

With regard to the *in vitro* study, glucose electrodes were previously used in a collagen gel to determine glucose diffusion coefficient using a computational model to simulate sensor dynamic response [30]. Glucose concentration transients were computed to mimic initial and boundary conditions and then compared to experimental data. A lactate diffusion coefficient in collagen has been similarly determined here.

3.2 Experimental

3.2.1 Chemicals and Reagents

Lactate oxidase (*Pediococcus*), lithium lactate, glutaraldehyde (25% v/v aqueous solution) and bovine serum albumin were from Sigma, Dorset, UK. Tetrahydrofuran, dimethylsulphoxide, di-sodium hydrogen phosphate, sodium di-hydrogen phosphate, sodium chloride and sodium hydroxide were from BDH, Dorset, UK. The outer covering layer of polyurethane was based on a proprietary prepolymer; Trixene SC7602 (a kind gift from Baxenden Chemicals Ltd, Accrington, UK). Sulphonated Polyether Ether Sulphone – Polyether Sulphone (SPEES|PES) copolymer was a kind gift from ICI Colloids and Polymer Group, Runcorn, UK. Superglue was from Loctite, Herts, UK. 10× concentration Eagle Minimum Essential Medium (EMEM) was from Gibco Chemical, Invitrogen, Scotland UK. 2.16 mg/ml protein in 0.6% acetic acid solution of native acid soluble type I rat tail collagen was from First Link (UK) Ltd, West Midlands, UK.

3.2.2 Electrode Fabrication

Polyester insulated platinum wire of diameter 0.125 mm and stainless steel tubing of inner diameter 0.38 mm and outer diameter 0.50 mm were from Goodfellow, Cambridge, UK; they were cut into 80 and 70 mm length pieces, respectively. The platinum wire was inserted into the stainless steel tube, and the non-sensing end connected to co-axial wire for further connection to the instrument, the sensing end penetrated 0.5 mm beyond the tubing and was coated variously with SPEES|PES inner membrane, enzyme and outer polyurethane.

The polyester insulation on the platinum tip had been scraped off, and the platinum tip cleaned with acetone and ethanol, respectively. After being dried at ambient room temperature, the tip was dip coated with the SPEES|PES membrane solution which was 10% w/v in dimethylsulphoxide and then dried overnight at ambient room temperature. The electrode tip was then drop coated with a mixture of 8 µl lactate enzyme–albumin solution and 4 µl 0.5% v/v glutaraldehyde solution. 114 U lactate oxidase and 60 mg bovine serum albumin were dissolved in 200 µl phosphate buffer to prepare this enzyme solution. 4 µl 25% v/v glutaraldehyde was diluted in 200 µl phosphate buffer to prepare a 0.5% working solution. The electrode tip was left in ambient air crosslinking for 10 min and washed for 2 min using phosphate buffer to remove excess glutaraldehyde and to halt crosslinking. After overnight drying, the electrode tip was sequentially dip coated with outer membrane solutions, comprising a sequence of 20, 30, 40 and 50% v/v Trixene, used as received and dissolved in tetrahydrofuran with a 30 minutes interval between the depositions. After washing and drying overnight at ambient temperature the electrode was ready for calibration.

3.2.3 Initial Electrode Calibration

An AUTOLAB PGSTAT10 potentiostat instrument (Eco Chemie, Utrecht, Netherlands) was used for all measurements. A potential of +0.65 V was applied to the platinum working electrode *vs*. stainless steel, used as a combined reference and counter electrode. Typical conditioning curves of two lactate electrodes in buffer solution are shown in Figure 3.1, the exponential curves were observed which illustrated the formation of electrical double layers on the electrode surfaces and demonstrate a finite stabilisation period required from open circuit. After the baseline currents were reached, monotonically incremental lactate concentrations in a series of 1-2-3-5-7-9-11 mM were realised by stepwise addition of 100 mM lactate stock solution. Once lactate was added to the assay buffer, the mixture was stirred rapidly for a few seconds and then left unstirred for several minutes to test the electrodes without stirring. Alternatively, after lactate was added to the assay buffer, the mixture was stirred rapidly for a few seconds and then stirred gently to test the electrodes. A typical response curve of a lactate electrode with and without stirring is shown in Figure 3.2. The electrodes were tested with and without stirring to confirm they were stir independent. Since oxygen partial pressure is different within different compartments of the body, lactate electrodes were tested with oxygen partial pressures of 40 and 70 mmHg equivalent to pO_2 in venous and low arterial respectively as shown in Figure 3.3. The electrodes were tested under different oxygen pressures to confirm they were oxygen independent under normal physiological conditions. Compared to the electrodes in Figure 3.2, electrodes with different sensitivities are observed. Electrode sensitivity is a function of temperature, so electrodes were either calibrated at room temperature (25 °C) or body temperature (37 °C) depending on application.

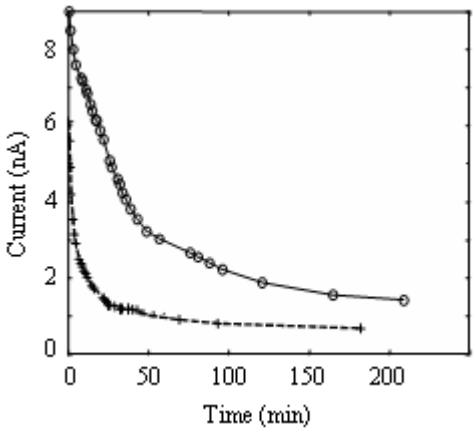

Figure 3.1 Typical conditioning curves for 2 lactate needle electrodes [31]. After the electrodes were placed in phosphate buffer solution and applying +0.65V polarisation on platinum working electrode *vs*. stainless pseudo reference electrode, the exponential curves were observed which illustrated the formation of electrical double layers on the electrode surfaces.

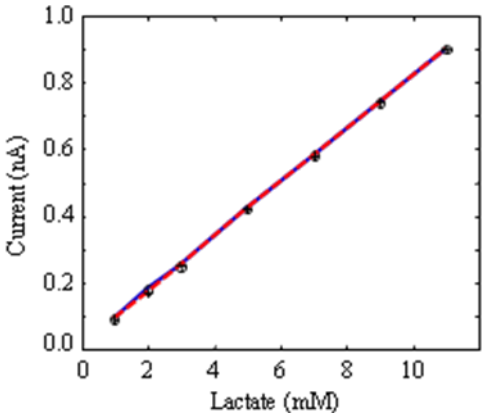

Figure 3.2 Typical lactate needle electrode calibration curves in buffer solution [31]. After needle electrodes were conditioned in phosphate buffer solution to give a stable baseline response, as shown in Figure 3.1, the electrodes were then tested by stepwise addition of 100 mM lactate solution with the lactate concentration increasing in a series of 1-2-3-5-7-9-11 mM. The electrodes were tested with (o) and without (+) stirring to confirm they were stir independent.

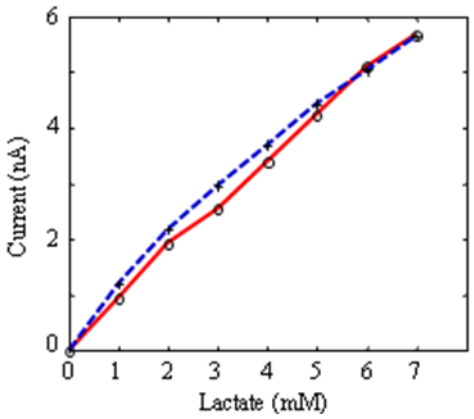

Figure 3.3 Lactate needle electrode calibration curves in buffer solution [31]. After needle electrodes were conditioned in phosphate buffer solution to give a stable baseline response, as shown in Figure 3.1, the electrodes were then tested by stepwise addition of 100 mM lactate solution with the lactate concentration increasing in a series of 1-2-3-4-5-6-7 mM. The electrodes were tested under different oxygen pressures, 40 (+) and 70 (o) mmHg, to confirm they were oxygen independent under normal physiological conditions. Compared to the electrodes in Figure 3.2, different sensitivities are observed.

3.2.4 Lactate Measurement *In Vivo*

Sterilisation is necessary for *in vivo* measurement. A prior investigation of the sterilization of lactate biosensors had shown that only beta and gamma irradiation was compatible with a functional enzyme. Gamma irradiation was chosen because the procedure was more convenient for sterilisation compared to beta irradiation. Since sterilisation studies had shown that the standard dose of 22.5 KGy allowed survival of the enzyme without loses of linearity, response time or sensitivity, this was the dose used.

Wistar rats weighing between 270 g and 320 g were used for *in vivo* monitoring, in accordance with authorised UK Home Office procedure. The rats were anaesthetised with sodium pentobarbitone (0.75 mg/kg body weight), maintained full anaesthesia during all experiments and were sacrificed after experiments. The animal body superficial temperature was kept at 37 °C with the aid of a 20 W anglepoise lamp. The temperature was monitored by means of a rectal probe. An intravenous catheter of 0.6 mm outer diameter was introduced into the tail artery for blood withdrawal and one tail vein was cannulated for blood pressure monitoring and anaesthetic infusion. The electrodes were inserted subcutaneously singly or in pairs, either in the scruff or lumbar region after being conditioned in phosphate buffer overnight. In order to assess the influence of fluid perfusion over the sensor tip by Open Microflow [92] *in vivo*, a perfusion rate of ~ 1 μl/min was used. In the Open Microflow method, a cannula housed the needle electrode and delivered perfusion fluid with the cannula open ended in the implant site and the other end connected to a reservoir.

Approximately 15 min before shock induction, the whole animal was heparinised by infusion of Monoparin to prevent blood clotting. *In vitro* calibration before *in vivo* measurements is undertaken but unlike other studies *in vivo* calibration was avoided. After *in vivo* measurement the electrodes were recalibrated following explanation to determine sensitivity drift.

The normal lactate level in rat serum is approximately 1 mM, and there is a total blood volume in the rat of approximately 16 ml. After the sensors were left to stabilise *in vivo*, haemorrhagic shock was induced in the animal by arterial blood withdrawal. The maximum withdrawal rate was 0.33 ml/min as was permitted by the

animal experimentation licence. The response of the sensor was continuously recorded. Blood samples were taken at successive time points, and kept refrigerated at 4 °C in fluoride / oxalate tubes for a maximum of 24 hours. Lactate concentrations in blood were determined using a clinical analyzer (Yellow Springs Instrument 2300 Stat Plus) for later correlation with the values acquired by the sensor. Lactate concentrations were measured respectively during a low shock (2 ml blood withdrawn) Figure 3.4 and high shock (3 ml blood withdrawn) Figure 3.5. After *in vivo* measurement, electrodes were calibrated for validation of measurements as shown in Figure 3.6.

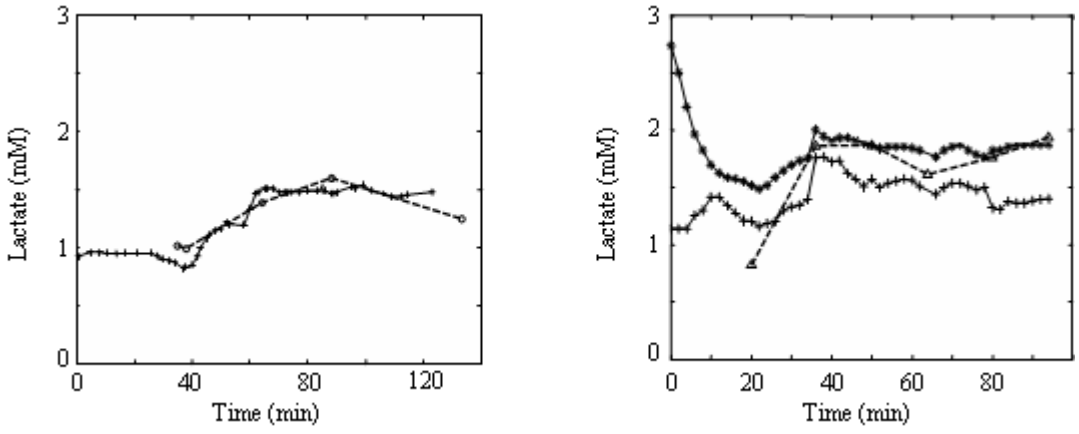

(a) (b)

Figure 3.4 (a) Observed lactate concentration measured subcutaneously in intra-scapular region of rat tissue (+) is compared with lactate concentration in blood plasma (o) at a low shock level (less than 2 ml blood withdrawal from 16 ml total blood volume). (b) Observed lactate concentrations measured subcutaneously in intra-scapular region (+) and lower back region (*) of rat tissue are compared with lactate concentration in blood (Δ) at a low shock level (less than 2 ml blood withdrawal from 16 ml total blood volume) [31].

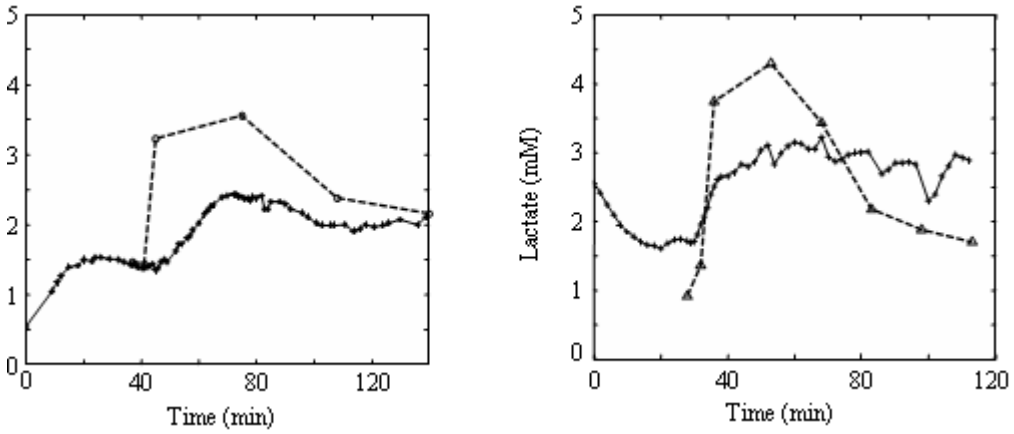

(a) (b)

Figure 3.5 (a) Observed lactate concentration measured subcutaneously in low back region of rat tissue (*) is compared with lactate concentration in blood plasma (o) at a high shock level (more than 3 ml blood withdrawal from 16 ml total blood volume). (b) Observed lactate concentration measured subcutaneously in intra-scapular region of rat tissue (+) is compared with lactate concentration in blood (Δ) at high shock level (more than 3 ml blood withdrawal from 16 ml total blood volume) [31].

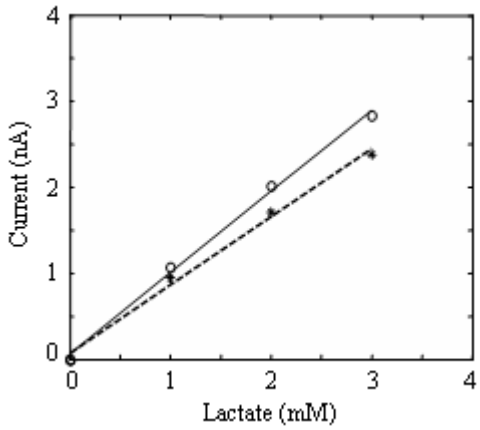

Figure 3.6 Lactate needle electrode calibration curves in buffer before (*) and after (o) *in vivo* measurement [31]. After needle electrodes were conditioned in phosphate buffer solution to give a stable baseline response, the electrodes were then tested by stepwise addition of 100 mM lactate solution with the lactate concentration increasing in a series of 1-2-3 mM. It can be seen that the minor sensitivity dropped after *in vivo* measurement.

3.2.5 Lactate Measurement in Collagen Gel

A collagen gel was prepared by mixing 4 ml of type I rat tail collagen with 1 ml of 10× concentration EMEM [30]. The mixture was neutralised by dropwise addition of 5 M NaOH and 1 M NaOH. This mixture was then poured into a mould (33×20×10 mm^3). The gel was then compressed with 125 grams for 5 minutes. Finally, the gel was rolled with a surgical blade to form a cylinder. The cylindrical collagen gel was 1.73 mm in diameter and 26.8 mm in length.

The electrode was axially inserted into the radial centre of the collagen gel to half way from the bottom, so the needle tip was in the centre of the gel segment immersed in the solution. The bottom of the collagen gel was sealed with superglue to prevent axial lactate diffusion through the gel. The needle tip was in the middle of the collagen gel so that any marginal effect was minimised through symmetry, and diffusion in a finite cylinder was approximated as in an infinite cylinder. For the stainless steel reference electrode, the reference electrode area to working electrode area ratio was required to be 50:1 to avoid the voltage polarising effects of current flow at the working electrode; the needle electrode was inserted $\geq$ 1 cm into the gel. Lactate needle electrodes and the set collagen gel was immersed in lactate solution as shown in Figure 3.7a, a typical concentration transient curve are shown in Figure 3.7b for a collagen gel free of lactate immersed in lactate solution.

3.3. Lactate Diffusion Coefficient Determination

Diffusion coefficient determination was based on a dynamic simulation as previously reported [30]. A brief description of the model is given and an improved formula for diffusion coefficient estimation is derived here. Lactate diffuses into a cylindrical

collagen gel with a radius of R without lactate immersed into a lactate solution with concentration c_0. For convenience, the dimensionless concentration $C = c/c_0$ and time $T = Dt/R^2$ are introduced. A simple but accurate expression for solution is given [30]:

$$C = \frac{\exp(-1/8T)}{\sqrt{\pi T}}\left[K_{\frac{1}{4}}(\frac{1}{8T}) - \frac{T}{4}K_{\frac{3}{4}}(\frac{1}{8T})\right] \text{ for } T \le 0.06301. \qquad 3.1a$$

$$C = 1 - 2\sum_{n=1}^{3}\frac{\exp(-\alpha_n^2 T)}{\alpha_n J_1(\alpha_n)} \text{ for } T \ge 0.06301, \qquad 3.1b$$

When $T = 0.06301$, equations 3.1a and 3.1b give the same values $C = 0.03575$.

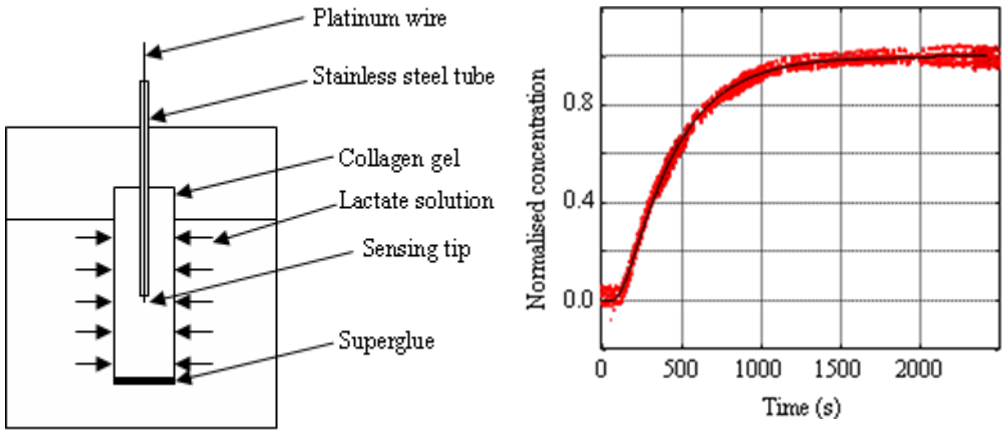

(a) (b)

Figure 3.7 (a) Schematic diagram of experiment setup for determining lactate diffusion coefficient in a cylindrical collagen gel. (b) The normalised observed (·) and simulated (-) concentration evolution with time. The observed curve and simulated curve virtually overlap [31].

Equation 3.1 is a function of dimensionless time, T, and can be considered as a function of parameter D as:

$$C_s = C\big(D(t - t_0)\big) \qquad 3.2$$

where t_0 is the time when the boundary condition changed.

To be compared with the simulated concentration, the experimental concentration c_e should be normalised as:

$$C_e = \frac{c_e - c_b}{c_m - c_b} \tag{3.3}$$

where c_m and c_b are the steady state concentration and baseline concentration.

Agreement between equation 3.2 and 3.3 can be achieved by adjusting parameters c_m, c_b, t_0 and D by minimising the standard deviation as [30]:

$$\sigma = \sqrt{\frac{1}{m-1}\sum (C_s - C_e)^2} \tag{3.4}$$

Table 3.1 Parameters for the dynamic model simulating lactate diffusion in a cylindrical collagen gel

parameter	unit	initial	optimised
c_m	nA	3.2	3.18
c_b	nA	0.2	0.222
t_0	s	100	133
$D \times 10^6$	cm^2/s	4.3	3.54
σ		0.06	0.019

As a normalised concentration was used for the best fit, electrode calibration was not necessary when the electrode operated over a linear range.

Four initial parameters c_m, c_b, t_0 and D are required for a best fit. The first three initial parameters are straightforward as respectively steady state concentration, baseline concentration, and time when the boundary condition changes. The D value was estimated from $D = R^2/t_1$ when t_1 is the time the normalised concentration

reaches 0.9951 of the steady state concentration [30]. Here the initial value for *D* was estimated from:

$$D = 0.2005R^2 / t_{0.5} = R^2 / 5t_{0.5} \qquad 3.5$$

where $t_{0.5}$ is the time when the normalised concentration reaches half of the steady state value. The initial parameters for the dynamic model simulating lactate diffusion in a collagen gel are shown in Table 3.1.

3.4 Results and Discussion

The extended conditioning times for lactate electrodes, the extreme periods shown in Figure 3.1 indicate a variable but significant stabilising time, from 30 min up to 120 min. Platinum working electrodes were believed to be responsible for these effects, due to the adsorption of oxygen onto the platinum surface, double layer charging and the formation of oxide layers [97, 98]. The central role of the platinum was tested in a 3 electrode set-up using a standard Ag/AgCl electrode as the reference, a platinum mesh as the counter and platinum as the working electrode; interchanging of the Ag/AgCl electrode with stainless steel did not alter the conditioning current, confirming this to be a platinum polarisation effect.

For either subcutaneous lactate measurements or lactate diffusion coefficient measurements in collagen, stirring is not possible in the target matrices since there is no dynamic fluidic flow. Electrode response may be affected by some fluid convection, stirring artefact [99], so stir independence was vital. The lactate electrodes satisfied this requirement; Figure 3.2 shows negligible change with rapid stirring, but more importantly, in quiescent solution, stable steady state readings were obtained with response times ~ 3 min, and notably, a linear range well above the Km

of the enzyme. The outer polyurethane diffusion barrier membrane was critical in reducing lactate transport whilst avoiding over-extended response times. Moreover, the independence from pO_2 between 40–70 mmHg (i.e., down to venous blood level) (Figure 3.3) showed that sufficient O_2 reached the oxidase layer to avoid O_2 reaction limitation.

In our previous work on glucose, Open Microflow gave *in vivo* tissue glucose readings that matched blood [92]. Importantly this glucose correlation was obtained without the need for *in vivo* recalibration. It was anticipated that a similar benefit would accrue for lactate. The current traces show firstly that electrodes coupled with Open Microflow required 1 hour to stabilise, with no evident sustained effect of the Open Microflow on lactate response subsequently.

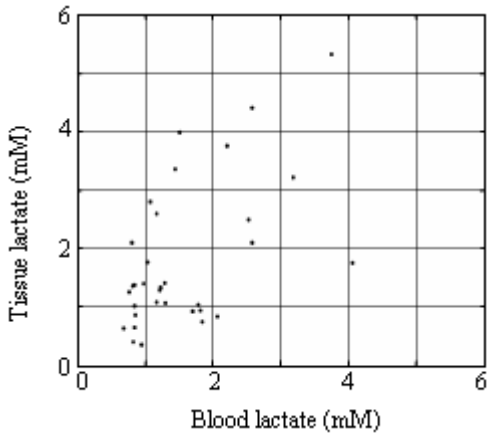

Figure 3.8 The measured lactate concentrations in blood and in tissue for 11 electrodes [31].

For *in vivo* measurement, a key issue of biosensor calibration; electrodes are calibrated *in vitro*, including for extracorporeal systems [73, 84, 86, 88, 90] or *in vivo* [74, 75, 87, 100]; only for the latter is a true tissue blood correlation attempted *in vivo*,

either one-point or two-point, based on blood measurement, which assumes blood-tissue equivalence. Two-point calibration can help define sensitivity and background. However, a disadvantage of the two-point method is that it is time consuming and vulnerable to measurement error. Here electrodes were calibrated *in vitro*, a much simplified protocol with subcutaneous measurements compared directly with blood *in vivo*.

During the studies, multi-point calibrations were carried out for 11 electrodes (one electrode with two points, nine electrodes with three points and one electrode with four points) *in vivo* as shown in Figure 3.8. No obvious correlation was observed, which is probably due to: animal movement, the formation of blood clots inside the sampling cannula and the administration of anaesthetic and heparin (which caused transient current fluctuations) - the significance of the latter is unclear. Lactate concentrations in blood and tissue are assumed to be the same for *in vivo* calibration which may be questionable. More importantly, the lactate concentration should be changed for a two-point *in vivo* calibration. If the lactate concentration change is small, the calibration error would be significant. If the lactate concentration is changed significantly then the lactate change in tissue might not follow the lactate change in blood. Hence, *in vivo* calibration was not adopted here. However, once a sensor signal was stabilised, and shock induced by haemorrhage, the electrode signals rose progressively - typically 5 to 10 min after haemorrhage, accompanied by a decrease in blood pressure; the electrode current, reflecting lactate, then reached a maximum before decreasing steadily. Blood for lactate determination was taken at several time points within the allowed Home Office protocol, notably at the beginning of haemorrhage, when maximum current was attained and before overdosing the

animal with anaesthetic. Representative traces for lactate monitoring for low and high shock levels are shown in Figures 3.4 and 3.5.

In a low shock level haemorrhage (2 rats), 2 ml blood was withdrawn from a rat through arterial and the minimum mean artery pressure (MAP) was kept greater than 80 mmHg. Lactate concentrations of two rats were measured in blood and blood plasma and were less than 2 mM as shown in Figure 3.4. Lactate levels measured in the intra-scapular region and lower back region were also less than 2 mM, once electrode response had stabilised. Electrode sensitivities were mostly retained (~80%) after 3 hours implantation, though monitoring periods of only 1.5 and 2 hours are shown in Figure 3.6. So lactate measurements *in vivo* using electrodes were sufficiently stable, at least for tracking rapid changes. From Figure 3.4 it is seen that lactate levels increased after haemorrhage for both blood and tissue and that the tissue location of the implanted device has no significant effect on measured lactate level.

Two rats were used for lactate measurement at a high shock level and electrodes were implanted in the lower back regions. 3 ml blood was withdrawn over 11 min. MAP was approximately 120 mmHg prior to the haemorrhage and was approximately 60 mmHg after the haemorrhage for one rat (Figure 3.5a) while MAP fell from 100 mmHg to 40 mmHg for the other (Figure 3.5b). An obvious lactate level rise in tissue is observed, with absolute values, > 2 mM, however, lactate level rise in tissue was less marked than in blood, though the electrodes were not affected by significant drift.

Comparison of Figures 3.4 and 3.5 shows that haemorrhage causes lactate concentration rises in both blood and tissue, but that whilst tissue and blood are

similar for low shock, for high shock, the lactate concentration in blood increases to a greater extent than in tissue. This result is consistent with lactate in muscle interstitium being lower than that in blood after acute haemorrhage [74, 75]. A lactate rise in the arterial blood is likely to be due to both an increase in lactate entry and a decrease in removal. In haemorrhage of 33% of total blood volume, peak lactate was 7.2 mM, while 40% haemorrhage caused a peak lactate of 10.5 mM; notably, lactate levels in tissue fell short of this by ~ 50%. More experiments are needed to determine the physiological relevance of the observed inter-compartment differences under severe shock. Animals respond to blood loss by a parallel loss of tissue hydration, which could have compromised tissue transport of lactate but, if this was the problem, Open Microflow based tissue hydration would have corrected the mismatch. It is possible that during shock with reduced tissue perfusion and a parallel reduced O_2 supply, a very low pO_2 could have led to device under-responsiveness. However, notably, Open Microflow can supply O_2, so if O_2 is not a limiting factor, this raises the further possibility that lactate as an anion equilibrates less rapidly across the capillary / tissue barrier than glucose, and that a true tissue difference is being demonstrated here.

Ellmerer et al [90] measured lactate concentration in tissue and in blood and found that whilst lactate concentrations in both blood and tissue increased during exercise, tissue lactate change was less pronounced than in blood. There was also a delay in the lactate level increase in tissue compared to the lactate level increase in blood. This finding is similar to the study by the group, but the *ex vivo* assay of Ellmerer et al [90] utilising added buffer will not have been O_2 limited, again suggesting a true lactate compartmentalisation.

Calibration curves performed before and after *in vivo* experiments shown in Figure 3.6 assess electrode fouling *in vivo* suggest a minor effect on lactate sensitivity which for normal clinical monitoring purposes would be acceptable. The electrode was calibrated up to 3 mM because the subcutaneous lactate concentration was recorded as up to 3 mM as shown in Figures 3.4 and 3.5. The effect of biofouling would be to cause a reduction of effective diffusion coefficients through barrier membranes and a reduced response; we have modelled this phenomenon [36]. With a suitable mathematical model a true concentration related signal might be uncoupled from the biofouling effect.

For the studies of *in vitro* lactate transport in collagen, four initial parameters c_m, c_b, t_0 and D in Table 3.1, a Microsoft Excel spreadsheet were used to obtain a best fit between the simulated and experimental concentration profiles. The corresponding fitted parameters c_m, c_b, t_0 and D are also shown in Table 3.1. Good agreement between simulated and experimental curves was observed (Figure 3.8) which verified use of the bipartite expression. For Table 3.1, the standard deviation decreased from 0.06 to 0.019 for the best fit, obtained by iteratively fitting the data on the Microsoft Excel Solver. From this, the D value was assessed to be 3.54×10^{-6} cm^2/s from the original 4.3×10^{-6} cm^2/s. This gives a high degree of accuracy, but even the initial value only differs by 20%.

The lactate diffusion coefficient in aqueous solution is 5.62×10^{-6} cm^2/s [95], higher as expected than in tumours [93, 94]. The apparent lactate diffusion coefficient in collagen of 3.54×10^{-6} cm^2/s obtained here is intermediate between aqueous solution and in xenograft tumour (2.1×10^{-6} cm^2/s) [93], and glioma tumour (1.3×10^{-6} cm^2/s)

[94]. The diffusion coefficient for lactate in tissue according to these results are of the same order of magnitude as in water, and probably sufficient for reliable tissue monitoring (Figure 3.4). The loss of correlation for more extensive haemorrhage (Figure 3.5) suggests that anionic lactate may not exchange readily across the capillary membrane and that the surrounding connective tissue matrix is less important as a barrier. The dynamic simulation method is extendable to other metabolites in gels and to other geometric shapes, including those loaded with cells.

3.5 Conclusion

Enzyme needle electrodes were fabricated to measure lactate concentration *in vitro* and *in vivo*. The electrodes were stir independent and oxygen independent down to venous blood pO_2. The sensor *in vitro* performance, namely its response time and stability, make it a candidate for *in vivo* application.

In the group, needle electrodes were able to monitor changes continuously in tissue lactate at different haemorrhagic shock levels. It was found that at a low shock level, lactate concentration changes in blood and tissue were of similar magnitude. At a high shock level, lactate concentration in blood increased much more than lactate in tissue.

A simple formula was derived to estimate solute diffusion coefficient in a cylindrical matrix which was further refined through dynamic simulation to avoid noise contamination of the experimental data. It is believed that this is the first high precision measurement of the lactate diffusion coefficient in collagen by this approach.

Chapter 4 Bipartite Expressions for Diffusive Mass Transport in BioMembranes

Analytical expressions for solute diffusion through a membrane barrier for different initial and boundary conditions are available in literature. The three most common initial and boundary conditions are for a membrane without solute respectively: (1) immersed in a solution of constant concentration, (2) immersed in such a solution for one side but with the other side isolated and (3) immersed in such a solution for one side and with the other side kept at zero concentration. The physical quantities for the first two initial and boundary conditions are concentration and average concentration (the total solute entering the membrane), with amperometric current (flux) and solute that permeates through the membrane (charge passed) for the third initial and boundary condition. Expressions for these methods in literature are inconvenient for practical application because of the infinite mathematical series required. An investigation of the convergence of these expressions was therefore carried out. Simple but accurate bipartite expressions for these methods were constructed and provided theoretical support for studies on mass transport characterisation of bio-membranes. As a specific application, these expressions enabled a direct fit of the simulated observables to experimental values to obtain diffusion coefficients. For these initial and boundary conditions and corresponding physical quantities, simple one point methods for diffusion coefficient estimation are also suggested. These latter diffusion coefficients can be initial values for numerical fit methods.

4.1 Introduction

Solute transport is of fundamental relevance in a broad range of applied scientific areas, including the biomedical and pharmaceutical. Fundamental diffusive processes are of relevance to transport studies of metabolic, drug and signalling molecules in tissue culture and across natural tissue boundaries. Theoretical models have been developed in parallel with experimental monitoring techniques. Thus, Bashkatov et al. [48] determined diffusion coefficients of glucose and mannitol in human *dura mater* from time-dependent optical transmittance data, which resulted from local concentration evolution of glucose and mannitol. Gredell et al. [101] determined the diffusion coefficient of Propofol through rat brain tissue, where propofol concentration was measured by extraction and HPLC. More recently, Goteti et al. [102] determined the diffusion coefficient of dipyridamole in a thermo-sensitive polymer where dipyridamole concentration was measured using a fluorescence spectrophotometer. Mitchem et al. [7] delivered nitroglycerin through skin mimetic and monitored diffusion by photoacoustic spectroscopy (PAS) and attenuated total reflectance (ATR) spectroscopy. Akimoto et al. [103] determined the diffusion coefficient of indomethacin and antipyrine through rat abdominal skin with HPLC. We measured the diffusion coefficient of electrochemically active acetaminophen and catechol through mixed cellulose esters membranes using planar electrochemical electrodes [36].

The key approach in mass transfer characterisation is that a set boundary condition defines the concentration profiles and therefore changes, which in turn are accessible experimental techniques, either directly or indirectly [7, 36, 48, 101–103]. Concentration evolution in a membrane barrier can be calculated according to Fick's Second Law. By fitting computed concentration profiles or their derivatives to

experimental values, numerical quantities, diffusion coefficients, can be obtained. Three kinds of initial and boundary conditions are most commonly used for mass transport studies at membranes depending on the analytical solution used and the experimental set up. All, however, are based on concentration c as determined by Fick's Second Law as:

$$\frac{\partial c(x,t)}{\partial t} = D\frac{\partial^2 c(x,t)}{\partial x^2} \qquad 4.1$$

where D is the diffusion coefficient, cm^2/s; t is time, s; and x is the spatial coordinate, cm. The solutions to equation 4.1 for three kinds of initial and boundary conditions are analysed here, as follows:

(1) A membrane of thickness $2L$ without solute is immersed in solution with concentration c_0; mathematically, $c_1(-L < x < L, t = 0) = 0$ and $c_1(-L, t \geq 0) = c_1(L, t \geq 0) = c_0$. The solution to Fick's Second Law is given as [1, 68]:

$$\frac{c_1(x,t)}{c_0} = 1 - \frac{4}{\pi}\sum_{n=0}^{\infty}\frac{(-1)^n}{2n+1}\cos\left(\frac{(2n+1)\pi x}{2L}\right)\exp\left(-\frac{(2n+1)^2\pi^2 Dt}{4L^2}\right) \qquad 4.2$$

The integral of equation 4.2 over x gives another physical quantity, average concentration (total solute entering the membrane) as [1, 68]:

$$\frac{c_1(t)}{c_0} = 1 - \frac{8}{\pi^2}\sum_{n=0}^{\infty}\frac{1}{(2n+1)^2}\exp\left(-\frac{(2n+1)^2\pi^2 Dt}{4L^2}\right) \qquad 4.3$$

(2) A membrane of thickness L without solute, but one side is in contact with a solution with concentration c_0 and the other side is isolated; mathematically, $c_2(0 < x < L, 0) = 0$ and $\partial c_2(x,t)/\partial x|_{x = 0,\ t \geq 0} = 0$, $c_2(L, t \geq 0) = c_0$. The solution to Fick's Second Law is the same as for the first kind of initial and boundary condition, i.e.,

$c_2(x,t) = c_1(x,t)$, as would be expected from symmetry. Also, the average concentrations are equivalent, i.e., $c_2(t) = c_1(t)$.

(3) A membrane of thickness $2L$ without solute, where one side is in contact with a solution with concentration c_0 and the other side is kept at zero concentration; mathematically, $c_3(0 < x < 2L, 0) = 0$ and $c_2(0, t \geq 0) = c_0$, $c_3(2L, t \geq 0) = 0$. The solution to Fick's Second Law is given as (1, 68):

$$\frac{c_3(x,t)}{c_0} = 1 - \frac{x}{2L} - \frac{2}{\pi}\sum_{n=1}^{\infty}\frac{1}{n}\sin(\frac{n\pi x}{2L})\exp(-\frac{n^2\pi^2 Dt}{4L^2}) \qquad 4.4$$

The corresponding integral of equation 4.4 over x is half of the integral of equation 4.2 (equation 4.3), i.e., $c_3(t) = c_1(t)/2$.

Under the third initial and boundary condition, two derivative quantities of concentration, i.e., the first derivative of the concentration and an integral of the first derivative are used for practically characterizing solute mass transport. For a membrane covered electrochemical sensor [36], responding to a redox active solute, the amperometric current is proportional to solute flux, i.e., the first derivative of concentration to x, $\partial c_3(x,t)/\partial x|_{x=2L}$. The normalised amperometric current (normalised to steady state current, I_s) is given as [1, 36, 38]:

$$I_3 = 1 + 2\sum_{n=1}^{\infty}(-1)^n \exp(-\frac{n^2\pi^2 Dt}{4L^2}) \qquad 4.5$$

The integral of equation 4.5 over time gives the total charges passed as:

$$\frac{I_3 D}{4L^2} = \frac{Dt}{4L^2} - \frac{1}{6} - \frac{2}{\pi^2}\sum_{n=1}^{\infty}\frac{(-1)^n}{n^2}\exp(-\frac{n^2\pi^2 Dt}{4L^2}) \qquad 4.6$$

The total solute permeation through the membrane [103] has the same expression for the dimensionless transient part as the right side of equation 4.6.

A variety of experimental methods have been adopted based on the above theoretical models, i.e., equation 4.2, 4.3, 4.5 and 4.6 [7, 36, 48, 101–103]. Bashkatov et al. [48] calculated the time-dependent optical transmittance of human *dura mater* due to glucose and mannitol and compared this to experimental values to determine diffusion coefficients. They recognised that equation 4.3 was too complex for practical use and simplified it to:

$$c_1(t)/c_0 = 1 - \exp(-\pi^2 Dt/4L^2) \qquad 4.7$$

where the factor $8/\pi^2$ was omitted for keeping equation 4.7 valid at $t = 0$, i.e., $c_1(0) = 0$. Gredell et al. [101] compared the calculated concentration profiles using a mono-exponential function of equation 4.3 to link to the experimental data to determine the diffusion coefficient. They employed a mono- or bi-exponential function of equation 4.2 to calculate the concentration of propofol as a function of x and t. Goteti et al. [102] fitted equation 4.3 to experimental data to obtain an effective drug diffusion coefficient with special software. Mitchem et al. [7] calculated normalised PAS data for nitroglycerin measurement with an equation similar to equation 4.3 but with an integral over a smaller distance than membrane thickness, where they added together the first 100 terms of the equation. They also calculated ATR absorbance data using the first 100 terms of equation 4.2 at $x = 0$, subsequently fitting calculated data to experimental values to determine the diffusion coefficient. Akimoto et al. [103] fitted computed values from an equation with the same dimensionless transient part as the right side of equation 4.6 to experimental values to obtain diffusion coefficient values.

In previous work, an expression for the amperometric currents for small time values was given [1, 35, 36, 68] as:

$$I_3 = \frac{4L}{(\pi Dt)^{1/2}} \sum_{n=0}^{\infty} \exp\left(-\frac{(2n+1)^2 L^2}{Dt} \right) \quad 4.8$$

After an investigation of the convergence of equation 4.5 and 4.8, a simple bipartite expression for amperometric current was constructed as [35, 36]:

$$I_3 = 1 - 2\exp(-\pi^2 Dt / 4L^2) \text{ for } t \geq 0.2369(2L)^2/D,\ I_3 \geq 0.8072 \quad 4.9a$$

$$I_3 = 4L/(\pi Dt)^{1/2} \exp(-L^2 / Dt) \text{ for } t \leq 0.2369(2L)^2/D,\ I_3 \leq 0.8072 \quad 4.9b$$

Equation 4.9 was used to directly fit calculated currents to experimental values to more accurately determine the diffusion coefficient [36]. A preliminary value for the diffusion coefficient was estimated from $T = Dt_1/L^2 = 0.5$, i.e., when the transient current reaches 0.9856 of the steady state current. In this study, we selected a more suitable point to estimate the diffusion coefficient, also suitable for other methods.

Previous improper simplified expressions or expressions with infinite series have hindered reliable experimental data processing, so we analysed the convergence of equations 4.2, 4.3, 4.4, 4.6 and their complementary counterparts for small time values and then construct the corresponding bipartite expressions. These simple but accurate expressions are proposed here as a generalisable tool for reliable mass transport characterisation in membranes with the specific capability for determining diffusion coefficient by fitting simulated to experimental data.

4.2 Mathematical Analysis

Solute concentration under the first kind of initial and boundary condition, i.e., equation 4.2, is a function of two variables, x and t. Initially, equation 4.2 at $x = 0$ is analysed, and for a simplified mathematical analysis, dimensionless time $T = Dt/4L^2$ is introduced. Equation 4.2 at $x = 0$ is written as:

$$\frac{c_1(0,T)}{c_0} = 1 - \frac{4}{\pi}\sum_{n=0}^{\infty}\frac{(-1)^n}{2n+1}\exp[-(2n+1)^2\pi^2 T] \qquad 4.10$$

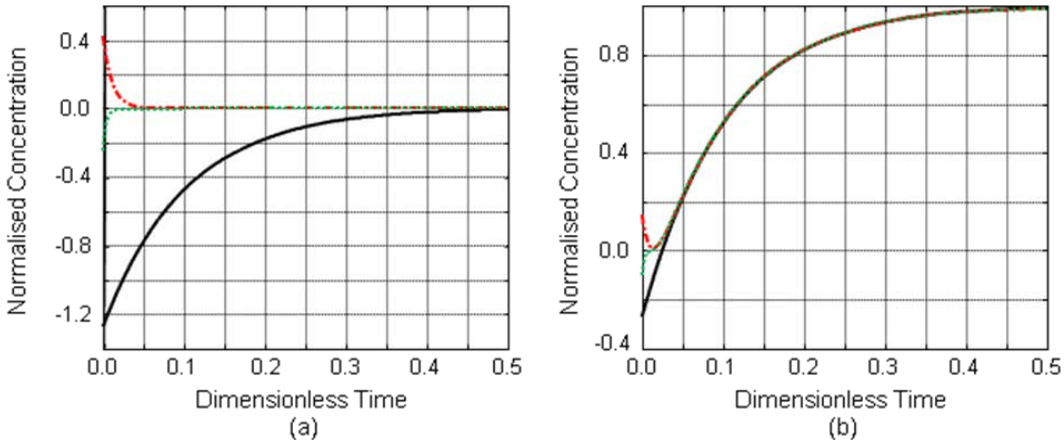

Figure 4.1 (a) Normalised concentration versus dimensionless time for terms of equation 4.10 in the text, corresponding to *n* equals to 0 (-), 1 (-·) and 2 (··) respectively; (b) normalised concentration versus dimensionless time for equation 4.10 in the text, with *n* limited to 0 (-), 1 (-·) and 2 (··) respectively [33].

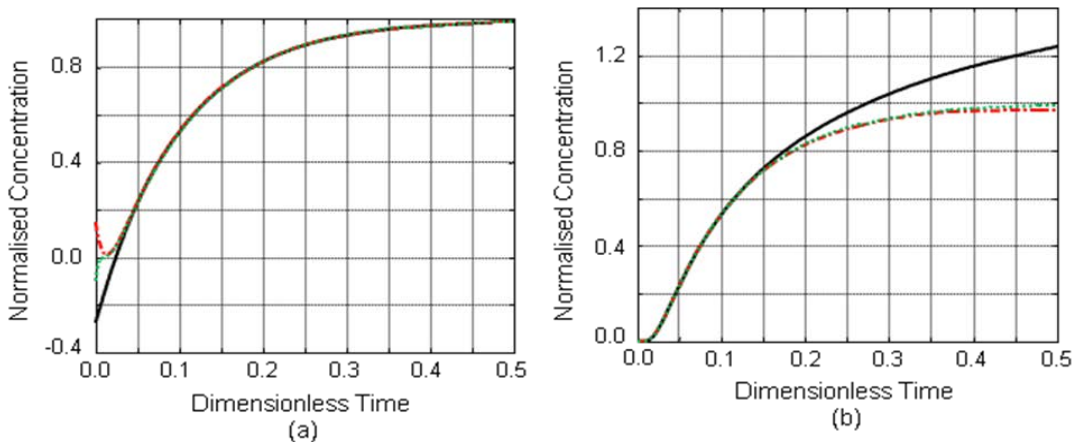

Figure 4.2 (a) Normalised concentration versus dimensionless time for terms of equation 4.12 in the text, corresponding to *n* equals to 0 (-), 1 (-·) and 2 (··) respectively; (b) normalised concentration versus dimensionless time for equation 4.12 in the text, with *n* limited to 0 (-), 1 (-·) and 2 (··) respectively [33].

The terms of equation 4.10 corresponding to n equals to 0, 1 and 2 are shown in Figure 4.1a. It can be seen from Figure. 4.1a that the absolute value of the term decreases with increasing n or T and this tendency is also true for $n > 2$. For $T > 0.06$, the terms with $n > 0$ become negligible. Equation 4.10 with n limited to 0, 1 and 2 are represented in Figure 4.1b for comparison. It can be seen that equation 4.10 with n limited to 0 can represent the whole solution to Fick's Second Law because the curves with different terms are overlapping for $T > 0.06$. In other words, equation 4.10 converges rapidly for large T, but slowly for small T, and it is therefore inappropriate to use equation 4.10 for numerical calculation for small T. Fortunately, a solution of equation 4.1 for small T is available as [1, 68]:

$$\frac{c_1(x,t)}{c_0} = \sum_{n=0}^{\infty}(-1)^n\left[\operatorname{erfc}\left(\frac{(2n+1)L-x}{2(Dt)^{1/2}}\right)+\operatorname{erfc}\left(\frac{(2n+1)L+x}{2(Dt)^{1/2}}\right)\right] \qquad 4.11$$

where erfc is the error function (10). At $x = 0$, equation 4.11 is written as:

$$\frac{c_1(0,T)}{c_0} = 2\sum_{n=0}^{\infty}(-1)^n\operatorname{erfc}\left(\frac{2n+1}{4T^{1/2}}\right) \qquad 4.12$$

The terms of equation 4.12 corresponding to n equals to 0, 1 and 2 are shown in Figure 4.2a. It can be seen from Figure 4.2a that the absolute value of the term of equation 4.12 increases with T increasing and decreases with n increasing; this tendency is also true for $n > 2$. Equation 4.12 with n limited to 0, 1 and 2 are shown in Figure 4.2b for comparison. For $T < 0.10$, the terms with $n > 0$ are negligible therefore the first term of equation 4.12 represents the whole solution as the curves with different terms overlap.

4.3 Results and Discussion

From the above analysis, it is possible to construct a solution function that combines the rapid convergent parts of equations 4.10 and 4.12. For a smooth connection, the two function curves are required to intersect and to have the same value or similar values for the first derivatives at the intersection point. After balancing accuracy *versus* complexity, a function was constructed as follows:

$$c_1(0,T)/c_0 = 1-(4/\pi)\exp(-\pi^2 T) \text{ for } T \geq 0.07958,\ c_1(0,T)/c_0 \geq 0.4199 \qquad 4.13a$$

$$c_1(0,T)/c_0 = 2\text{erfc}(1/4T^{1/2}) \text{ for } T \leq 0.07958,\ c_1(0,T)/c_0 \leq 0.4199 \qquad 4.13b$$

The rapid convergent parts of equation 4.10 and equation 4.12 overlap, and therefore a complete solution function, equation 4.13, can be constructed, with the expressions cut into fast and slow convergent parts respectively and the two fast convergent parts then joined to form a practical function for an entire time range. At the joint point (T = 0.07958), the absolute values of the terms of equation 4.10 corresponding to n equals to 0, 1, 2, 3 and 4, are 0.5805, 3.613×10^{-4}, 7.556×10^{-10}, 3.513×10^{-18} and 3.320×10^{-29}, respectively, which decreases dramatically with n increasing. This tendency is also true for $n > 4$. Therefore, the terms with $n > 0$ are negligible for $T > 0.07958$. At the joint point, the absolute values of the first five terms of equation 4.12 are 0.4202, 3.400×10^{-4}, 7.386×10^{-10}, 3.478×10^{-18} and 3.308×10^{-29}, respectively, which decreases dramatically with n increasing. This tendency is again also true for $n > 4$. The terms with $n > 0$ are negligible for $T < 0.07958$. Therefore, it is reasonable that only the term with n limited to 0 of equation 4.10 and the first term of equation 4.12 are sufficient to construct the full solution function, i.e., equation 4.13. From the values of equation 4.10 and equation 4.12 at the joint point, the maximum error of the properly simplified expression, i.e., equation 4.13 is less than 0.04%.

The diffusion coefficient can be estimated from time $t_{0.5}$ when concentration (equation 4.10 or equation 4.12) reaches half of the steady state value as:

$$D = 0.09469(2L)^2 / t_{0.5} \qquad 4.14$$

After the bipartite expression for concentration at $x = 0$, i.e., $c(0,t)$ is constructed, a bipartite expression for the concentration function, $c(x,t)$, can be constructed with the same accuracy and joint point as equation 4.13. The bipartite expression consists of equation 4.2 with n limited to 0 for $T \geq 0.07958$ and equation 4.11 with n limited to 1 for $T \leq 0.07958$. Because $\cos(x) \leq 1$, n is limited to 0 for equation 4.2 whereas n is limited to 1 for equation 4.11 because of a variable domain in the error function. Explicitly, the terms with absolute values larger than $\text{erfc}(3/4T^{1/2})$ are retained.

For average concentration defined by equation 4.3, a solution for small t is given as [1, 68]:

$$\frac{c_1(t)}{c_0} = \frac{2}{L}\left(\frac{Dt}{\pi}\right)^{1/2} + \frac{4(Dt)^{1/2}}{L}\sum_{n=1}^{\infty}(-1)^n \text{ierfc}\left(\frac{nL}{(Dt)^{1/2}}\right) \qquad 4.15$$

where ierfc(y) is the integral of the error function erfc(y) and $\text{ierfc}(y) = \exp(-y^2)/\pi^{1/2} - y\text{erfc}(y)$ [2]. Similarly a bipartite expression can be constructed as follows [43]:

$$c_1(T)/c_0 = 1 - (8/\pi^2)\exp(-\pi^2 T) \text{ for } T \geq 0.05326,\ c_1(T)/c_0 \geq 0.5200 \qquad 4.16a$$

$$c_1(T)/c_0 = 4(T/\pi)^{1/2} \text{ for } T \leq 0.05326,\ c_1(T)/c_0 \leq 0.5200 \qquad 4.16b$$

At the joint point ($T = 0.05326$), the absolute values of the terms of equation 4.3 corresponding to n equals 0, 1, 2, 3 and 4, are 0.4792, 7.942×10^{-4}, 6.362×10^{-8}, 1.078×10^{-13} and 3.228×10^{-21}, respectively. At the joint point, the absolute values of the terms of equation 4.15 corresponding to n equals 1, 2, 3, 4 and 5, are 7.946×10^{-4},

1.807×10^{-10}, 5.359×10^{-21}, 1.643×10^{-35} and 4.762×10^{-54}, respectively, which thus decreases dramatically with n increasing. From the values of equation 4.3 and equation 4.15 at the joint point, the maximum error of the final simplified expression, i.e., equation 4.16 is less than 0.08%.

For a one point method, the diffusion coefficient can, in principle, be relatively easily estimated from time $t_{0.5}$ when the average concentration (equation 4.3 or equation 4.15) reaches half of the steady state concentration [43] as:

$$D = 0.04918(2L)^2 / t_{0.5} \tag{4.17}$$

In the case of the concentration under the third kind of initial and boundary condition, i.e., equation 4.4, the complementary counterpart expression for small time values is given as:

$$\frac{c_3(x,t)}{c_0} = \sum_{n=0}^{\infty}\left[\operatorname{erfc}\left(\frac{4nL+x}{2(Dt)^{1/2}}\right) - \operatorname{erfc}\left(\frac{4(n+1)L-x}{2(Dt)^{1/2}}\right)\right] \tag{4.18}$$

By comparison of equation 4.2 with 4.4, and equation 4.11 with 4.18, respectively, it is found that $c_3(L,t) = c_1(0,t)/2$. A bipartite expression for $c_3(L,t)$ can be constructed as for $c_1(0,t)$ with the same joint point, terms used and accuracy. Subsequently, a bipartite expression for $c_3(x,t)$ can be constructed by combining equation 4.4 with n limited to 2 for $T \geq 0.07958$ and equation 4.18 with n limited to 0 for $T \leq 0.07958$. It should be pointed out that equation 4.4 with $n = 2$ is needed and equation 4.18 with only $n = 0$ is sufficient in the construction because of variable domains in the functions.

In our previous work, a bipartite expression for amperometric current was constructed [35, 36], there, the corresponding one point method can be improved. The diffusion coefficient can be determined from time $t_{0.5}$ when transient current (equation 4.5 or equation 4.8) reaches half of the steady state current as:

$$D = 0.1388(2L)^2 / t_{0.5} \qquad 4.19$$

Equation 4.19 provides a more direct and precise method of estimating the diffusion coefficient because the transient current curve is steeper at I_3 = 0.5 than at I_3 = 0.9856, therefore, the time when the current reaches half of the steady state current is likely to be more accurately estimated.

For the charge passed in the case of an electrochemical sensor used to monitor the flux of an electrochemically active compound (equation 4.6), the complementary counterpart expression of charge passed for small time values is given as [68]:

$$\frac{I_3 D}{4L^2} = \frac{2(Dt)^{1/2}}{L} \sum_{n=0}^{\infty} \text{ierfc}\left(\frac{(2n+1)L}{(Dt)^{1/2}} \right) \qquad 4.20$$

Similarly a bipartite expression can be constructed from equation 4.6 and 4.20 as

$$I_3 D/(4L^2) = T - 1/6 + (2/\pi^2)\exp(-\pi^2 T) \text{ for } T \geq 0.2369,\ I_3 D/(4L^2) \geq 0.08979 \qquad 4.21a$$

$$I_3 D/(4L^2) = 4T^{1/2}\text{ierfc}\left(1/2T^{1/2}\right) \text{ for } T \leq 0.2369,\ I_3 D/(4L^2) \leq 0.08979 \qquad 4.21b$$

At the joint point (T = 0.2369), the absolute values of the terms of equation 4.6 corresponding to n equals 1, 2, 3, 4 and 5, are 0.01956, 4.395×10^{-6}, 1.635×10^{-11}, 7.174×10^{-19}, and 3.335×10^{-28}, respectively. At the joint point, the first five terms of equation 4.20 are 0.08978, 3.788×10^{-6}, 6.678×10^{-14}, 3.604×10^{-25} and 4.757×10^{-40}, respectively. From the values of equation 4.6 and 4.20 at the joint point, the maximum error of the final simplified expression, i.e., equation 4.21 is 0.0004%.

Because of the lack of a steady state value for the charge passed (total solute permeated), there is another way to estimate the diffusion coefficient. If equation 4.6 is plotted, i.e., total charge versus time, the asymptotic line intersects the time axis at t_L, and the diffusion coefficient can then be estimated as [104]:

$$D = (2L)^2/(6t_L) \qquad 4.22$$

This is the well known time lag method and was first defined by Dynes [104]. The diffusion coefficient estimated from equation 4.22 can be refined by fitting equation 4.21 to the experimental data.

Above, various bipartite expressions are constructed and one point methods developed. By way of illustration, a bipartite expression is used to analyse previous work. Bashkatov et al. [48] used a simplified expression, equation 4.7, for averaged concentration, but this led to source error, the difference between equation 4.7 and 4.16 versus dimensionless time, as shown in Figure 4.3. According to the analysis of *dura mater* tissue samples used by Bashkatov et al. [48], $D = 1.31\times10^{-6}$ cm^2/s, $2L$ = 0.43 mm, 0.52 mm, 0.65 mm for mannitol, and $D = 1.63\times10^{-6}$ cm^2/s, $2L$ = 0.52 mm, 0.56 mm, 0.59 mm for glucose, the corresponding dimensionless times for t = 15 min measurement time, are: T = 0.64, 0.44, 0.28 for mannitol and T = 0.54, 0.47, 0.42 for glucose. The error distribution in Figure 4.3 shows that the maximum error is up to 14 %. The mean errors of equation 4.7 were obtained by averaging the curve in Figure 4.3 over 15 min (the corresponding dimensionless time is different in each case because of a different diffusion coefficient and tissue sample thickness) and the average error values are 2.8%, 4.0% and 6.0% for mannitol diffusion in 0.43 mm, 0.52 mm and 0.65 mm *dura mater*, and 3.3%, 3.8% and 4.2% for glucose diffusion in 0.52 mm, 0.56 mm and 0.59 mm *dura mater*. Membrane swelling was not taken into

account at the times the average errors of equation 4.7 were calculated. However, swelling of a tissue sample will increase tissue thickness and therefore will reduce the dimensionless time further to increase the average error (Figure 4.3) even further. The error in average concentration would have led to an error in calculated optical transmittance, which was therefore likely to be greater than the 1% suggested. These workers actually fitted calculated (transmittance) curves to a data range of experimental curves within one standard deviation, whereas conventionally for an experiment with such errors, the defined experimental value is considered to be precisely at the statistical mean value, not any free standard deviation data range around a mean. There is, thus, less reliability in the curve fitting method, particularly when, as reported, the mean transmittance value changes during two experiments were less than the standard deviation range for glucose and mannitol measurements. A more appropriate fitting approach would be to best fit the calculated optical transmittance with a bipartite expression (equation 4.16) for average concentration to the experimental mean values. Curve fitting here essentially involves a baseline shift or a curvature change to the calculated curve by iterative adjustment of the diffusion coefficient. The curves reported by Bashkatov et al. [48] can in fact be shifted and their curvature changed to improve the fit, providing more accurate diffusion coefficients with a best match to the observed data.

If instead of equation 4.7, a mono-exponential, equation 4.3 with $n = 0$ approximates equation 4.3, the maximum error (difference between equation 4.3 with $n = 0$ and equation 4.13) occurs at $t = 0$ as 18.9%. Thus, only the bipartite expression can provide a simple but accurate solution.

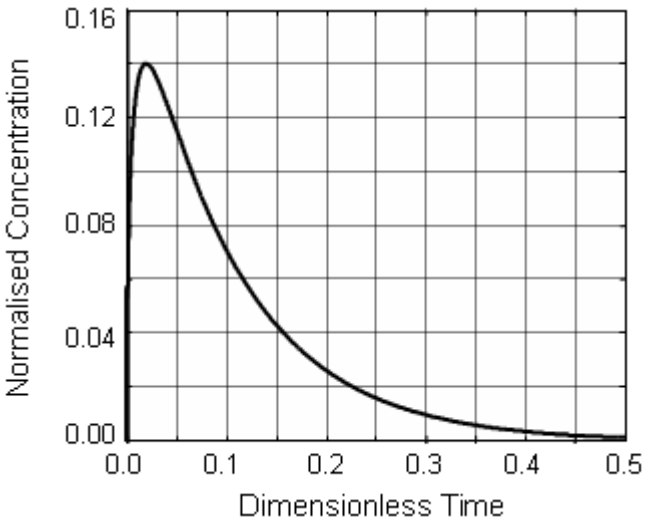

Figure 4.3 The error of equation 4.7 in the text *versus* dimensionless time, i.e., the difference between equation 4.7 and equation 4.16 in the text [33].

Mitchem et al. [7] used the first 100 terms of equation 4.10 to calculate the ATR absorbance data. The 101st term at $t = 0$ equals 0.006, and gives the order of the maximum error. Therefore, the accuracy of equation 4.10 summing the first 100 terms is still one order of magnitude lower than that of the bipartite equation as equation 4.13, so again, a bipartite expression is preferred.

4.4 Conclusion

For studies on diffusive mass transport through membrane barriers with initially no solute in the membrane, three kinds of boundary conditions are commonly used, in which one side of the membrane contacts a solution with constant solute concentration c_0 whereas the other contacts the same solution, is isolated or is kept at zero concentration. Accurate, but simple, bipartite expressions have been constructed for concentration and average concentration (total solute entering the membrane) for three boundary conditions, and amperometric current (flux) and charge passed (solute

permeated through the membrane) for the third boundary condition. The nature of the bipartite expression is that the slow convergent part of an expression is replaced by a fast convergent part of its complementary counterpart expression. So the expression is simple but accuracy is retained. The error of a bipartite expression can be estimated from the values of the original expression at its joint point. The term of the bipartite expression used was based upon a practical assumption of an accuracy of 0.1%. The accuracy of a bipartite expression can, in fact, be improved upon by increasing the number of terms. For an ideal system a bipartite expression and one point method are equivalent for diffusion coefficient determination. Because of experimental errors and theoretical approximation, a one point method, though simple, may contain greater errors. However, a one point method is suggested for an initial estimate of diffusion coefficient, which can be refined by a direct fit of the calculated observables to experimental data. The direct fit method with the bipartite expressions has general applications for mass transport studies in biophysical systems, where a one dimensional model is valid and helps to improve reliability in a measurement field notoriously susceptible to high experimental variability.

Chapter 5 Bipartite Expressions for Amperometric Currents of Recessed, Membrane Covered Planar and Hanging Mercury Drop Electrodes

An investigation of dynamic amperometric currents at recessed, membrane covered planar and hanging mercury drop electrodes has been conducted. Two expressions for current transients were found to have different convergent properties depending on the value of dimensionless time $T = Dt/L^2$, where D is the diffusion coefficient, t is time and L is the recess depth for a recessed electrode, the membrane thickness for a membrane covered electrode and the radius of the mercury drop for a hanging mercury drop electrode. A simple but accurate solution function was derived which consisted of the rapid convergent elements of these two expressions; this proved to be valid for the entire response time range allowing a dynamic simulation and a route to computing the diffusion coefficient of an electrochemically active solute through the diffusive barriers at the working electrode.

5.1 Introduction

Solute transport within bulk media or barrier layers is of great importance in a host of scientific and technical fields, not least in biology where solute flux at cells defines their metabolic behaviour. Electrochemical techniques have been used to study electrochemically active analyte diffusion through the use of voltage polarisation conditions where the rate of the electrode surface reaction is mass transfer controlled. Recently, experimental [105, 106] and numerical [107, 108] studies on recessed

electrodes have attracted great attention. Bond et al [109] derived expressions for normalised amperometric currents as:

$$I_{11} = (\pi T)^{-1/2} + 2(\pi T)^{-1/2} \sum_{m=1}^{\infty} \exp(-m^2 / T) \text{ for short time} \quad 5.1$$

$$I_{11} = 1 + 2 \sum_{m=1}^{\infty} \exp(-m^2 \pi^2 T) \text{ for long time} \quad 5.2$$

where dimensionless time $T = Dt/L^2$ is introduced for convenience, D is the diffusion coefficient, t is time and L is the recess depth. The amperometric current is normalised by a factor, $nFcDA/L$ for convenience, where n is the number of electrons in the electrode redox reaction, F is the Faraday constant, c is the bulk solute concentration and A is the working electrode surface area.

For recessed electrodes, solute transport in the recessed column is considered to follow the one dimensional Fick's model,

$$\frac{\partial c}{\partial t} = D \frac{\partial^2 c}{\partial x^2} \quad 5.3$$

where c is the solute concentration with the initial condition 1: $c(0 < x < L, t = 0) = c_0$ at the recess column and the boundary condition 1: $c(x = 0, t > 0) = 0$ at the inner surface and $c(x = L, t > 0) = c_0$ at the external surface, which provides the basis for derived current transients. The same one dimensional mass transfer model can be realised at a membrane covered planar electrode. Kralj and Dryfe [110], for example, applied expressions of transient amperometric currents for recessed electrodes to the membrane covered planar electrodes. The first study of membrane covered electrodes can probably be attributed to Bowers and Wilson [111], who presented expressions for transient amperometric currents under two initial conditions: (1) a membrane with initial solute $c(0 < x < L, t = 0) = c_0$ and (2) a membrane without initial solute $c(0 < x$

< L, t = 0) = 0 respectively when voltage was applied to the electrodes. Equations 5.1 and 5.2 are expressions for initial condition 1 and boundary condition 1. For initial condition 2 and boundary condition 1, the expressions for transient amperometric currents are:

$$I_{21} = 2(\pi T)^{-1/2} \sum_{m=0}^{\infty} \exp\left(-(m+1/2)^2/T\right) \text{ for short time} \quad 5.4$$

$$I_{21} = 1 + 2\sum_{m=1}^{\infty} (-1)^m \exp(-m^2\pi^2 T) \text{ for long time} \quad 5.5$$

A further boundary condition for a membrane covered electrode, boundary condition 2: $c(x = 0, t > 0) = 0$, $\partial c/\partial x(x = L, t > 0) = 0$, i.e. the external surface of the membrane was isolated, was reported [112] and used to study charge transport through ultrathin films [113]. The expressions for transient amperometric currents here were given as:

$$I_{12} = (\pi T)^{-1/2} + 2(\pi T)^{-1/2} \sum_{m=1}^{\infty} (-1)^m \exp(-m^2/T) \text{ for short time} \quad 5.6$$

$$I_{12} = 2\sum_{m=0}^{\infty} \exp(-(m+1/2)^2 \pi^2 T) \text{ for long time} \quad 5.7$$

Before further analysing expressions for recessed electrodes and membrane covered electrodes, hanging mercury drop electrodes are introduced because these electrodes can be defined by similar expressions as recessed electrodes. Hanging mercury drop electrodes are characteristically used in striping voltammetry, regarded as one of the most sensitive techniques for trace metal analysis [114, 115]. Kao and Chang [116] derived an expression for a normalised amperometric current for hanging mercury drop electrodes as:

$$I_2 = -1 + (\pi T)^{-1/2} + 2(\pi T)^{-1/2} \sum_{m=1}^{\infty} \exp(-m^2/T) \text{ for short time} \quad 5.8$$

which was used to determine diffusion coefficients for a series of metals in mercury [117]. Chovnyk and Vashchenko [118] derived an expression for a normalised transient amperometric current at a hanging mercury drop electrode as:

$$I_2 = 2\sum_{m=1}^{\infty}\exp(-m^2\pi^2 T) \text{ for long time} \qquad 5.9$$

used subsequently to determine the diffusion coefficients of cadmium, lead and zinc in mercury [118].

Equations 5.1, 5.2, 5.4–5.9 are expressed using infinite mathematical series and so, whilst mathematically satisfying, are not convenient for practical application; we therefore sought further analysis for practical application. This study was inspired by the recent work of Mahon and Oldham [13] on inlaid disc electrodes. For the specific case of inlaid disc electrodes, Aoki and Osteryoung [119] were the first to obtain two expressions in infinite series for both short and long time transient amperometeric currents, improved by Shoup and Szabo [120] soon after. Mahon and Oldham [13] recently suggested a simple but accurate bipartite expression for inlaid electrodes as:

$$I = \pi^{-1/2}T^{-1/2} + 1 + 0.5\pi^{-1/2}T^{1/2} - 0.12003T + 0.013273T^{3/2} \text{ for } T \le 1.281 \qquad 5.10a$$

$$I = 4\pi^{-1} + 8\pi^{-5/2}T^{-1/2} + 16\pi^{-9/2}(9^{-1}\pi^2 - 1)T^{-3/2} - 2.5664\times10^{-4}T^{-5/2} - 2.2312\times10^{-4}T^{-7/2} + 2.7628\times10^{-5}T^{-9/2} \text{ for } T \ge 1.281 \qquad 5.10b$$

In this work a comprehensive investigation of expressions for transient amperometric currents for recessed, membrane covered planar and hanging mercury drop electrodes is given. Mirroring our previous approach, simple, accurate bipartite expressions for these transient currents are then provided. The proposed bipartite expressions are operated for the entire time range and so are suitable for the simulation of electrochemical active solute transport through barriers.

5.2 Mathematical Analysis I

The normalised amperometric currents for recessed electrodes for the first term and the second term corresponding to *m* equals 1 and 2 of equation 5.1 are shown in Figure 5.1a.

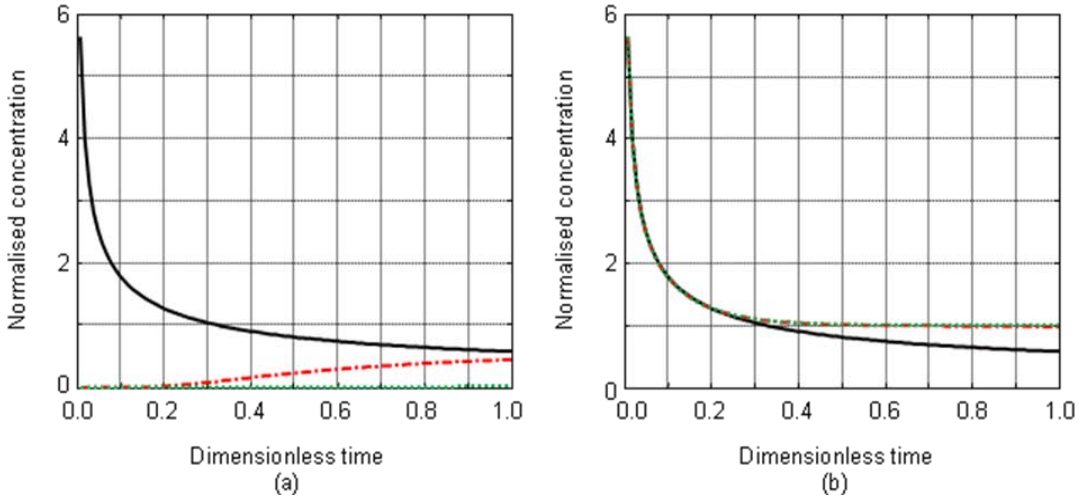

Figure 5.1 (a) For equation 5.1, normalised current against dimensionless time for the first term (-) and the second term corresponding to *m* equals 1 (-·) and 2 (··). (b) For equation 5.1, normalised current against dimensionless time limited to the first term (-) and the second term with *m* limited to 1(-·) and 2 (··) [34].

From Figure 5.1a, it can be seen that the second term with $m = 1$ is very small for $T < 0.15$ whereas the second term with $m = 2$ is very small (near zero) for $T < 0.80$. It can also be seen that the second term increases with T but decreases considerably with m. The corresponding profiles for equation 5.1 limited to the first term and including the second term with *m* limited to 1 and 2 are shown in Figure 5.1b for comparison. It can be seen that the convergence of equation 5.1 is rapid for small T, but slow for large T. For $T < 0.15$, the second term of equation 5.1 is negligible as shown in

Figure 5.1a and the first term represents well the complete solution as shown in Figure 5.1b where the curves of equation 5.1 limited to the first term and including the second term with *m* limited to 1 and 2 are virtually identical.

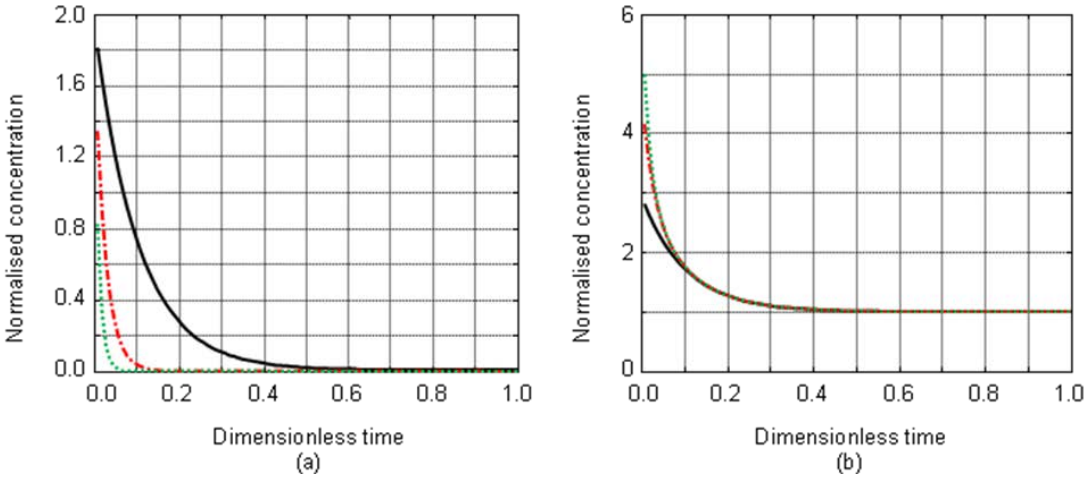

Figure 5.2 (a) For equation 5.2, normalised current against dimensionless time for terms corresponding to *m* equals 1 (-), 2 (-·) and 3 (··). (b) For equation 5.2, normalised current against dimensionless time for *m* limited to 1 (-), 2 (-·), and 3 (··) [34].

Equation 5.1 converged slowly for a long time, thus equation 5.2 was analysed. The terms corresponding to *m* equals 1, 2 and 3 of equation 5.2, respectively are shown in Figure 5.2a. It can be seen that the value of the term with $m = 2$ is very small for $T > 0.20$ and the term with $m = 3$ is very small for $T > 0.08$. The value of the second term in equation 5.2 thus decreases with both *m* and *T*. Equation 5.2 with *m* limited to 1, 2 and 3 are represented in Figure 5.2b for comparison. It can be seen that the convergence of equation 5.2 is rapid for large *T* and slow for a small *T*. For $T > 0.18$, the term with $m > 1$ is negligible as shown in Figure 5.2a and the first term alone

adequately represents the whole solution as shown in Figure 5.2b as the curves of equation 5.2 with *m* limited to 1, 2 and 3 overlap.

With analysis of the convergent properties of equations 5.1 and 5.2, an effort was made to construct a single solution function by combining the rapid convergent parts of equations 5.1 and 5.2. Both equations are solutions of the same differential equation and therefore these equations have the same values, as might be expected. As a suitable connection, it is expected to have both simplicity and accuracy. A bipartite expression for normalised amperometric currents was constructed as:

$$I_{11} = (\pi T)^{-1/2} \quad \text{for } T \le 0.1547 \qquad 5.11a$$

$$I_{11} = 1 + 2\exp(-\pi^2 T) \quad \text{for } T \ge 0.1547 \qquad 5.11b$$

When T = 0.1547, equations 5.11a and 5.11b give the same value I = 1.44. The maximum error of equation 5.11, which occurs at the joint point, is 0.0045.

For a higher accuracy the bipartite expression can be written as:

$$I_{11} = (\pi T)^{-1/2} + 2(\pi T)^{-1/2}\exp(-1/T) \quad \text{for } T \le 0.3183 \qquad 5.12a$$

$$I_{11} = 1 + 2\exp(-\pi^2 T) \quad \text{for } T \ge 0.3183 \qquad 5.12b$$

At the joint point T = 0.3183, equations 5.12a and 5.12b give the same value I = 1.0864. The first five values of the second terms of equation 5.1 are 0.086, 7.0×10^{-6}, 1.1×10^{-12}, 3.0×10^{-22} and 1.6×10^{-34}, respectively, which decrease dramatically with *m* increasing; the tendency is also true for $m > 5$. The second term of equation 5.1 is smaller than the corresponding values at the joint point as shown in Figure 5.1a therefore, the higher order terms of equation 5.1 are negligible for $T < 0.3183$. At the joint point, the first five values of the second term of equation 5.2 are 0.086, 7.0×10^{-6},

1.1×10^{-12}, 3.0×10^{-22} and 1.6×10^{-34}, respectively, which decreases very quickly with m increasing; again this tendency is true for $m > 5$, and for $T > 0.3183$, the second term of equation 5.2 is less than the corresponding values at the joint point. Therefore, the higher order terms of equation 5.2 are negligible. Overall, it is reasonable that equation 5.1 with m limited to 1 and equation 5.2 with m limited to 1 are used to construct the solution function. The maximum error of equation 5.12 occurs at the joint point and has a value of 7×10^{-6}, which is clearly sufficient for practical application.

Equation 5.12 is relatively simple and allows for simulating of experimental currents. For this purpose, an initial value for the diffusion coefficient can be estimated as:

$$D_{11} = 0.07958L^2 / t_2 = L^2 /(4\pi t_2) \qquad 5.13$$

where t_2 is the time when the normalised transient current reaches 2. It is interesting to point out that equation 5.11a has the form of the well known Cottrell equation [121], which means at short time periods, the Cottrell equation is sufficient to represent transient currents, as the second term of equation 5.12a is only 1.4×10^{-5} at $T = 0.07958$ ($I = 2$).

5.3 Mathematical Analysis II

The second terms of equation 5.5 corresponding to $m = 1, 2, 3$ and 4, respectively are shown in Figure 5.3a. It can be seen that the absolute value of any term with $m > 1$ is very small for $T > 0.18$, indeed, absolute values decrease with m increasing or T increasing. Equation 5.5 with m limited to 1, 2, 3 and 4 are represented in Figure 5.3b for comparison. It can be seen that convergence of equation 5.5 is rapid for large T and slow for small T. For $T > 0.18$, the term with m larger than 1 is negligible as

shown in Figure 5.3a, in other words, equation 5.5 with *m* limited to 1 adequately represents the whole solution as shown in Figure 5.4b, as the curves overlap. Because equation 5.5 converges slowly for small *T*, it does not have practical convenience for numerical calculation. Therefore, it is inappropriate for the early phase electrode response, and another solution is needed for small *T*.

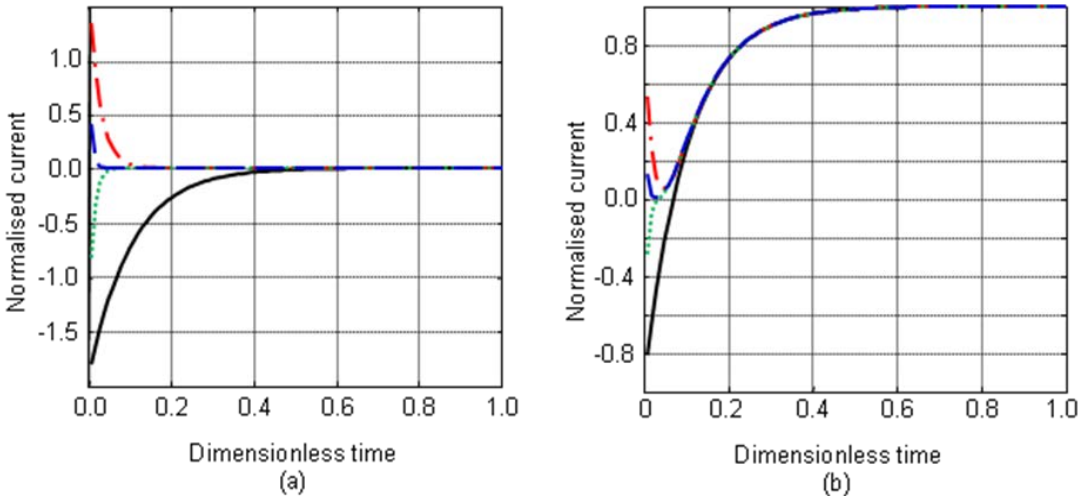

Figure 5.3 (a) Normalised current against dimensionless time for terms of equation 5.5, corresponding to *m* equals 1 (-), 2 (-·), 3 (··) and 4 (--). (b) Normalised current against dimensionless time for equation 5.5, with *m* limited to 1 (-), 2 (-·), 3 (··) and 4 (--) respectively [36].

The terms of equation 5.4 corresponding to *m* equals 0, 1, 2 and 3 are shown in Figure 5.4a. Here the terms with $m = 1, 2$ and 3 are very small for $T < 0.30$, the term value decreases with *m* increasing, and increases with *T*. The corresponding profiles for equation 5.4 with *m* limited to 0, 1, 2 and 3 are shown in Figure 5.4b. It can be seen that convergence of equation 5.4 is rapid for small *T*, but slow for large *T*. For $T <$ 0.30, the terms of equation 5.4 with *m* larger than 0, are negligible as shown in Figure

5.4a. Therefore, for $T < 0.30$, the first term represents the whole solution well as shown in Figure 5.4b where the curves are virtually identical.

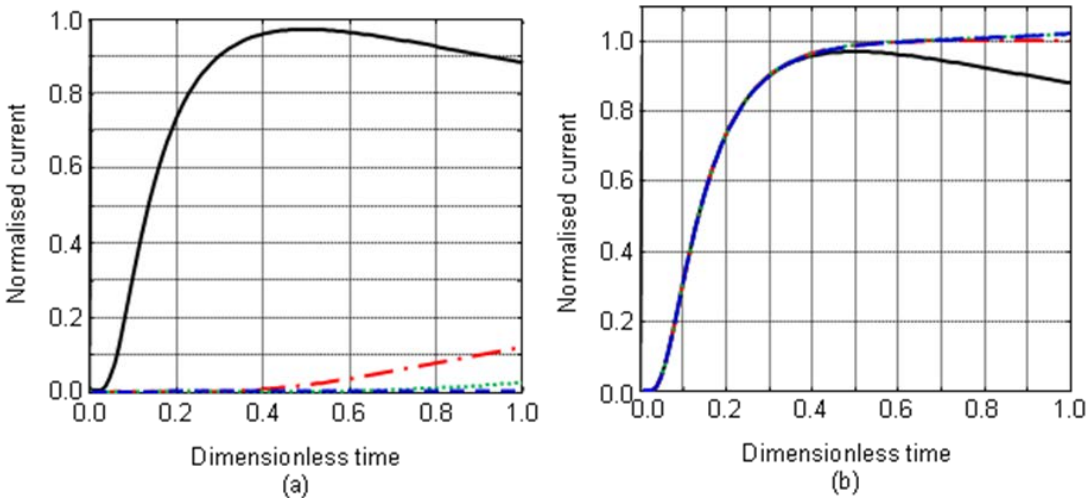

Figure 5.4 (a) Normalised current against dimensionless time for terms of equation 5.4, corresponding to *m* equals 0 (-), 1 (-·), 2 (··) and 3 (--). (b) Normalised current against dimensionless time for equation 5.4, with *m* limited to 0 (-), 1 (-·), 2 (··) and 3 (--) [36].

Through analysis of the convergent properties of equations 5.5 and 5.4, a solution function was constructed by combining the rapid convergent parts of equations 5.5 and 5.4, respectively. For a smooth connection, it would be expected that the two curves intersected and that they had the same or similar values for first derivatives at the intersection point. The rapid convergent domains of the two expressions in fact overlap and a simple bipartite expression for normalised amperometric current function *I* can be constructed by combining the rapid convergent parts:

$$I_{21} = 2(\pi T)^{-1/2} \exp\left(-1/(4T)\right) \text{ for } T \leq 0.2368 \qquad 5.14a$$

$$I_{21} = 1 - 2\exp(-\pi^2 T) \quad \text{for } T \geq 0.2368 \qquad 5.14b$$

These equations were used to determine the diffusion coefficients of acetaminophen and catechol through a mixed cellulose acetate membrane [36] and to analyse oxygen diffusion through a hydrogel layer [35] by a simulation, where the initial value for the diffusion coefficient was obtained from the time $t_{0.5}$ when the transient electrode current reached the half steady state:

$$D_{21} = 0.1388L^2 / t_{0.5} \qquad 5.15$$

From Figure 5.3a it can be seen that for terms of equation 5.5 corresponding to *m* equals 0, 1, 2 and 3, absolute values decrease with *T* and *m* increasing. At the joint point, *T* = 0.237, the first five absolute values of the second part of equation 5.5 decreases dramatically: 0.193, 1.73×10^{-4}, 1.44×10^{-9}, 1.12×10^{-16} and 8.03×10^{-26}. For *T* > 0.237, the same terms are smaller and so higher order terms become negligible. From Figure 5.4a it can be seen that for the terms of equation 5.4 corresponding to *m* equals 0, 1, 2 and 3, absolute values increase with *T* increasing and decrease with *m* increasing. At the joint point *T* = 0.237, the first five terms are 0.807, 1.75×10^{-4}, 1.08×10^{-7}, 8.17×10^{-12} and 7.46×10^{-17}, respectively, a sharp decrease with *m* increasing. For *T* < 0.237, these terms are again less than the values at the joint point, higher order terms are negligible. Thus, it is reasonable that for equation 5.5 *m* is limited to 1 and for equation 5.4 *m* is limited to 0, the solution function, equation 5.14, operates across the entire time range. When *T* = 0.2368, equations 5.14a and 5.14b give the same values *I* = 0.8072. The maximum error of the bipartite expressions to equations 5.4 or 5.5 is 1.7×10^{-4}, which satisfies practical applications.

Similarly, a bipartite expression can be constructed for equations 5.6 and 5.7 as

$$I_{12} = (\pi T)^{-1/2} - 2(\pi T)^{-1/2}\exp(-1/T) \quad \text{for } T \le 0.4278 \qquad 5.16a$$

$$I_{12} = 2\exp(-\pi^2 T/4) \quad \text{for } T \geq 0.4278 \qquad 5.16b$$

At T = 0.4278, equations 5.16a and 5.16b give the same values I = 0.6961. The maximum error of equation 5.16 at the joint point is 1.5×10^{-4}, which is also sufficient for practical application. If only the first term is used for equation 5.16a then at the joint point T = 0.2094 (I = 1.2121), the error of 0.04 is probably not of sufficient accuracy for application. Equation 5.13, however, is used to determine an initial diffusion coefficient for initial condition 1 and boundary condition 2 because in such a short time period the Cottrell formulation predominates at initial condition 1 and both boundary conditions 1 and 2.

When equations 5.8 and 5.9 and equations 5.1 and 5.2 are compared, it is found that the differences between equations 5.8 and 5.1, and 5.9 and 5.2 are 1. Bipartite expressions for hanging mercury drop electrodes are ready from the expressions for recessed electrodes under initial condition 1 and boundary condition 1, $I_2 = I_{11} - 1$. The similarity of these two electrodes comes from solute transport. Solute transport in a hanging mercury drop electrode follows Fick's Second Law as:

$$\frac{\partial(rc)}{\partial t} = D\frac{\partial^2(rc)}{\partial r^2} \qquad 5.17$$

where r is the radial coordinate with the initial condition: $rc(0 < r < L, t = 0) = rC$ in the mercury drop and the boundary condition: $rc(r = 0, t > 0) = 0$ at the centre of the mercury drop and $rc(r = L, t > 0) = 0$ at the external surface of the mercury drop, which provides the basis for derived current transients. The initial estimated diffusion coefficient at a hanging mercury drop electrode is obtained from equation 5.15 as:

$$D_2 = 0.07958L^2/t_1 = L^2/(4\pi t_1) \qquad 5.18$$

where t_1 is the time when the normalised transient current reaches 1.

5.4 Results and Discussion

Two main categories of electrochemical techniques can be used, notably the steady state and dynamic. For steady state methods, a single experimental response of an electrode, notably final current is used, but multiple experimental variables are needed for the computation of the diffusion coefficient; these are, notably, the number of electrons in the electrode redox reaction (n), working electrode surface area (A), bulk solute concentration (c) and the dimension of the barrier (L). Alternatively, for dynamic methods, a range of transient data is used but only the dimension of the barrier is required to calculate the diffusion coefficient. Because experimental values may be noise contaminated, the dynamic method would be expected to offer a greater accuracy than the steady state method. The use of simulation and best fit allows manipulation of the calculated current allowing its comparison with experimental current.

We have fitted simulated transient currents under initial condition 2 and boundary condition 1 to the experimental data by stretching and shifting the experimental current curve vertically and stretching and shifting the calculated current curve horizontally [36]. Similarly, for other initial and boundary conditions, the experimental current curve can be stretched and shifted vertically and a simulated curve stretched and shifted horizontally for a best fit and therefore D value. Because an experimental current value may be different from one experiment (e.g. nA) to the next (e.g. mA), comparison of normalised currents generally characterises the agreement between simulated to experimental data. It should be noted that the percentage error in barrier thickness doubles the percentage error in the diffusion coefficient.

5.5 Conclusion

An investigation of dynamic amperometric currents at recessed, membrane covered planar and hanging mercury drop electrodes has been made. A one dimensional mass transport model has been realised in these three kinds of electrodes. Solute transport through a planar sheet, a recessed column or a membrane, is governed by three common initial and boundary conditions. In this work, solute concentration was assumed to remain at zero at the inner surface in contact with the working electrode. Solute concentration at the external surface was held at constant concentration as the bulk solution with initial solute concentration in the planar sheet or zero. When the external surface of the membrane is isolated, the initial solute concentration in the planar sheet cannot be zero. It was shown that the normalised amperometric currents of hanging mercury drop electrodes are less than the normalised currents of recessed electrodes under initial condition 1 and boundary condition 1 by 1.

Solutions for the transient currents of these various types of electrodes have different expressions for short and long time. Convergence of these two expressions is also different, depending on the value of dimensionless time. However, for all, the rapid convergent parts of the equation pairs overlap to form a practical bipartite expression.

Chapter 6 Dynamic Simulation Method to Characterise Oxygen Transport in Hydrogel Membranes

Characterisation of solute transport through polymeric barrier materials is of great importance in designing many functional clinical devices where permeability is required *viz*. drug release system and haemodialysis / haemofiltration membranes. Recently, Compañ and co-workers [122] used an oxygen electrode to determine O_2 diffusion coefficient through hydrogel membranes that are used for contact lenses, because of the central importance of O_2 availability to the surface of the cornea. There were, however, significant errors in their calculated diffusion coefficients. Their results are represented for convenience using the original reported data (Figure 6.1 and Table 6.1).

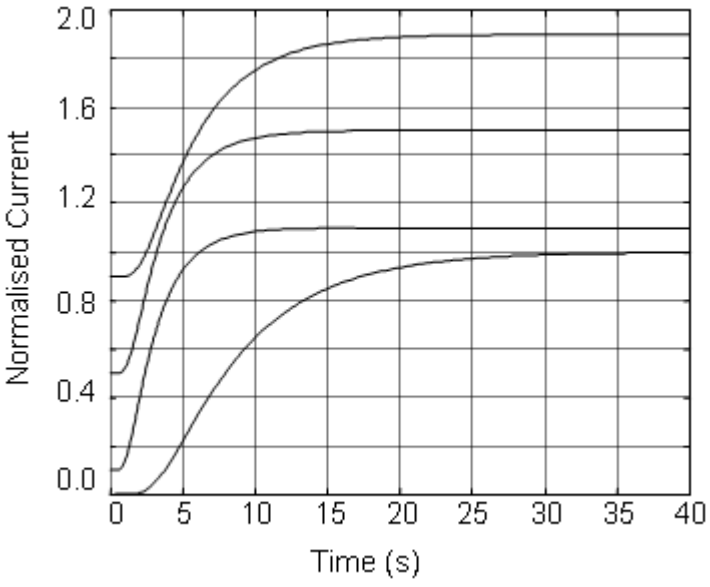

Figure 6.1 Simulated normalised amperometric current at 35°C for hydrogel with varying proportions in *x*EEMA (in the order of 0.90, 0.60, 0.50 and 0.25 for curves

from bottom to top) which are offset 0.1, 0.4 and 0.4 respectively for clarity. The corresponding parameters: diffusion coefficient (D = 2.31×10^{-6}, 5.53×10^{-6}, 6.74×10^{-6}, 15.2×10^{-6} cm^2/s) and membrane thickness (L = 115, 106, 125, 240 μm) are from ref 122 [35].

Table 6.1 Oxygen transport parameter and 2-ethoxyethyl methacrylate (EEMA) concentration for hydrogel at 35°C.

x_{EEMA}	L[a] μm	10^6D[a] cm^2/s	t_c[b] s	t_{e1}[a] s	t_{e2}[a] s	10^6D_{e1}[c] cm^2/s	10^6D_{e2}[c] cm^2/s
1.00	106	1.62	35	280	300	0.20	0.19
0.90	115	2.31	29	280	300	0.24	0.22
0.80	106	3.33	17	280	300	0.20	0.19
0.70	105	4.50	12	280	300	0.20	0.18
0.60	106	5.53	10	280	300	0.20	0.19
0.50	125	6.74	12	280	300	0.28	0.26
0.25	240	15.2	19	280	300	1.03	0.96

[a]Diffusion coefficient D, membrane thickness L, the time when the current reaches the steady state t_{e1}, t_{e2} values are from ref 122.

[b]$t_c = L^2/2D$ is the time when the current reaches steady state (T = 0.500, I = 0.9856).

[c]$D_{ei} = L^2/2t_{ei}$ calculated from the time when the current reaches steady state (T = 0.500, I = 0.9856) where i =1 and 2.

With the use of their core parameters: diffusion coefficient and membrane thickness, time to steady state current are computed by us to be between 10 and 35 s shown in Figure 6.1 and Table 6.1. However, the experimental values Compañ et al actually

obtained were between 280 and 300 s; there is an order of magnitude difference. Moreover, even with the incorporation of their times when current reaches steady state and their reported measured membrane thickness, diffusion coefficients by our computation are actually 0.18×10^{-6} to 1.03×10^{-6} cm^2/s, shown in Table 6.1 as against their reported values of 1.62×10^{-6} to 15.2×10^{-6} cm^2/s, a further computation deviation. In this chapter, a dynamic simulation method to accurately determine diffusion coefficients by a precise fit of the simulated transient current to the experimental currents is proposed.

At a membrane covered planar amperometric electrode, solute first diffuses down a concentration gradient through the membrane to be electrochemically consumed at the electrode, producing a current that depends on the concentration gradient at the electrode surface and therefore a mass transfer condition immediately adjacent to the electrode. Experimentally, electrochemically active solute can be considered to diffuse from solution ($x = L$) and be consumed at the electrode ($x = 0$), with L the thickness of the membrane. The boundary assumption is that the reaction is mass transfer and not kinetic limited and that concentration is zero at the electrode surface, applicable for polarising voltage above the solute redox potential, and employed for O_2 measurement [122]. Mathematically, diffusion in the membrane will follow Fick's Second Law as:

$$\frac{\partial c(x,t)}{\partial t} = D\frac{\partial^2 c(x,t)}{\partial x^2} \qquad 6.1$$

where D is diffusion coefficient, c is concentration, x is displacement and t is time. Initial and boundary conditions are: $c(0 \le x \le L, t < 0) = 0$; $c(x = 0, t \ge 0) = 0$ and $c(x = L, t \ge 0) = c_o$.

Three dimensionless quantities, for time ($T = Dt/L^2$), concentration ($C = c/c_0$) and displacement ($X = x/L$) can be introduced for convenience. Equation 6.1 can be solved as [1, 68]:

$$C = 1 = X - (2/\pi)\sum_{m=1}^{\infty}(1/m)\sin(m\pi X)\exp(-\pi^2 m^2 T) \qquad 6.2$$

where m is an integer. Under mass transfer limited mode, amperometric current is proportional to solute flux, i.e., the first derivative of concentration. By using a normalised amperometric current (normalised to final steady state current, $i_s = nFADkp_L/L$, where n is the number of electrons, F is the Faraday constant, A is the surface area of the electrode, k is the apparent solubility in the hydrogel, p_L is the O_2 partial pressure), for $X = 0$, I is given as [1, 68, 122]:

$$I = 1 + 2\sum_{m=1}^{\infty}(-1)^m \exp(-\pi^2 m^2 T) \qquad 6.3$$

Because equation 6.3 is an infinite series, it is not convenient for any practical calculation, therefore, current is integrated to give charge q_t, i.e. the quantity of oxygen transferred through the membrane as [1, 122]:

$$\frac{q_t D}{I_s L^2} = T - \frac{1}{6} - \frac{2}{\pi^2}\sum_{m=1}^{\infty}\frac{(-1)^m}{m^2}\exp(-\pi^2 m^2 T) \qquad 6.4$$

When T is sufficiently large, the exponential terms can be neglected and equation.6.4 simplifies to:

$$\frac{q_t D}{I_s L^2} = T - \frac{1}{6} \qquad 6.5$$

Compañ et al [122] determined their oxygen diffusion coefficients by rearranging equation 6.5 to $D = L^2 I_s/6(I_s t - q_t)$.

$$D = \frac{I_s L^2}{6(I_s t - q_t)} \qquad 6.6$$

Similar to the derivation of equation 6.3, a solution for equation 6.1 can be obtained for small T and a normalised current obtained as [1, 68]:

$$I = (2/\sqrt{\pi T})\sum_{m=0}^{\infty} \exp\left(-(m+1/2)^2/T\right) \qquad 6.7$$

By analysis of the convergent properties of equation 6.3 and equation 6.7, a simple expression for the normalised amperometric current can be constructed by combining the rapid convergence elements of equation 6.3 and equation 6.7, which was shown in equation 5.14. I in equation 6.7 is 0.9856 when $T = Dt_1/L^2 = 0.5$, so $D = L^2/(2t_1)$ can be estimated from the time where the normalised current reaches 0.9856.

For the method used by Compañ et al [122], experimental errors were not dealt with so there was significant error in the diffusion coefficients. This chapter presents a simple but accurate expression for transient current at planar electrodes bounded by mass controlling membranes. The dynamic simulation model developed here to simulate current transients allows a direct fit of the simulated current to the experimental data. The maximum experimental current I_m, baseline I_b, zero time t_0 and diffusion coefficient containing parameter D/L^2 have all been optimised to give a best fit. The experimental errors due to noise, baseline and zero time determination are minimised by this method. Thus the simple bipartite expression provides an easy way to verify the calculated diffusion coefficient. From Table 6.1, if the time when the current reaches the steady state shifts from just 280 to 300 s (7%), then the calculated diffusion coefficient changes 7%. A diffusion coefficient can instead be easily determined from the time when the current reaches the steady state.

Chapter 7 Bipartite Expressions for Transient Amperometric Currents at a Membrane Covered Planar Electrode to Characterise Solute Diffusion through a Membrane

A simple bipartite expression for transient amperometric currents at a membrane covered planar electrode has been derived. This expression, uniquely, applied across the entire measurement time frame and enabled rapid, full dynamic simulation of solute diffusion through the membrane. Hence rapid determination of effective diffusion coefficients through membranes for electrochemically active solutes was made by employing a simple curve fitting routine. Diffusion coefficients of acetaminophen through 0.05 and 0.025 μm pore size mixed cellulose esters membranes were determined to be 1.96×10^{-7} and 1.21×10^{-7} cm^2/s, respectively. For catechol the respective values were 1.55×10^{-7} and 1.15×10^{-7} cm^2/s, respectively. These diffusion coefficients decreased further after bovine serum albumin exposure and the change in effective coefficients provided a functional measure rather than the conventional structural measure of surface biofouling of relevance to sensors and membrane separation systems in biomedicine. This technique offered rapid assessment of biofouling.

7.1 Introduction

Solute transport within polymeric membranes has received significant attention in recent years since diffusive behaviour through such solid phases, whether natural, biopolymeric or synthetic can strongly influence the efficiency of reactive phases,

including, for example, for sensors [123]. In two key examples in medicine, oxygen transfer across the membrane in an artificial lung and across contact lens material affects clinical utility [124, 125]. Electrochemical methods, particularly amperometry have especially been used to characterise electrochemically active solute transport across membrane barriers [1, 122, 126–131]. McBreen et al [126] proposed a planar electrode for the amperometric detection of hydrogen transport through a metal membrane forty years ago, and more recently, Kimble et al [128] estimated the hydrogen diffusion coefficient through a propriety ion exchange membrane. For a refunctionalised fluoropolymeric membrane, Tarnowski et al [129] were similarly able to characterise oxygen transport; Compañ et al [122,130] characterised oxygen diffusion through silicone and hydrogel membranes; Kim et al [131] followed oxygen transport at a fluorinated ethylene propylene membrane barrier.

Commercial mixed cellulose ester membranes of defined pore sizes were used as model membrane structures to characterise the mass transport of acetaminophen and catechol as a fundamental study towards understanding diffusion resistance and biofouling, such an assessment has particular relevance to biosensors, where selective transport may be required, and where surface deposition of proteins and cells may distort response. Also in a particular application to engineering, fouling of mixed cellulose ester membranes by activated sludge was determined to be mainly caused by the formation of a cake layer on the membrane surface [132]. For the model solutes selected here, acetaminophen and catechol, diffusive transport is relevant to the pharmaceutical industry and clinical chemistry [133].

Two main categories of electrochemical techniques are generally used; steady state and dynamic [1]. For steady state methods, a single experimental response parameter, notably final current is used, but this requires multiple experimental variables, notably current, working electrode area, concentration, and membrane thickness, for final computation of the diffusion coefficient. Alternatively, for dynamic methods, a range of transient data is used though only the thickness of the membrane is required to calculate the diffusion coefficient.

For a membrane covered planar electrode system, solute diffusing through the membrane is electrochemically consumed and produces a current that depends simply on concentration gradients; importantly, only a single solution compartment is required. Theoretically, for membrane covered planar electrodes, electrochemically active solutes can be considered to diffuse from bulk solution ($x = 0$) through a membrane to be fully consumed at the electrode surface ($x = L$), where L is the thickness of the membrane, provided the polarising voltage is well above the redox potential of the solute. Assuming thus the electrochemical reaction is mass transfer limited and concentration at the electrode surface is zero, for a solution reservoir that is infinitely large, stirred solution concentration at the membrane surface will be constant. Mathematically, solute diffusion at the membrane then has a simple Fick's Second Law relationship:

$$\frac{\partial c}{\partial t} = D\frac{\partial^2 c}{\partial x^2} \qquad 7.1$$

where D is the diffusion coefficient, c is the concentration, x is the spatial coordinate and t is the time. The initial and boundary conditions are: $c(0 \le x \le L, t < 0) = 0$; $c(x = 0, t \ge 0) = c_0$ and $c(x = L, t \ge 0) = 0$.

Three dimensionless quantities, time $T = Dt/L^2$, concentration ($C = c/c_0$), and displacement $X = x/L$ can be used for convenience, and equation 7.1 is solved as [1, 68]:

$$C = 1 - X - (2/\pi)\sum_{m=1}^{\infty}(1/m)\sin(m\pi X)\exp(-\pi^2 m^2 T) \qquad 7.2$$

where m is an integer. Under mass transfer limited mode, amperometric current is proportional to solute flux, i.e. the first derivative of concentration. The corresponding transient amperometric current, normalised to the final steady state current $I_s = nFADc_0/L$ (n is the amount of electrons transferred, F is the Faraday constant and A is the effective area of the planar electrode), at $X = 1$ is given as [1]:

$$I = 1 + 2\sum_{m=1}^{\infty}(-1)^m \exp(-\pi^2 m^2 T) \qquad 7.3$$

Under a first order approximation, i.e. terms with $m > 1$ neglected, equation 7.3 simplifies to [126, 128]:

$$I = 1 - 2\exp(-\pi^2 T) \qquad 7.4$$

Equation 7.3 is an infinite series, and so is not practically convenient for calculation, therefore, current is integrated to give the total charge passed q_t as [1, 104]:

$$\frac{q_t D}{I_s L^2} = T - \frac{1}{6} - \frac{2}{\pi^2}\sum_{m=1}^{\infty}\frac{(-1)^m}{m^2}\exp(-\pi^2 m^2 T) \qquad 7.5$$

When T is sufficiently large, the exponential terms can be neglected and equation 7.5 simplifies to:

$$\frac{q_t D}{I_s L^2} = T - \frac{1}{6} \qquad 7.6$$

For the line, charge against time, the point where equation 7.6 intersects the time axis at $L^2/6D$, can be used to determine the diffusion coefficient, the time lag first reported by Daynes [104].

As with the derivation of equations 7.2 and 7.3, a solution to equation 7.1 can also be obtained for small T and corresponding normalised current obtained as [1]:

$$I = \frac{2}{\sqrt{\pi T}} \sum_{m=0}^{\infty} \exp\left(- \frac{(2m+1)^2}{4T} \right) \qquad 7.7$$

Under zero order approximation, i.e. the terms with $m > 0$ are set to zero, equation 7.7 simplifies to [126, 128]:

$$I = \frac{2}{\sqrt{\pi T}} \exp(\frac{-1}{4T}) \qquad 7.8$$

Yen and Shih [127] used the Laplace transformation method with approximation in the transformation to give a simpler expression as:

$$I = 1 - \exp(-6T) \qquad 7.9$$

McBreen et al [126] compared the curve of equation 7.8 for $T < 0.3$ and equation 7.4 for $T > 0.3$ against $\log(T)$ to a normalised experimental curve to determine $\log(D/L^2)$. This is an embryonic version of the bipartite expression for a membrane covered planar electrode. Recently Kimble et al [128] determined diffusion coefficients by fitting equations 7.4, 7.8 and 7.9, and numerical solutions to the observed current with a least square fit. The numerical solution was calculated in finite difference form [128]. They concluded that the numerical method provided the only accurate solution to equation 7.1. Tarnowski et al [8] used a variation of the expression of equation 7.4

with $\ln[(1-I)/2]=-\pi^2 Dt/L^2$ for $t > 1$ s to determine oxygen diffusion coefficients in membranes, while Compañ et al [130] fitted experimental data to a variation of equation 7.9 with $\ln[1/(1-I)]=6Dt/L^2$ to obtain oxygen diffusion coefficients. Kim et al [131] determined the oxygen diffusion coefficient with the established time lag method of equation 7.6. More recently Compañ et al [122] have determined oxygen diffusion coefficients in membranes by rearranging equation 7.6, i.e. $L^2 I_s/6(I_s t-q_t)$, possibly to reduce errors associated with equation 7.9.

For practical computation, equations 7.3 and 7.7 are not convenient because of the infinite terms involved. Mathematically, as T approaches 0, equation 7.3 jumps from 1 to -1, alternately with the addition of extra terms. Because the solution does not approach zero when T approaches zero the equation fails. When T approaches 0, equation 7.4 approaches -1 and so also fails. Experimentally, for T approaching infinity, normalised current approaches 1, but this then leads to equations 7.7 and 7.8 tending to zero so these equations fail, and equation 7.9 is only correct when T approaches 0, infinity and at one intermediate value [128]. None of the above expressions except the bipartite expression thus offers a description over the entire time range. Whilst the simple time lag method is reasonably accurate [131], indeed with perfect fit claimed, there remains method-dependent disparity between experimental and simulated currents.

This study evolved the above computation approaches by investigating expressions for current transients for membrane covered planar electrodes. The bipartite expression obtained worked for the entire time range as equation 5.14. The result is a practical, and self-contained, model that can give more accurate and reliable diffusion

coefficients. This expression with dynamic simulation was used for the determination of diffusion coefficients for acetaminophen and catechol through a complex membrane structure in both simple buffer solution and following bovine serum albumin exposure.

7.2 Experiment

The composition of the phosphate buffer was: di-sodium hydrogen phosphate (Na_2HPO_4) (BDH, Dorset, UK), 52.8 mM, 7.50 g/l; sodium di-hydrogen phosphate (NaH_2PO_4) (BDH, Dorset, UK), 15.6 mM, 1.87 g/l; sodium chloride (NaCl) (Sigma, Dorset, UK), 5.1 mM, 2.98 g/l. The salts were dissolved in 1 litre of distilled water with pH adjusted to 7.4 by drop-wise addition of concentrated sodium hydroxide solution (5 M NaOH (BDH, Dorset, UK)). 0.3024 g acetaminophen (Sigma, Dorset, UK) was dissolved in 20 ml buffer solution to prepare 0.1 M saturated stock solution. The final concentration used was 0.09 M because of the solubility limit of acetaminophen. 0.2202 g catechol (Sigma, Dorset, UK) was dissolved in 20 ml buffer solution to obtain 0.1 M stock solution. 8 g of bovine serum albumin (Sigma, Dorset, UK) was dissolved in 200 ml buffer solution to obtain 40 g/l BSA solution.

Experiments were carried out at room temperature (25±1 ºC). The model membranes studied were porous mixed cellulose esters (kind gift from Millipore, Hatters Lane, Watford, United Kingdom) placed over the platinum working electrode of a Rank cell (Rank Brothers Ltd, Bottisham, Cambridge, United Kingdom). The diameter of the working electrode disc was 2 mm. A MW-1032 platinum wire (Bioanalytical System Inc., Kenilworth, Warwickshire, United Kingdom) and a MF-2052 silver/silver chloride electrode (Bioanalytical System Inc., Kenilworth, Warwickshire, United

Kingdom) were used as counter and reference electrodes, respectively. The diameter of the counter electrode was 0.5 mm with a length of 75 mm. 5 ml buffer solution was put into the Rank cell and stirred with a MR 100 magnetic stirrer (Heidolph, Kelheim, Germany). For amperometric measurements, an AUTOLAB PGSTAT10 potentiostat instrument (Eco Chemie, Utrecht, Netherlands) was used following application voltage of +0.65V versus the reference electrode. After the current reached a steady base line, the electrochemically active diffusant, acetaminophen or catechol, was added to the solution in the Rank cell. For practical measurement of a planar diffusion profile, membrane thickness should be less than one tenth of effective membrane diameter, i.e. here a thickness < 200 μm is used to avoid edge effects [1]. Experiments were carried out for membranes with different nominal pore sizes of 0.05 and 0.025 μm and thickness of 105 μm. Measurements were taken in buffer solution with and without timed BSA exposure. A three-electrode cell arrangement was adopted except for the measurement of acetaminophen with 0.05 μm pore membrane in buffer solution. Where the measured maximum current is less than 2 μA, a two-electrode cell is sufficient [134].

For maintaining such current, acetaminophen consumption (~10^{-11} mol/s) is negligible compared to acetaminophen (~10^{-4} mol) in the Rank cell. Because the signal current (2 μA) is much less than the main line current (2 A), the recorded current may be affected by the environment. Two typical transient currents of acetaminophen and catechol are shown in Figure 7.3 with two extreme examples of experimental noise, which provided me with an opportunity to test whether our mathematical model works for noisy data.

7.3 Simulation and Best Fit

A theoretical current I of equation 5.14 is normalised, therefore it needs to be multiplied with a steady state current I_s in order to be compared with an experimental current. A simulated current also needs to be added onto a baseline I_b (background current), which always exists experimentally. In practice, it is more convenient and meaningful to scale the experimental data and to compare it with the normalised value. The experimental current I_e is divided by the maximum (steady state) current I_s to a normalised value I_{en} with subtraction of the baseline I_b as:

$$I_{en} = (I_e - I_b)/(I_s - I_b) \qquad 7.10$$

Theoretically the experiment can start exactly when the boundary condition changes. In practice, the boundary condition change takes time. After the solute is added into the Rank cell, time is required to form a homogeneous solution. The simulated current I_{sn} of equation 7.10 can be considered as:

$$I_{sn} = I((t - t_0)D / L^2) \qquad 7.11$$

where t_0 is the time of the increase of concentration in bulk solution.

Mathematically, I_s stretches or compresses the experimental current curve vertically; I_b shifts the overall experimental current curve vertically; t_0 shifts the calculated current curve horizontally; D/L^2 stretches or compresses the calculated current curve horizontally. In principle, a set of four parameters I_s, I_b, t_0 and D/L^2 can be adjusted to fit simulated curves to the experimental data.

The initial values for these four parameters I_s, I_b, t_0 and D/L^2 can be obtained in the following way. I_s, and I_b are obtained from the maximum and minimum of the

experimental values respectively; t_0 is estimated from when the experiment starts. $D/L^2 = 1/(2t_1)$ can be estimated from the time t_1 when the normalised current reaches 0.9856. D/L^2 is obtained from the optimization of the parameters I_s, I_b, t_0 and D/L^2, i.e. best fit of equation 7.11 to equation 7.10. The best fit procedure is to minimise the standard deviation value of the normalised current:

$$\sigma = \sqrt{\frac{1}{m-1}\sum (I_{en} - I_{sn})^2} \qquad 7.12$$

where m is the experimental point number and the summation is over all the experimental points. The standard deviation characterises the deviation between simulation and experiment. Experimental current values may differ from one experiment to another by orders of magnitude; therefore, standard deviation values of absolute current are not generally comparable so the standard deviation of normalised current is used. Nonlinear fitting can be carried out with commercial software or a numerical recipe. Here, manipulation of the model current and its comparison with experimental current was carried out with a Microsoft Excel spreadsheet.

For the initial experimental parameters, for catechol listed in Table 7.1, the best fit parameters were obtained. It can be seen from Table 7.1 that the standard deviation decreases from 0.08 to 0.008 following optimisation. Through best fit, D/L^2 changes from 8×10^{-4} s^{-1} to 9.220×10^{-4} s^{-1}. Thus, even without optimization of the transient response, the diffusion coefficient is close to the corrected value (< 15% difference). Once D/L^2 is obtained from the best fit, the diffusion coefficient is readily calculated as $(D/L^2)\times L^2$. In principle, one point of a current curve can determine the diffusion coefficient. In practice, noise always exists. Membrane swelling and electrode drift cause experimental current to depart from an ideal response. The effective diffusion

coefficients with BSA exposure are shown in Figure 7.1a for acetaminophen and Figure 7.1b for catechol.

Table 7.1 Parameters for catechol diffusion through a 0.025 μm mixed cellulose esters membrane after 6 hours of BSA exposure.

parameter	Unit	Initial	optimised
Maximum (I_s)	μA	1.1	1.151
Baseline ($I_b \times 10^2$)	μA	1.8	1.456
Initial time (t_0)	S	5	5.367
$D/L^2 \times 10^3$	s^{-1}	0.8	0.9220
Standard deviation σ		0.08	0.008

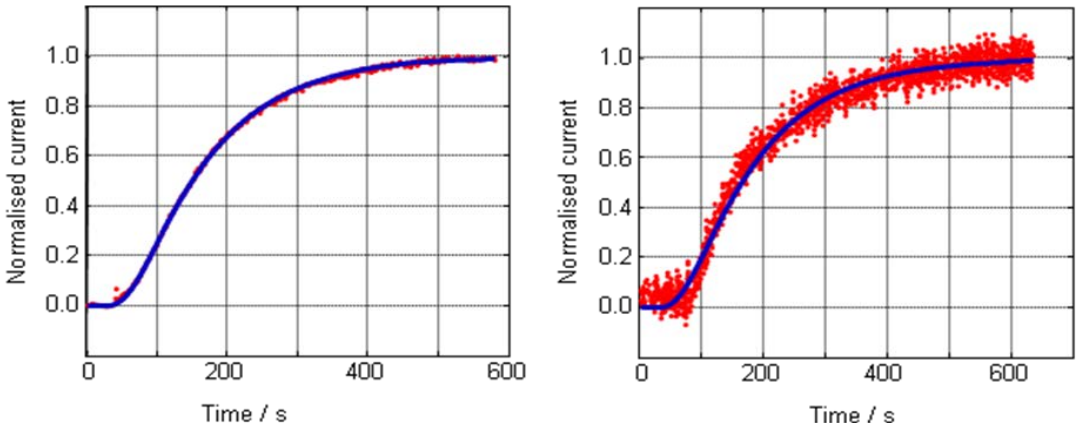

(a) (b)

Figure 7.1 (a) The normalised observed (··) and simulated (-) currents for catechol diffusion through 0.025 μm pore size mixed cellulose esters membrane after 5 hours of BSA exposure. The observed and simulated curves virtually overlap. (b) The normalised observed (··) and simulated (-) currents for acetaminophen diffusion through 0.05 μm pore size mixed cellulose esters membrane after 5 hours of BSA exposure [36].

7.4 Results and Discussion

The simulated curves (Figure 7.1) are seen to be nearly identical to the experimental curves, except for the background noise. This confirms the applicability of the bipartite expression. Kimble et al [128] compared their analytical solutions, i.e., equation 7.4 and equation 7.8 with the numerical solution, and found that equation 7.4 agreed with the numerical solution for $T > 0.12$, and equation 7.8 agreed with the numerical solution for $T < 0.4$, so different constructed expressions are required for different time domains.

A relative error of $\Delta L/L$ in membrane thickness here will lead to a relative error of $2\Delta L/L$ in the diffusion coefficient, but, with an extended time multi parameter fit, other significant errors are avoided. Because of its mathematical simplicity and straightforward applicability, the time lag alternative as a flexible technique is most commonly used in the characterisation of mass transport properties within membranes. This method fails, however, when permeability and flux are high, with diffusion coefficients overestimated [135]. For diffusion coefficient determination by the time lag method, time lag estimation leads to additional measurement uncertainty. The time lag error itself consists of two parts, the time lag calculation from curve fitting and the experimental determination of start time. Whilst curve fitting would be reasonably accurate, the error in start time determination would be more serious, and errors have been observed between experimental curves and simulated ones [131]. The computed curves started earlier than the experimental curves, i.e., the time lag value overestimated the actual value. Therefore, the diffusion coefficient is underestimated and simulated curves are less steep than the experimental curves. With the dynamic simulation method, the simulated curves can be right shifted and

compressed horizontally to fit the experimental curves better, and therefore accurate diffusion coefficients.

The bipartite expression was used to verify diffusion coefficients obtained from the other equation [35]. If diffusion coefficients are obtained by fitting equation 7.4 to experimental currents for $t > 1$ second [129], for $D = 1.2\times10^{-7}$ cm^2/s, $t = 1$ second and $L = 25.4$ and 50.8 μm, then $T = 0.0186$ and 0.00465, normalised currents of equation 7.4, $I = -0.66$ and -0.91 respectively whereas actual currents of equation 7.10 are 1.2×10^{-5} and 7.4×10^{-23} respectively. Again, equation 7.10 is the preferred option and is not only simple but offers a solution which adds considerable reliability to a parameter that is traditionally difficult to estimate reliably.

For acetaminophen, the diffusion coefficients through 0.05 and 0.025 μm pore size membranes in phosphate buffer are 1.96×10^{-7} and 1.21×10^{-7} cm^2/s, respectively. So available diffusion paths through the smaller pore size membrane are not reduced in proportion to pore size, this could be because pore density, tortuosity or connectivity was not equivalent. As might be expected both values are much smaller than those obtained through a macroporous chitosan hydrogel; $0.1 - 5\times10^{-4}$ cm^2/s [136]. Here the diffusion coefficients exhibited a strong dependence on pore size which was suggested to be due to ion complex formation between deprotonated acetaminophen and the chitosan [136]. Current values are, however, of the same order of magnitude as those reported through porous carbons; $0.5 - 5\times10^{-7}$ cm^2/s [137] presumably because of a similar reduction of available diffusion paths.

After exposure to BSA, diffusion coefficient values (Figure 7.2a) are reduced, with extended BSA exposure leading to further reduction. This is consistent with membrane surface fouling as would occur with any BSA exposed surface, but signifies also that the protein adsorbate poses a significant additional barrier to the transport of even a low molecule weight solute. It is likely to be due to mixed surfaces and some superficial intra-pore incorporation of albumin [132]. The different BSA exposure times used allowed an assessment of the dynamics of BSA adsorption; this shows a higher initial rate of deposition as assessed by the effective diffusion coefficient changes. The results are consistent with the work of Zhang et al [138] who demonstrated an initial period of rapid adsorption of BSA on a mixed cellulose ester membrane, followed by a slower approach to a limiting value [138].

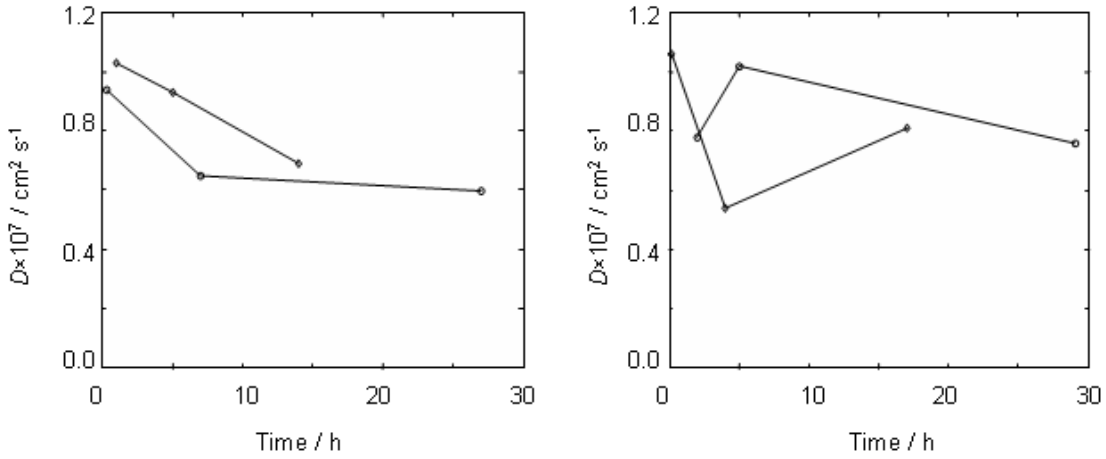

(a) (b)

Figure 7.2 (a) Diffusion coefficients of acetaminophen through 0.025 (○) and 0.05 (◊) μm pore diameter mixed cellulose esters membranes changes with BSA exposure time. (b) Diffusion coefficient of catechol through 0.025 (○) and 0.05 (◊) μm pore diameter mixed cellulose esters membranes changes with BSA exposure time [36].

For catechol transport, the diffusion coefficients in phosphate buffer decrease only from 1.55×10^{-7} to 1.15×10^{-7} cm^2/s for membrane pore sizes from 0.05 to 0.025 μm, so the reduced pore size has less relative effect than for acetaminophen, possibly because of some additional permeability of the less polar aromatic through the polymer matrix. However, both values are much smaller than the reported diffusion coefficient for catechol of 7.6×10^{-6} cm^2/s in solution as expected [133]. Whilst effective diffusion coefficients (Figure 7.2b) following BSA exposure are certainly further reduced, a consistent trend over time is not seen. This may reflect different permeability, partitioning or pore-wall interactions depending on the deposition profile of the BSA layer and its remodelling. Despite the similar molecular weights (molecular weight ratio of acetaminophen to catechol is 1.4:1.0), there is a substantial difference between acetaminophen and catechol diffusion coefficient evolutions with BSA exposure time, again suggesting different transport pathways and differences in diffusive activation energy [137].

7.5 Conclusion

A thorough investigation of the transient amperometric current of a planar disk electrode with an external mass controlling membrane has been made. A simple but complete bipartite expression has been derived which works for the entire time range, and facilitates measurement of permeability through film materials in general. Diffusion coefficients of acetaminophen and catechol through mixed cellulose esters membranes have been determined with and without BSA exposure.

Chapter 8 an Electrochemical Method for Measurement of Mass Transport in Polymer Membranes Using Acetaminophen as a Model System

An electrochemical approach has been used to model and measure acetaminophen transport through a microporous polycarbonate membrane. The dynamic response of a membrane covered planar electrode system was investigated to derive a simplified middle point formula, the time at which the amperometric current reaches its half steady state value, that provided reliable solute diffusion coefficients. Experimental values may be noise-contaminated; when this noise is significant, the diffusion coefficient by this method needs be refined. Here a direct simulation method with a bipartite mathematical expression for current transient was used, which fitted calculated current transients to experimental data. A best fit was reached by minimising the standard deviation between the simulated and experimental current profiles. Mathematically, the simulated curve was linear operated, i.e., shifted and stretched vertically, as well as shifted and stretched horizontally to coincide with the experimental curve. The single point formula, bipartite expression and simulation approach allowed the extraction of accurate diffusion values from a previously reported approximated method. The computation approach is not only valid for membrane covered electrodes, but is suitable for any experimental set up where a one dimensional Fickian diffusion model is valid.

8.1 Introduction

Acetaminophen (also 4-acetaminophenol, Paracetamol®) is an antipyretic analgesic, though with rather limited anti-inflammatory properties [139]. Because of its apparently innocuous character it is the most widely used over the counter drug. Acetaminophen is metabolized predominantly in the liver where it generates toxic metabolites, and overdose leads to major hepatic toxicity, in some cases associated with renal failure. Measurement of acetaminophen and its diffusion properties has value for both pharmaceutical processing and in medicine; moreover it is a useful electrochemical compound. Many methods such as titrimetry, chromatography, fluorometry, colorimetry and spectrophotometry have been used to detect acetaminophen, but electrochemical methods may be the most widely applied because of their high sensitivity, simplicity and reproducibility [140, 141].

Determination of molecular diffusion coefficients in tissue, and more generally, characterisation of solute transport through complex media is relevant to a broad range of scientific areas including controlled release drug delivery systems, membrane covered biosensors and sample separation systems. Basic diffusion coefficients of inorganic or organic compounds in aqueous solutions and organic solvents are readily available [142]. Diffusion is a process of solute transport in a specific medium so the value of a diffusion coefficient depends on both the solute and medium. When the value of a diffusion coefficient in a specific medium is sought, it is often unavailable or it cannot be directly applied to a given system because of differences in the measurement conditions where it was determined and applied [143].

In practice, the experimental determination of diffusion coefficients is a difficult task. Many techniques have been developed, and can be classified from different

perspectives. They can be categorised according to a solute monitoring method such as hydrodynamic voltammetry and optical light scattering, or they can be classified according to data collection and manipulation as either steady state or dynamic methods. Thus, a steady state method where the diffusion coefficient is determined by a single measurement, in the dynamic method, the diffusion coefficient is determined by fitting a whole concentration (or its derivative) profile to the experimental data.

For a membrane covered electrode in the steady state method, a final steady state current $I_s = nFADC_0/L$ (n is the amount of electrons transferred, F is the Faraday constant and A is the effective area of the planar electrode) is used as a single experimental response parameter. However, this requires the inclusion of multiple experimental variables, notably current, electrons transferred, working electrode area, concentration, and membrane thickness, for computation of the diffusion coefficient. Even electrons transferred may not be in ideal compliance with the theory. For example, due to complex electrochemical pathways related to oxygen reduction, Hahn [144] pointed out that the number of electrons, n, involved in molecular oxygen reduction can vary between $2 \leq n \leq 4$. Winlove et al [145] gave more precise values for electrons involved as 2.8±0.4 in his electrode system. Alternatively, for dynamic methods, whilst a range of transient data is required, only the thickness of the membrane is necessary to calculate the diffusion coefficient.

By means of a dynamic method, nitroglycerin diffusion coefficients through skin analogues have been determined [7], and in a materials study, oxygen diffusion through a membrane polymer has been determined by amperometry [130, 146]. The latter study established oxygen diffusion coefficient values from electrochemical

current transients for a polymer based on the original method of Yen and Shih [127]. Here, essentially, a single set of boundary conditions were used to provide a simple solution to Fick's Second Law for a planar membrane barrier. However, there was significant uncertainty in estimated diffusion coefficients by this approach because of an indirect experimental fit of an approximate and simplified equation.

We have previously constructed bipartite expressions as equation 5.14 [35] and derived a middle point formula (response at half maximum) [34] for amperometric currents at membrane covered electrodes. Such expressions provided to be highly reliable for membranes while being relatively simple to apply [36]. In this study, we use the middle point formula to specifically determine diffusion coefficients for acetaminophen through porous polycarbonate membranes. The estimated value is refined by fitting a simulated current transient to the experimental profile. In this study we analyse a four parameter fit and uncover the mathematical nature of the best fit method. We also compare an earlier model of Yen and Shih [127] as equation 8.1 and equation 5.14, and discuss its requirement for further refinement.

$$I = 1 - \exp(-6T) \qquad 8.1$$

Experiments were carried out like the one in chapter 7, except a 0.22 μm pore diameter polycarbonate membrane (Millipore, Hatters Lane, Watford, United Kingdom) with thickness of 0.021 mm was used here.

8.2 Simulation and best fit

A typical transient current response to a step change in acetaminophen concentration in the bulk solution is shown in Figure 8.1.

In principle, the corresponding amperometric current (equation 5.14) can be obtained as:

$$I_{ca} = I_s I\big(D(t - t_0)\big) + I_b \qquad 8.2$$

where I_b is the baseline current which experimentally can be of variable magnitude and t_0 is the time when the boundary condition changed. Parameters I_s, I_b, t_0 and $t_{0.5}$ are obtained directly from experiment and D is obtained from equation 5.15. The D value can be refined by fitting the simulated curve from equation 8.2 to experimental data, which is particularly necessary when the experimental errors are significant. In fact, the D value obtained from equation 5.15 is the same as from the best fit, provided the experimental error is negligible. On the other hand, it is precisely because of finite experimental errors, that the parameters I_s, I_b, t_0 and $t_{0.5}$ cannot be obtained precisely from experimental data, and a four parameter (I_s, I_b, t_0 and D) fit is needed, i.e., fitting the simulated curve as equation 8.2 to experimental data by iterative adjustment of I_s, I_b, t_0 and D.

For the four parameter fit, the simulated current curve is a linear function of I_s and I_b, and a nonlinear function of t_0 and D. Mathematically, it can be seen from equation 8.2 that I_s stretches the simulated curve and I_b shifts the curve vertically along the current axis. Also, t_0 shifts the curve and D stretches the simulated curves horizontally along the time axis. In principle, the simulated curves can be fitted to experimental data through linear operations, (stretched vertically and horizontally, and shifted vertically and horizontally) which is the mathematical base for a global minimisation in a four parameter fit. Even if the simulated currents are considered as a linear function of I_s and I_b, and a nonlinear function of t_0 and D, a global minimisation can still be reached through proper preparation of the initial parameters.

The initial values for these four parameters (I_s, I_b, t_0 and D) can be obtained in the following way. I_s and I_b are estimated from the steady state and baseline values of the experimental currents; t_0 is estimated from the start of the experiment; D is estimated from equation 5.15 and refined by a four parameter fit. With use of the bipartite expression, the best fit can easily be carried out with a Microsoft Excel Solver. Hence, global minimisation is ensured and local minimisation is avoided by simple visual comparison of simulated to experimental curve as shown in Figure 8.1.

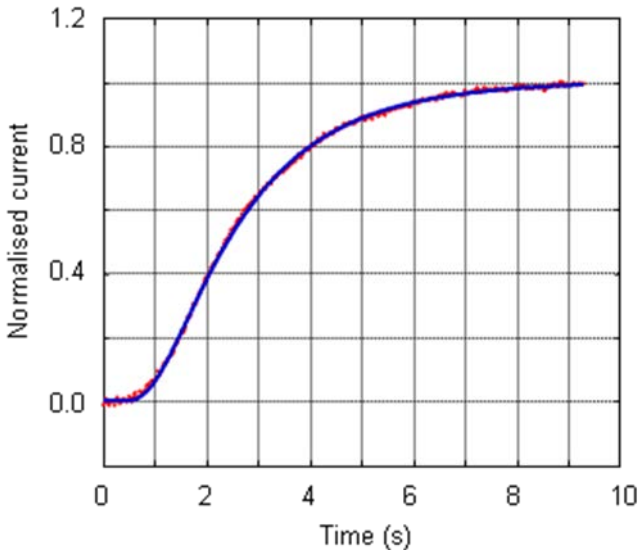

Figure 8.1 The normalised observed (··) and simulated (-) transient currents for acetaminophen diffusion through a 0.22 μm pore size polycarbonate membrane [37].

In practice, experimental values change from one experiment to another, so our fit of normalised simulated current to experimental data is realised through an experimental curve stretched (normalisation) and shifted vertically, and a simulated curve stretched (D value) and shifted horizontally. First an experimental current, I_e, is normalised by the steady state current, I_s, with subtraction of the baseline current I_b then:

$$I_{en} = (I_e - I_b)/(I_s - I_b) \qquad 8.3$$

The calculated current (equation 5.15) is then considered as:

$$I_{sn} = I\left(D(t - t_0)\right) \qquad 8.4$$

The key to the best fit procedure is minimisation of the standard deviation value of normalised current:

$$\sigma = \sqrt{\frac{1}{m-1}\sum (I_{en} - I_{sn})^2} \qquad 8.5$$

where m is the experimental point number. A typical fit of acetaminophen diffusion through a polycarbonate membrane is shown in Table 8.1.

Table 8.1 Parameters for acetaminophen diffusion through a 0.22 μm polycarbonate membrane in phosphate buffer solution.

Parameter	Unit	Initial	Optimised
Steady state current (I_s)	μA	2	1.986
Baseline current ($I_b \times 10^2$)	μA	3	2.831
Initial time (t_0)	s	0	0.01558
$D/L^2 \times 10^3$	s^{-1}	0.06	0.05758
Standard deviation σ		0.02	0.008

8.3 Results and Discussion

Electrochemical oxidation of acetaminophen is pH dependent [147]. In our experiment, at pH 7.4, acetaminophen is oxidised to *N*-acetyl-*p*-quinoneimine [147]. The number of electrons involved in the oxidation of acetaminophen has been reported to be 2.1±0.1 [147] and 1.899 [148]. So preferably a dynamic method is

used to determine the diffusion coefficient to avoid the parameter, *n*, i.e., the electrons transferred in the redox reaction.

Multiple measurements of the diffusion coefficients of acetaminophen were made through 0.22 μm pore diameter polycarbonate membranes with a porosity of 5-20%. The values obtained for the same membrane were 2.5, 2.2, 3.6, 3.6, 2.2 and 2.2×10^{-7} cm^2/s, respectively, which were in fact of the same order of magnitude as those reported through porous carbon; $0.8–4.4\times10^{-7}$ cm^2/s [137]. Compared with acetaminophen diffusion coefficients in 1.5% (w/v) pectin gels as 5.8×10^{-6} cm^2/s [149], acetaminophen diffusion coefficients in polycarbonate membranes decreased based on pore diameter and the pore density range specified by the manufacturer, overall membrane porosity would be 5–20%. If acetaminophen diffusion in pectin gel is similar to that in water, then the diffusion coefficients measured in our study are not accounted for by porosity effects alone. This could be because of wall interaction through the polycarbonate pores or simply a mismatch in the methods used, again underlying the difficulties of reliable diffusion coefficient measurement. Here, however, we provide a simple technique for reliable diffusion coefficient measurement. When the transient current reaches half its maximum at 2.4 s, the D/L^2 value can be estimated as 0.06 s^{-1} as shown in Table 8.1 which shows < 5% difference from the value by an optimised method, so even a simple one point method can offer a reliable estimate. This is not surprising, since the middle point obtained is the same as for a best fit where experimental noise (error) is negligible. The diffusion coefficient can also be estimated from the time when the normalised current reaches 0.9856 [36], i.e. at transient current $I = 0.9856$, $T = Dt_1/L^2 = 0.5$, so $D = L^2/(2t_1)$. However, $I = 0.5$, $T = Dt_{0.5}/L^2 = 0.1388$, so $D = 0.1388L^2/t_{0.5}$ provides the more precise method for

a diffusion coefficient because the transient current curve is steeper at (T = 0.1388, I = 0.5) than at (T = 0.5, I = 0.9856) as shown in Figure 8.1, though, a maximum slope of 5.9 occurs at (T = 0.09175, I = 0.24), with a slope of 4.7 at (T = 0.1388, I = 0.5) and a slope of 0.14 at (T = 0.5, I = 0.9856). There is a need for balancing accuracy with the inconvenience of a measurement; the middle point would be seen acceptable.

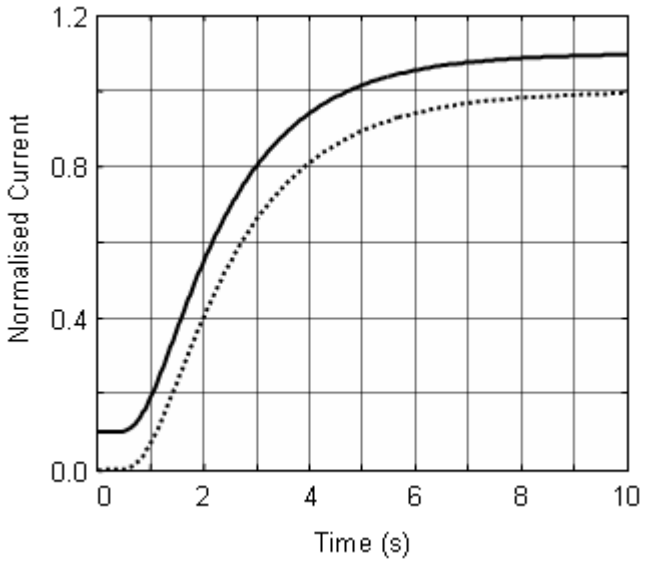

Figure 8.2 Simulated normalised current for an experimental setup of three moistened paper layers above the G0 (··) and G4 (-) membranes which is offset 0.1 for clarity. The corresponding parameters: diffusion coefficient (D = 10.1×10^{-6}, 12.6×10^{-6} cm^2/s) and membrane thickness (L = 0.13, 0.14 mm) are from ref 130 [37].

The results shown in Figure 8.2 and Table 8.2, using the parameters reported by Compañ et al [130], notably diffusion coefficient and membrane thickness, give times for the electrode steady state current by our method as 8 to 10 s, shown in Figure 8.2 and Table 2, whereas the actual experimental values reported by Compañ [130] were 30 to 40 min, a two orders of magnitude difference. With the incorporation of these original times to the steady state current, the diffusion coefficients we obtained by our

method were 0.035×10^{-6} to 0.063×10^{-6} cm^2/s (Table 8.2) against the reported values 10.1×10^{-6} to 12.6×10^{-6} cm^2/s [130], a major computation deviation therefore from the original method.

Table 8.2 Oxygen transport parameter for different silicone networks (Compañ et al [130]).

Network	L[a]	10^6D[a]	t_c[b]	t_{e1}[a]	t_{e2}[a]	10^6D_{e1}[c]	10^6D_{e2}[c]
	mm	cm^2/s	s	s	s	cm^2/s	cm^2/s
G0	0.13	10.1	8.4	1800	2400	0.047	0.035
G1	0.13	10.9	7.6	1800	2400	0.046	0.035
G2	0.15	11.4	9.9	1800	2400	0.063	0.047
G3	0.14	12.3	8.3	1800	2400	0.057	0.043
G4	0.14	12.6	7.6	1800	2400	0.053	0.040

[a]Diffusion coefficient D, membrane thickness L, the time, when the current reaches the steady state ranged between t_{e1} and t_{e2} are values from ref 130. The membrane thickness (L) was obtained from the transmissibility and permeability coefficient.

[b]$t_c = L^2/(2D)$ is the time when the current reaches the steady state ($T = 0.5$, $I = 0.9856$) by using the reported diffusion coefficient and membrane thickness value of ref 130.

[c]$D_{ei} = L^2/2t_{ei}$ calculated by using the reported time [9] when the current reaches the steady state ($T = 0.5$, $I = 0.9856$) where i =1 and 2.

In another study, Guzmán et al [146] determined oxygen diffusion coefficients through tetraethyleneglycol acrylate polymer at 25 °C as 11.5×10^{-6} cm^2/s. From the time reported to reach a steady state (400 s) [146], the membrane thickness would be estimated as $L = (2t_cD)^{0.5} = (2\times400\times11.5\times10^{-6})^{0.5} = 0.096$ cm. However, the

membrane was considerably thinner, being mounted in a gap of only 0.0375 cm between a cathode and anode [146]. The diffusion coefficient again seems to have been overestimated by at least one order of magnitude.

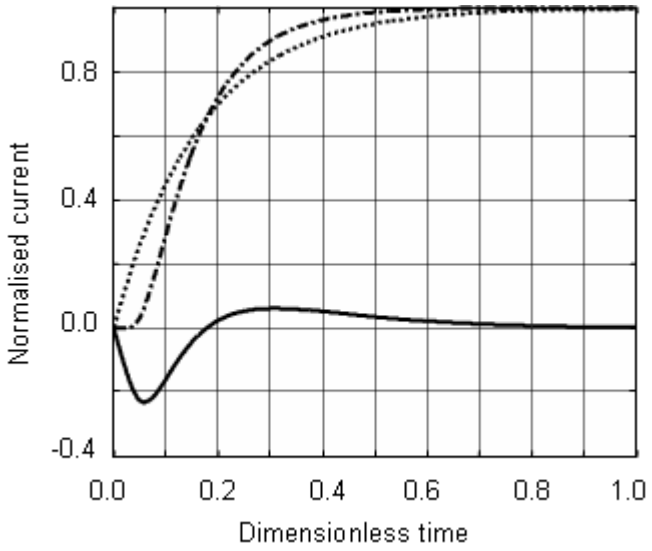

Figure 8.3 The Yen-Shih solution (··), i.e. equation 8.1, the bipartite expression (·-), i.e. equation 5.14 and the difference (-) between these two expressions [37].

When we analyse the result by Compañ et al [130] and Guzmán et al [146] by the normalised current obtained from the Yen and Shih model [127] *vs*. our own bipartite expression there is again a significant difference (Figure 8.3). The Yen and Shih model (equation 8.1) gives larger values than the current more accurate solution, (equation 5.14) for $T > 0.178$), and smaller values for $T < 0.178$. The maximum difference between equation 8.1 and equation 5.15 reaches 23% of the steady state current value. In the early phase of the electrode response up to $T = 0.084$, the error shown in equation 8.1 is actually greater than the actual response i.e. equation 5.15.

Compañ transformed the Yen and Shih formula as [130]:

$$\ln\left(1/(1-I)\right) = 6Dt/L^2 \qquad 8.6$$

and provided a fit of equation 8.6 to the experimental data to determine diffusion coefficients. However, the entire equation (equation 5.14) cannot be written in a simple form whereas equation 5.14b can be simplified to:

$$\ln\left(1/(1-I)\right) = \pi^2 Dt/L^2 - \ln 2 \qquad 8.7$$

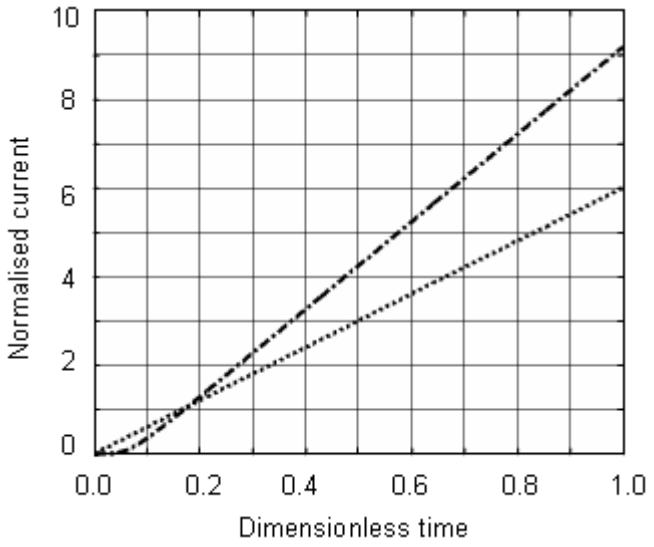

Figure 8.4 ln(1/(1-*I*)) against dimensionless time for the Yen-Shih formula (··) and the bipartite expression (·-) [37].

It can be seen that there is a significant difference between the coefficient of 6 in equation 8.6 and π^2 in equation 8.7. Figure 8.4 shows the ln(1/(1-*I*)) plot against dimensionless time for both the Yen and Shih formula and the bipartite expression. It can be seen that a significant difference between the Yen and Shih formula and the bipartite expression is retained for the entire time domain, though this is not seen in Figure 8.3 where the difference is reduced for dimensionless time T >0.178. Nevertheless, the ratio of the slopes of the two curves is $\pi^2/6$=1.6. A diffusion coefficient obtained from equation 8.6 would be expected to differ by that value from

the bipartite expression (equation 8.7). An order of magnitude error in diffusion coefficients can be avoided by directly fitting the simulated current to the experimental data, where the calculated diffusion coefficient is visually verified.

Our expression, above, a fit of calculated *vs*. experimental current curves would seem preferable to any indirect fit, not only to avoid calculation errors, but more importantly, to show by observation whether a direct fit can reproduce the entire experimental result to verify the reliability of the fit. It is well understood that background current needs to be subtracted from the response current, but less well understood that curve fitting should also consider an accurate initial time, when the theoretical boundary condition changed. By our method, zero time is more readily identified from a curve fit using a normalised transient current from equation 8.4.

Finally, practical applicability of the one dimensional mass transport model should be considered. In our experiments, the diameter of the working electrode was 2 mm and the diameter of the solution cylinder was 16 mm. To validate the one dimensional model, membrane thickness needs to be less than 0.2 mm to avoid edge effects [1]. A thicker membrane (> 0.2 mm) would require a larger working electrode. However, a large working electrode area leads to a large current (>10 μA), and so a three electrode system becomes necessary [134]. If the working electrode diameter increases to that of the solution cylinder, solute diffusion can be described by a one dimensional mass transport model for a membrane of any thickness. On the other hand, if the diameter of the cylinder decreases to less than that of the working electrode, the one dimensional mass transport model is also valid. This latter system is actually the well known recessed electrode [34, 110, 150]. A recessed electrode for

diffusion coefficient measurement appears a promising practical strategy. The one dimensional model originated from a planar electrode but is not limited to this. Compañ et al [130] and Guzmán et al [146] in fact approximated a cylindrical polarographic cell consisting of an inner cylindrical gold cathode (diameter of 4.25 mm and length of 6 mm) and an outer hollow cylindrical silver anode (inner and outer diameter of 5 and 10 mm and length of 7 mm) to the one dimensional model.

8.4 Conclusions

For a membrane covered electrode, where the electrochemical reaction is limited by a one dimensional mass transport model, if an amperometric current transient is recorded, then the solute diffusion coefficient through the membrane can be rapidly estimated from the time it takes to reach half of the steady state current as from equation 5.15. The diffusion coefficient can be further refined by a best fit of equation 5.14 to the experimental current transient. A more direct fit of the simulated current curve also ensures that the calculated D value can be verified. An approximate expression or use of an indirect fit can lead to significant errors in the diffusion coefficient determination that can go unrecognised, a potential pitfall with diffusion measurements in biological systems.

Chapter 9 Analytical Expressions for Mass Transport within Microfluidic Systems

The reliable modeling of solute and solvent transport within microfluidic systems is fundamental to their adaptation for practical analysis. Theoretical expressions for molecular transport, including across parallel laminar flows, are available in literature. However, they are rarely used in practical analysis because they involve infinite series and so approximate expressions or numerical solutions are conventionally used. Here an investigation of the convergence of these more exact infinite series expressions is conducted. Accurate but simple bipartite expressions for analyte concentrations and concentration gradients were constructed, and these enabled direct simulation, analysis by best fit, of experimental profiles for the exact determination of diffusion coefficients, and through this, molecular mass.

9.1 Introduction

The development of micro-electromechanical systems (MEMS) has led to a scientific research area: microfluidics. Scale reduction has provided obvious advantages in reagents conservation. Equally importantly, for the special case where two fluid streams flow side by side in a single micro channel, maintained laminar flow allows for precisely controlled liquid/liquid boundaries, which were termed *de facto* interfaces [151]. Under such laminar flow conditions, i.e. low Reynolds numbers, streams which contact each other, only allow sample mixing through diffusion. These interfaces can constitute virtual separation membranes, in contrast to real membranes needed in macro-scale systems, and will provide increasingly wide applications in analytical chemistry, biology and medicine [151]. In practical embodiments, T-sensor

or Y-sensor constructs are used, in which one stream contains the analyte and the other a receiving buffer stream which may, for example, contain fluorescent dye or a dye label for optical detection. Here, detection methods for following diffusion include refractive index gradient detection [152–154], fluorescent intensity imaging [155–158], fluorescence lifetime imaging microscopy [159] and transmitted light microscopy [160]. Typically, by comparing measured and calculated diffusion profiles, diffusion coefficients of the analyte can be determined.

Here, for convenience in describing the theoretical aspects of microfluidic systems, Fick's Second Law and solutions to relevant initial and boundary conditions are introduced first. In a three dimensional coordinate system the initial solute concentration is c_0 in left semi-infinite space, $x < 0$, and zero in right semi-infinite space, $x > 0$. Assuming these two semi-infinite solutions meet, the analyte concentration c follows Fick's Second Law as:

$$\frac{\partial c(x,t)}{\partial t} = D\frac{\partial^2 c(x,t)}{\partial x^2} \tag{9.1}$$

where D is diffusion coefficient and t is time. The solution is given as [1, 153, 154]:

$$\frac{c(x,t)}{c_0} = \frac{1}{2}\mathrm{erfc}\left(\frac{x}{2(Dt)^{1/2}}\right) \tag{9.2}$$

For a concentration gradient, the first derivative of concentration is given as [153]:

$$\frac{\mathrm{d}c(x,t)}{\mathrm{d}x} = \frac{-1}{2(\pi Dt)^{1/2}}\exp\left(\frac{-x^2}{4Dt}\right) \tag{9.3}$$

In the second model, the dimensions of the x coordinate are limited to a finite length L, and no flow of analyte through the boundaries takes place at $x = \pm L/2$. Initially, the concentration at the left fluid column between $-L/2$ and 0 is c_0 and at the right column

between 0 and $L/2$ is zero. The solution to Fick's Second Law is then given as [1, 156]:

$$\frac{C(x,t)}{C_0} = \frac{1}{2}\sum_{n=-\infty}^{\infty}\left\{\mathrm{erf}\left(\frac{2nL-x}{2(Dt)^{1/2}}\right)+\mathrm{erf}\left(\frac{x+L-2nL}{2(Dt)^{1/2}}\right)\right\} \quad 9.4$$

Synovec and co-worker [152–154] developed a microfluidic molecular mass determining system based on a T-sensor. They used equation 9.3 to calculate concentration gradients. Yang et al used equation 9.4 to calculate analyte concentration to study diffusive mixing in a microfluidic chip [155]. Yager's group used a numerical method to solve Fick's Second Law to analyze molecular diffusion in laminar flow [156–158]. They also recognized that computational demands for more complex 2 or 3-dimensional models, involving for example sheath flow [158], were too complex for effective curve fitting.

In our previous work, we proposed accurate but simple bipartite expressions for solutions to Fick's Second Law at defined initial and boundary conditions [30, 33, 35, 36, 43]. These expressions enabled us to provide a precise fit of calculated concentrations and concentration gradients, to experimentally determine amperometric electrode responses of electrochemically active solutes. Here, we investigate the convergence of the expressions for concentration, i.e., equation 9.4, and concentration gradients for microfluidic systems and then construct the bipartite expressions. These expressions enable one to directly simulate concentration and concentration gradient profiles.

9.2 Mathematical Analysis

For generality and convenience, three dimensionless quantities, i.e. time $T = Dt/L^2$, spatial coordinate $X = x/L$ and concentration $C = c/c_0$ are introduced. Also, because the erf function is a monotonously increasing function and the absolute values of erf functions (equation 9.4) increase with n, erfc is used in preference. Equation 9.4 is rewritten as:

$$C(X,T) = \frac{1}{2}\left\{\text{erfc}\left(\frac{X}{2T^{1/2}}\right) - \text{erfc}\left(\frac{1+X}{2T^{1/2}}\right)\right\} + \frac{1}{2}\sum_{n=1}^{\infty}\left\{\text{erfc}\left(\frac{2n-1-X}{2T^{1/2}}\right) + \text{erfc}\left(\frac{2n+X}{2T^{1/2}}\right) - \text{erfc}\left(\frac{2n-X}{2T^{1/2}}\right) - \text{erfc}\left(\frac{2n+1+X}{2T^{1/2}}\right)\right\} \quad 9.5$$

At $X = ½$, equation 9.5 simplifies to (*vide infra*):

$$C(1/2,T) = \sum_{n=0}^{\infty}\left\{(-1)^n \text{erfc}\left(\frac{2n+1}{4T^{1/2}}\right)\right\} \quad 9.6$$

Equation 9.6, with n limited to 0, 1 and 2, respectively, is represented in Figure 9.1a. It can be seen that the convergence of equation 9.6 is fast for small T but slow for large T. For $T < 0.1$ the terms of equation 9.6 with $n > 0$ are negligible and the term with $n = 0$ represents the whole solution well as shown in Figure 9.1a where the curves are superimposed. However, because equation 9.6 converges slowly at large T, it is not convenient for practical calculations. Equation 9.2, shown in Figure 9.1a for comparison, demonstrates substantial differences from equation 9.6 for all T values. Indeed for the early phase (small T), equation 9.2 has half the value of equation 9.6.

Fortunately, a complementary counterpart solution for equation 9.1 is available [1]:

$$C(X,T) = \frac{1}{2} - \frac{2}{\pi}\sum_{n=0}^{\infty}\frac{1}{2n+1}\sin\left((2n+1)\pi X\right)\exp\left(-(2n+1)^2\pi^2 T\right) \quad 9.7$$

At $X = ½$, equation 9.7 is simplified to:

$$C(1/2,T) = \frac{1}{2} - \frac{2}{\pi}\sum_{n=0}^{\infty}\frac{(-1)^n}{2n+1}\exp\left(-(2n+1)^2\pi^2 T\right) \qquad 9.8$$

Equation 9.8 with n limited to 0, 1 and 2, respectively, are shown in Figure 9.1b. It can be seen that equation 9.8 converges quickly for large T but slowly for small T. For $T > 0.07$, the terms of equation 9.8 with $n > 0$ are negligible, therefore, equation 9.8 with $n = 0$ is sufficient to represent the whole equation, the curves are essentially superimposed.

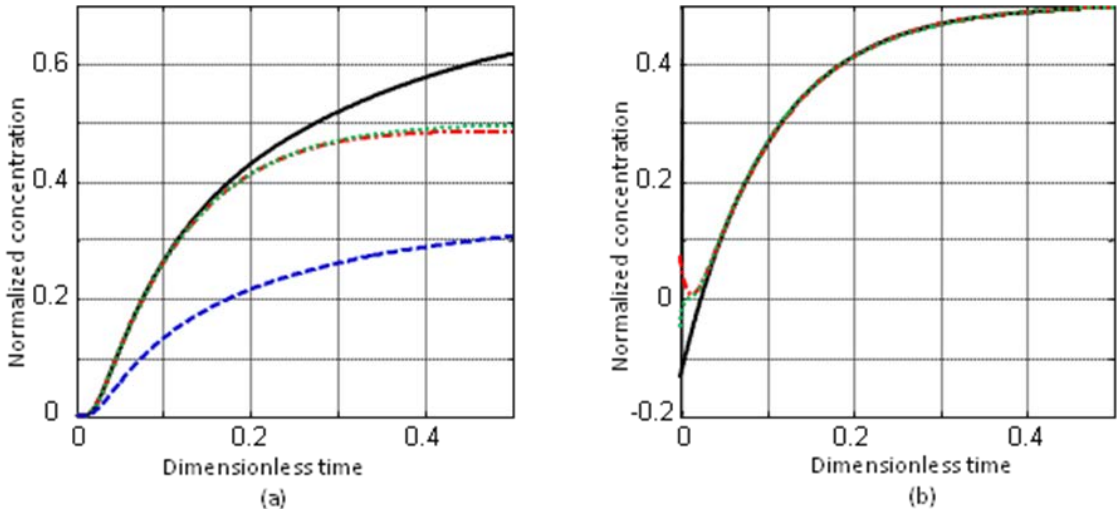

Figure 9.1 (a) Normalized concentration C at $X = ½$ *versus* dimensionless time T for equation 9.6 in the text with n limited to 0 (-), 1(-·) and 2 (··), respectively. Normalized concentration C at $X = ½$ *versus* dimensionless time T for equation 9.2 in the text (--) is also shown for comparison. (b) Normalized concentration C at $X = ½$ *versus* dimensionless time T for equation 9.8 in the text with n limited to 0 (-), 1(-·) and 2 (··), respectively.

9.3 Results and Discussion

Through analysis of the convergent properties of equation 9.6 and 9.8, a function can be constructed by combining the rapidly convergent parts of equation 9.6 and 9.8,

respectively. For a smooth connection, the two curves need to intersect, giving the same or very close values for their first derivatives at the intersection point. By a balance of complexity *versus* accuracy, a bipartite expression for solute concentration can be constructed as:

$$C(1/2,T) = \text{erfc}\left(1/(4T^{1/2})\right) \text{ for } T \le 0.07958 \qquad 9.9a$$

$$C(1/2,T) = 1/2 - (2/\pi)\exp(-\pi^2 T) \text{ for } T \ge 0.07958 \qquad 9.9b$$

At the joint point T = 0.07958, equation 9.6 and 9.8 give the same value of 0.2099. Also at the joint point, the first five absolute values of equation 9.6 decrease dramatically: 0.2101, 1.700×10^{-4}, 3.693×10^{-10}, 1.739×10^{-18} and 1.654×10^{-29}, respectively. Equation 9.6 shows the absolute value of the terms increases with T increasing, and so for T < 0.07958 these same terms become even smaller than their values at the joint point, and so the higher order terms become of even less significance. At the joint point, the absolute values of the first five terms of equation 9.8 are 0.2903, 1.806×10^{-4}, 3.778×10^{-10}, 1.757×10^{-18} and 1.660×10^{-29}, respectively, again a sharp decrease with n increasing. It can also be seen from equation 9.8 that the absolute values of the terms decrease with T increasing. So for T < 0.07958, these terms are again less than the values at the joint point, and higher order terms are negligible. Thus, it is reasonable that for equation 9.6 and 9.8, both with n limited to 0; the solution function (equation 9.9) operates across the entire time range. From the values of equation 9.6 and 9.8 at the joint point, the accuracy of equation 9.9 is obtained as 0.02%.

Following construction of equation 9.9, for equation 9.5, only absolute values of terms larger than erfc(3/(4$T^{1/2}$)) are kept, and for equation 9.7, terms with n > 0 are negligible as sin(πX) is not larger than 1. With the same accuracy as equation 9.9, a

bipartite expression is obtained by combining rapidly convergent parts of equation 9.5 and 9.7 as:

$$C(X,T)=\frac{1}{2}\left\{\operatorname{erfc}\left(\frac{X}{2T^{1/2}}\right)-\operatorname{erfc}\left(\frac{1+X}{2T^{1/2}}\right)+\operatorname{erfc}\left(\frac{1-X}{2T^{1/2}}\right)\right\} \text{ for } T\le 0.07958 \qquad 9.10a$$

$$C(X,T)=1/2-(2/\pi)\sin(\pi X)\exp(-\pi^2 T) \text{ for } T\ge 0.07958 \qquad 9.10b$$

Equation 9.10 is also correct with 0.02% accuracy for both arbitrary time and position.

The concentration gradient, i.e. the first derivative of the concentration, was used for the refractive index gradient calculation by Synovec et al [153, 154]. The first derivative of equation 9.5 at $X = 0$ is given as:

$$\frac{\mathrm{d}C(0,T)}{\mathrm{d}X}=-\frac{1}{2(\pi T)^{1/2}}-\frac{1}{(\pi T)^{1/2}}\sum_{n=1}^{\infty}(-1)^n\exp\left(-\frac{n^2}{4T}\right) \qquad 9.11$$

The first derivative of equation 9.7 at $X = 0$ is given as:

$$\frac{\mathrm{d}C(0,T)}{\mathrm{d}X}=-2\sum_{n=0}^{\infty}\exp\left(-(2n+1)^2\pi^2 T\right) \qquad 9.12$$

Similarly to the derivation of equation 9.9, the analysis of equation 9.11 and 9.12 is as follows. For equation 9.11, the first part and the terms of the second part with $n = 1$ and 2 are shown in Figure 9.2a. It can be seen that the first term represents the whole equation for $T < 0.03$. For equation 9.12, the terms with $n = 0$, 1 and 2 are shown in Figure 9.2b. It can be seen that the first term represents the whole equation for $T > 0.08$. More terms are needed in the construction of the bipartite expression for the concentration gradient. The final result is given as:

$$\mathrm{d}C(0,T)/\mathrm{d}X=-1/\left(2(\pi T)^{1/2}\right)+1/(\pi T)^{1/2}\exp\left(-1/(4T)\right) \text{ for } T\le 0.10694 \qquad 9.13a$$

$$\mathrm{d}C(0,T)/\mathrm{d}X=-2\exp(-\pi^2 T) \text{ for } T\ge 0.10694 \qquad 9.13b$$

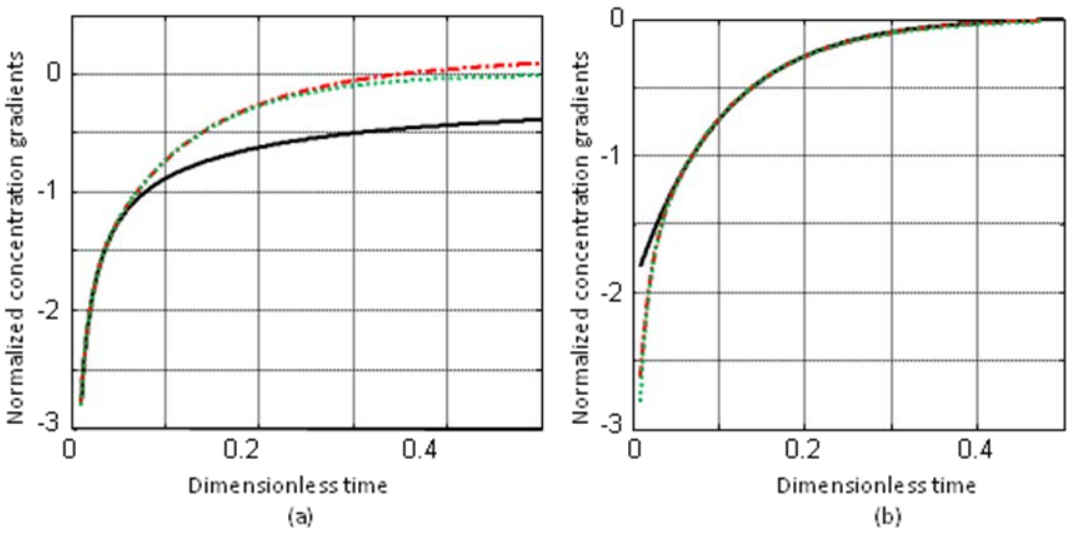

Figure 9.2 (a) Normalized concentration gradients d*C*/d*X* at *X* = 0 *versus* dimensionless time *T* for equation 9.11 in the text is limited to the first part (-), the second part with *n* equal to 1(-·) and 2 (··), respectively. Normalized concentration gradient d*C*/d*X* at *X* = 0 as equation 9.11 in the text with *n* limited to 0 is the same as equation 9.3 at *X* = 0. (b) Normalized concentration gradient d*C*/d*X* at *X* = 0 *versus* dimensionless time *T* for equation 9.12 in the text with *n* limited to 0 (-), 1(-·) and 2 (··).

At the joint point *T* = 0.10694, equations 9.11 and 9.12 have the same value of –0.6962. The absolute values of the first part and the terms of the second part of equation 9.11 with *n* = 1, 2, 3, 4 and 5 are 0.8626, 0.1666, 1.499×10^{-4}, 1.257×10^{-9}, 9.827×10^{-17} and 7.161×10^{-26}, respectively. The absolute values of the terms of equation 9.12 with *n* = 0, 1, 2, 3 and 4 are 0.6961, 1.498×10^{-4}, 6.943×10^{-12}, 6.926×10^{-23} and 1.487×10^{-37}, respectively. From these absolute values of equation 9.11 and

9.12 at the joint point, the accuracy of equation 9.13 for concentration gradients is determined as 0.02% of c_0/L.

With the same accuracy as equation 9.13, the bipartite expression for the concentration gradient in general is obtained as:

$$\frac{\mathrm{d}C(X,T)}{\mathrm{d}X} = -\frac{1}{2(\pi T)^{1/2}}\left\{\exp\left(-\frac{X^2}{4T}\right) - \exp\left(-\frac{(1+X)^2}{4T}\right) - \exp\left(-\frac{(1-X)^2}{4T}\right)\right\}$$

for $T \le 0.10694$ 9.14a

$$\mathrm{d}C(X,T)/\mathrm{d}X = -2\cos(\pi X)\exp(-\pi^2 T) \text{ for } T \ge 0.10694$$ 9.14b

Again equation 9.14 for concentration gradients is correct with an accuracy of 0.02% of c_0/L for both arbitrary time and position.

The constructed bipartite expression for concentration gradients was used to analyze the experimental T-sensor data of Costin et al [153]. For one set of experimental parameters: width of channel L = 0.5 mm, depth of channel h = 0.2 mm, flow rate u = 16 μL/min, downstream detection position past the T-junction d = 50 mm, and diffusion coefficient D = 1000 $\mu m^2/s$, equivalent dimensionless time was T = 0.075. The diameter of the probe laser beam was 0.586 mm with equivalent dimensionless spatial coordinate X = 1. Whilst Costin et al [153] found that the experimental light deflection ratio of a small beam (0.158 mm) agreed with the theoretical plot (equation 9.2), the experimental deflection ratio with a large beam (0.586 mm) agreed with the theoretical plot for only a larger molecular mass but not for a smaller molecular mass. The differences between equation 9.14 and equation 9.3 within the domain, $0 \le X \le 1$, $0 \le T \le 0.075$, are shown in Figure 9.3. It can be seen that errors of equation 9.3 increase with increasing T or absolute values of X. A smaller molecular mass results

in a larger diffusion coefficient, therefore a larger dimensionless time; as the error of equation 9.3 is larger for larger dimensionless time and larger spatial coordinates (absolute value), experimental deviation from the original theory (equation 9.3) would be expected. It is suggested that use of equation 9.14 instead of equation 9.3 would eliminate this error.

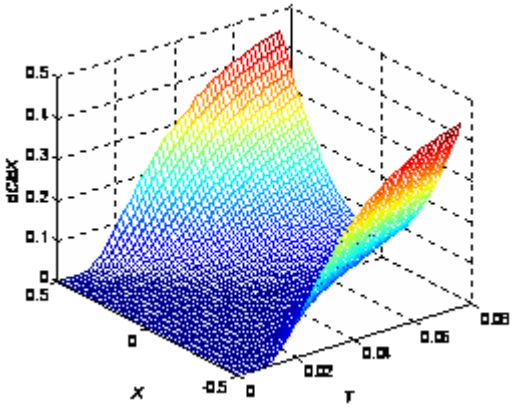

Figure 9.3 Error of equation 9.3 in the text, i.e., the difference between equation 9.14 and 9.3 in the text *versus* dimensionless time $T \in [0, 0.075]$ and dimensionless spatial coordinate $X \in [0, 1]$.

In the above, diffusion between infinite columns (temporal frame) is used to mimic diffusion through a moving interface (spatial frame) in microfluidic systems. Nguyen et al [161, 162] considered a microfluidic channel in a different fashion, in a steady state two dimensional model as:

$$D\left(\frac{\partial^2 c(x,z)}{\partial x^2}+\frac{\partial^2 c(x,z)}{\partial z^2}\right)=v\frac{\partial c(x,z)}{\partial z} \qquad 9.15$$

where flow is assumed to be in the z direction with velocity v. The solution is [161, 162]:

$$C(X,Z)=\frac{1}{2}-\frac{2}{\pi}\sum_{n=0}^{\infty}\frac{1}{2n+1}\sin\left((2n+1)\pi X\right)\exp\left(-\frac{2(2n+1)^2\pi^2 Z}{Pe+\left(Pe^2+4(2n+1)^2\pi^2\right)^{1/2}}\right) \qquad 9.16$$

where $Pe = vL/D$ is the Peclet number and $Z = z/L$ is a normalised spatial coordinate. When Pe is sufficiently large, the diffusion term along the z direction in equation 9.15 is much smaller than the convective term and equation 9.15 becomes equation 9.1 with use of $t = z/v$. Also, with use of $t = z/v$ equation 9.16 becomes equation 9.7, and for large Pe numbers, equation 9.10 is correct for both arbitrary x and z. Here the bipartite expressions are obtained for equal mixing ratios between two streams, but general expressions for arbitrary mixing ratios, are available in literature [1,162] and can be similarly analyzed.

9.4 Conclusions

Through analysis of expressions for concentration and concentration gradients we have derived accurate but simple bipartite expressions, which are valid for both arbitrary time and position. The nature of the bipartite expression is that the slow convergent part of an expression is replaced by a fast convergent part of its complementary counterpart expression. We believe these bipartite expressions are of general applicability in mass transport related studies in microfluidic systems.

Chapter 10 Simple Expression for Diffusion Coefficient Determination of Adsorption within Spherical and Cylindrical Adsorbents Using Direct Simulation Method

Various analytical expressions for solute adsorption kinetics within porous adsorbents of defined geometry (planar sheet, cylinder and sphere) are available in literature. However, these expressions are limited for practical numerical evaluation because they are based on infinite series. An investigation of these expressions has been carried out and then accurate and simple expressions were derived that enable rapid determination of effective diffusion coefficients for adsorption within geometrically categorical absorbents. These involve directly fitting calculated kinetic adsorption curves to experimental ones. A simple one point method is also proposed to estimate the effective diffusion coefficient for an adsorption process within these simple geometrical absorbents as an initial value for a best fit.

10.1 Introduction

Adsorption is the adhesion of atoms, ions, or molecules from a gas, liquid or dissolved solid to a surface. According to the nature of the bonding, the adsorption process is generally classified as physisorption (van der Waals forces) or chemisorption (covalent bonding). The word adsorption was first coined by Heinrich Kayser in 1881. An isotherm is used to describe adsorption, the amount of adsorbate on the adsorbent as a function of its pressure (if gas) or concentration (if liquid) at a constant temperature. Freundich Küster was the first to use an empirical mathematical

formula to describe an isotherm in1894. Irving Langmuir reported a novel model isotherm for gases adsorbed to solids in 1916. Stephen Brunauer, Paul Emmett and Edward Teller developed a model isotherm called BET theory in 1938. The Langmuir isotherm is usually better for chemisorption and the BET isotherm is better for physisorption. Silica gel, zeolites and activated carbon are common adsorbents.

Solute adsorption from solution constitutes one of the most important practical applications of high surface area carbon. Drug species may be removed this way, e.g. for detoxification. Terzyk et al [137, 163, 164] studied the adsorption kinetics of the analgesic drug acetaminophen (paracetamol®) at adsorbing carbon surfaces in a series of studies. Complete analytical solutions to Fick's Second Law of diffusion for the kinetics of adsorption in spherical and cylindrical adsorbents are well known, but numerical application is limited because the solutions are expressed as infinite series. In the specific studies of Terzyk et al [163, 164] a method to determine the acetaminophen diffusion coefficient within cylindrical and spherical carbon granules was developed. They expressed the diffusion coefficient as a function of normalised adsorption for spherical adsorbents and for both normalised adsorption and the length / radius ratios for cylindrical adsorbents. In this work we provide an alternative practical approach to adsorption kinetics for spherical and cylindrical absorbents.

The computations used here envisage a spherical granule with radius *R*, without solute, immersed in an acetaminophen solution. Time dependent adsorption in the granule follows Fick's Laws and the solution is given as [1, 68]:

$$\frac{a_t}{a_{\max}} = 1 - \frac{6}{\pi^2}\sum_{n=1}^{\infty}\frac{1}{n^2}\exp(-\frac{\pi^2 n^2 Dt}{R^2}) \qquad 10.1$$

where a_t and $a_{\max}$ are adsorption at time t and saturated adsorption respectively, D is the effective diffusion coefficient.

Similarly, an expression for a finite cylinder with radius R and length of L is given as [1, 68]:

$$\frac{a_t}{a_{\max}} = 1 - \left(4\sum_{n=1}^{\infty} \frac{1}{\alpha_n^2} \exp(-\frac{\alpha_n^2 Dt}{R^2}) \right) \left(\frac{8}{\pi^2} \sum_{m=1}^{\infty} \frac{1}{2m-1} \exp(-\frac{\pi^2 (2m-1)^2 Dt}{L^2}) \right) \qquad 10.2$$

where α_n are the roots of the zero order Bessel function: $J_0(\alpha_n) = 0$. Equations 10.1 and 10.2 are computationally exact but are inconvenient for practical numerical valuation. Here, instead, equation 10.2 is expressed in a format different from that in literature to enable further analysis.

The expression for adsorption within a spherical granule as from equation 10.1 was simplified as [165]:

$$\frac{a_t}{a_{\max}} = \frac{6}{R} \left(\frac{Dt}{\pi} \right)^{0.5} \text{ for } a_t/a_{\max} < 0.2 \qquad 10.3a$$

$$\frac{a_t}{a_{\max}} = \frac{6}{R} \left(\frac{Dt}{\pi} \right)^{0.5} - \frac{3Dt}{R^2} \text{ for } 0.2 < a_t/a_{\max} < 0.8 \qquad 10.3b$$

$$\frac{a_t}{a_{\max}} = 1 - \frac{6}{\pi^2} \exp(-\frac{\pi^2 Dt}{R^2}) \text{ for } 0.8 < a_t/a_{\max} \qquad 10.3c$$

We previously modelled solute uptake in a cylindrical geometry gel without solute immersed in a solute containing solution as a concentration c_0. The concentration at the centre of the cylinder follows Fick's Laws and was expressed as [30]:

$$\frac{c}{c_0} = \frac{R}{\pi Dt} \exp(-\frac{R^2}{8Dt}) \left(K_{\frac{1}{4}}(\frac{R^2}{8Dt}) - \frac{Dt}{4R^2} K_{\frac{3}{4}}(\frac{R^2}{8Dt}) \right) \text{ for } t < 0.063R^2/D \qquad 10.4a$$

$$\frac{c}{c_0} = 1 - 2\sum_{n=1}^{3} \frac{1}{\alpha_n J_1(\alpha_n)} \exp(-\frac{\alpha_n^2 Dt}{R^2}) \text{ for } t > 0.063R^2/D \quad 10.4b$$

where $J_1(\alpha_n)$ are the first order Bessel functions. We directly fitted a calculated concentration evolution profile using equation 10.4 to the experimental concentration profile to determine the solute diffusion coefficient within the gel using a Microsoft Excel spreadsheet. When compared with equation 10.4, equation 10.3 appears simple enough to be used for practical diffusion coefficient determination for an adsorption process within a spherical absorbent by direct fit of the calculated adsorption curve to an experimental one.

In this work we also derive accurate but simple expressions for adsorption within a finite cylinder. During the derivation, expressions for adsorption within an infinite slab and an infinite cylinder are also obtained. These expressions thus enable us to accurately determine the effective diffusion coefficient by directly fitting calculated and experimental adsorption curves to defined geometric structure. Timofiejev [166] proposed a one point method to estimate the diffusion coefficient based on adsorption in a sphere as

$$D = 0.308\frac{R^2}{\pi^2 t_{0.5}} = 0.0312\frac{R^2}{t_{0.5}} \quad 10.5$$

where $t_{0.5}$ is the time when adsorption reaches half saturation. The estimated diffusion coefficient can be used as an initial value for a best fit. We report a simple one point method to estimate the diffusion coefficient for adsorption respectively within an infinite slab, an infinite cylinder and a finite cylinder.

10.2 Mathematical Analysis

It can be seen from equation 10.2 that the expression for adsorption within a finite cylinder could be obtained using the expression for adsorption within an infinite cylinder and the expression of adsorption within an infinite planar sheet. An expression for adsorption within an infinite planar sheet with thickness L is given as [1, 68]:

$$\frac{a_t}{a_{\max}} = 1 - \frac{8}{\pi^2}\sum_{m=1}^{\infty}\frac{1}{(2m-1)^2}\exp[-\frac{\pi^2(2m-1)^2 Dt}{L^2}] \qquad 10.6$$

For simplicity, here dimensionless time $T = Dt/L^2$ is introduced, and equation 10.6 is rewritten as [1, 68]:

$$\frac{a_t}{a_{\max}} = 1 - \frac{8}{\pi^2}\sum_{m=1}^{\infty}\frac{1}{(2m-1)^2}\exp[-(2m-1)^2\pi^2 T] \qquad 10.7$$

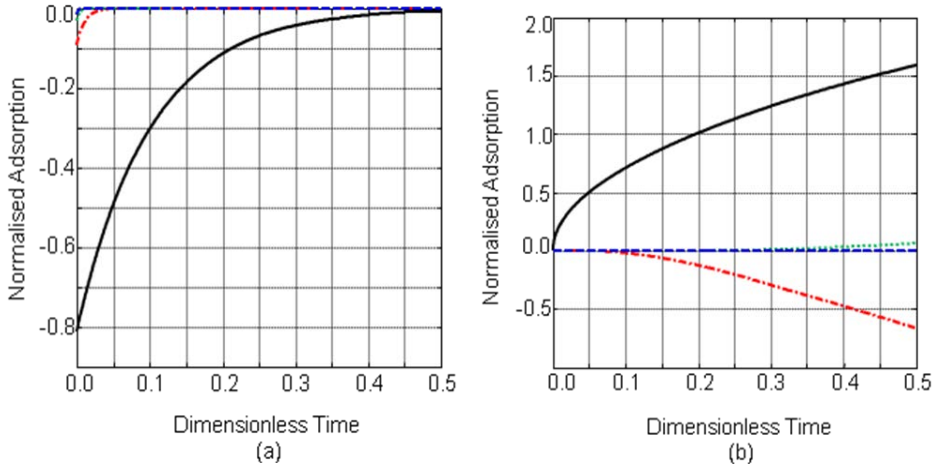

Figure 10.1 (a) The terms corresponding to m equals 0 (-), 1 (-·), 2 (··) and 3 (--) of adsorption as equation 10.7 in the text, respectively [43]. (b) The first part (-) and the terms of the second part corresponding to m equals 1 (-·), 2 (··) and 3 (--) of adsorption as equation 10.8 in the text, respectively [43].

Analysis of equation 10.7 is needed to determine convergence for two different time domains. The terms of equation 10.7 corresponding to m equals 0, 1, 2, and 3 are

shown in Figure 10.1a. It can be seen from Figure 10.1a that the absolute value of the term decreases with m or T increasing and this tendency is also true for $m > 3$. For $T > 0.04$, the terms with $m > 0$ become negligible; therefore equation 10.7 with m limited to 0 can represent the whole solution. In other words, equation 10.7 converges rapidly for large T and slowly for small T. It is inappropriate to use equation 10.7 for the numerical calculation for small T. Fortunately, a solution for small T is given as [1, 68]:

$$\frac{a_t}{a_{\max}} = 4\left(\frac{T}{\pi}\right)^{0.5} + 8T^{0.5}\sum_{m=1}^{\infty}(-1)^m \text{ierfc}(\frac{m}{2T^{0.5}}) \qquad 10.8$$

where ierfc(y) is the integral of the error function erfc(y) and ierfc(y) = $\exp(-y^2)/\pi^{0.5} - y\text{erfc}(y)$ [2]. The first part of equation 10.8 and the terms of the second part of equation 10.8 corresponding to m equals 1, 2, and 3 are shown in Figure 10.1b. It can be seen from Figure 10.1b that the absolute value of the term of the second part of equation 10.8 increases with T increasing and decreases with m increasing, this tendency is again also true for $m > 3$. For $T < 0.08$, the second part of equation 10.8 is negligible therefore the first part of equation 10.8 represents the whole equation 10.8.

10.3 Results and Discussion

A computational approach was used to construct a solution function by combining the rapidly convergent parts of equation 10.7 and equation 10.8. For a smooth connection, the two function curves are required to intersect and to have the same or similar values for the first derivatives at the intersection point. After balancing accuracy versus complexity, we constructed an expression for adsorption within an infinite planar sheet as follows:

$$f_{is} = \frac{a}{a_{\max}} = 1 - \frac{8}{\pi^2}\exp(-\frac{\pi^2 Dt}{L^2}) \quad \text{for } t > 0.05326L^2/D,\ a_t/a_{\max} > 0.5200 \qquad 10.9a$$

$$f_{is} = \frac{a_t}{a_{\max}} = \frac{4}{L}\left(\frac{Dt}{\pi}\right)^{0.5} \quad \text{for } t < 0.05326L^2/D,\ a_t/a_{\max} < 0.5200 \qquad 10.9b$$

The rapidly convergent parts of equation 10.7 and equation 10.8 overlap, and therefore a complete solution function can be constructed, with the expressions cut into fast and slow convergent parts and two fast convergent parts joined to form a practical function for an entire time range. At the joint point (T = 0.05326), the absolute values of the terms of equation 10.7 corresponding to m equals 0, 1, 2, 3 and 4, are 0.4792, 7.942×10^{-4}, 6.362×10^{-8}, 1.078×10^{-13} and 3.228×10^{-21}, respectively, which decreases dramatically with m increasing. This tendency is also true for $m > 4$. Therefore, the terms with $m > 0$ are negligible for $T > 0.05326$. At the joint point (T = 0.05326), the absolute values of the first part of equation 10.8 is 0.5200 and the first four terms of the second part of equation 10.8 are 7.946×10^{-4}, 1.807×10^{-10}, 5.359×10^{-21} and 1.643×10^{-35}, respectively, which decreases dramatically with m increasing. This tendency is also true for $m > 4$. The second part of equation 10.8 is negligible for $T < 0.05326$. Therefore, it is reasonable that only the first part and the first term of the second part of equation 10.7 and the first part of equation 10.8 are used to construct the solution function, i.e., equation 10.9. The nature of the bipartite expression is that for $T < 0.05326$, equation 10.9b is as accurate as including high order terms but a simpler way to express equation 10.7. From the values of equation 10.7 and equation 10.8 at the joint point, the maximum error of the final simplified expression, i.e., equation 10.9 is less than 0.08%.

The diffusion coefficient is estimated from the time when adsorption reaches half saturation as:

$$D = 0.04918\frac{L^2}{t_{0.5}} \qquad 10.10$$

A similar expression for adsorption within an infinite cylindrical granule with radius R is given as [1, 68]:

$$\frac{a_t}{a_{\max}} = 1 - 4\sum_{n=1}^{\infty}\frac{1}{\alpha_n^2}\exp(-\frac{\alpha_n^2 Dt}{R^2}) \qquad 10.11$$

where α_n are roots of the zero order Bessel function: $J_0(\alpha_n) = 0$. This expression is also based on an infinite series. The expression for adsorption within an infinite cylinder for small dimensionless time ($T = Dt/R^2$) is given as [1, 68]:

$$\frac{a_t}{a_{\max}} = \frac{4}{R}\left(\frac{Dt}{\pi}\right)^{0.5} - \frac{Dt}{R^2} - \frac{(Dt)^{1.5}}{3\pi^{0.5}R^3} \qquad 10.12$$

Similar to the construction of equation 10.9 for an infinite planar sheet, a bipartite expression for adsorption within an infinite cylinder can be constructed from equation 10.11 and equation 10.12 as:

$$f_{ic} = \frac{a_t}{a_{\max}} = 1 - 4\sum_{n=1}^{3}\frac{1}{\alpha_n^2}\exp(-\frac{\alpha^2 Dt}{R^2}) \text{ for } t > 0.02908L^2/D,\ a_t/a_{\max} > 0.3552 \qquad 10.13a$$

$$f_{ic} = \frac{a_t}{a_{\max}} = \frac{4}{R}\left(\frac{Dt}{\pi}\right)^{0.5} - \frac{Dt}{R^2} - \frac{(Dt)^{1.5}}{3\pi^{0.5}R^3} \text{ for } t < 0.02908L^2/D,\ a_t/a_{\max} < 0.3552$$

10.13b

The maximum error of equation 10.13 at the joint point here is 0.05%.

The diffusion coefficient is estimated from the time when adsorption reaches half saturation as:

$$D = 0.06307\frac{R^2}{t_{0.5}} \tag{10.14}$$

According to the relationship between equation 10.2, equation 10.6 and equation 10.11, it is observed that the normalised adsorption for a finite cylinder is equal to the sum of the normalised adsorption of an infinite cylinder and an infinite planar sheet minus their product. The expression for adsorption within a finite cylinder is thus obtained from equation 10.9 and equation 10.13 as:

$$f_{fc} = f_{is} + f_{ic} - f_{is} f_{ic} \tag{10.15}$$

Equation 10.15 is still simple enough to allow use of a Microsoft Excel spreadsheet to handle the data.

For a specific geometrical model where R = 0.0615 cm and L = 0.3864 cm Terzyk used [137, 163], and equation 10.15 is a function of Dt, then the diffusion coefficient D can be estimated from time $t_{0.5}$ when adsorption reaches half saturation as:

$$D = \frac{1.927\times10^{-4}}{t_{0.5}}\,[\mathrm{cm^2/s}] \tag{10.16}$$

For further analysis of adsorption within a sphere, the expression for small dimensionless time ($T = Dt/R^2$) is given as [1, 68]:

$$\frac{a_t}{a_{\max}} = \frac{6}{R}\left(\frac{Dt}{\pi}\right)^{0.5} - \frac{3Dt}{R^2} + \frac{12}{R}(Dt)^{0.5}\sum_{n=1}^{\infty}\mathrm{ierfc}\left(\frac{nR}{(Dt)^{0.5}}\right) \tag{10.17}$$

The expression for adsorption within a sphere had been expressed as a tripartite expression [165], however, this is not necessary because the complexity of equation 10.3a is similar to that of equation 10.3b. A bipartite expression is sufficient as:

$$\frac{a_t}{a_{\max}} = \frac{6}{R}\left(\frac{Dt}{\pi}\right)^{0.5} - \frac{3Dt}{R^2} \text{ for } t < 0.15465R^2/D,\ a_t/a_{\max} < 0.8675 \qquad 10.18a$$

$$\frac{a_t}{a_{\max}} = 1 - \frac{6}{\pi^2}\exp(-\frac{\pi^2 Dt}{R^2}) \text{ for } t > 0.15465R^2/D,\ a_t/a_{\max} > 0.8675 \qquad 10.18b$$

The maximum error of this expression at the joint point is 0.03%. Timofiejev [166] proposed a one point method to estimate the diffusion coefficient for adsorption in a sphere as equation 10.5. A more accurate expression than equation 10.5 for estimating the diffusion coefficient is given from the above as

$$D = 0.03055\frac{R^2}{t_{0.5}} \qquad 10.19$$

By way of example, equation 10.13, equation 10.15 and equation 10.18 are used to reproduce experimental results in Figure 10.3 for two kind of spherical carbon granules (R = 0.488 mm and D = 1.0×10^{-7} cm^2/s) and (R = 1 mm and D = 2.8×10^{-7} cm^2/s) respectively, and for a finite cylindrical carbon granule (R = 0.615 mm, L = 3.684 mm and D = 1×10^{-7} cm^2/s) and its infinite cylinder approximation (R = 0.615 mm, L = ∞ and D = 1×10^{-7} cm^2/s). The diffusion coefficients 1×10^{-7} cm^2/s and 2.8×10^{-7} cm^2/s for spherical granules were calculated with exact numerical calculations assuming constant diffusivity (Figure 2 of ref 163). The diffusion coefficient 1×10^{-7} cm^2/s for cylindrical granules was selected from reported data (Figure 2 of ref 137) where consistency was observed by comparison with the observed normalised adsorption (Figure 1 of ref 137) and the simulated normalised adsorption (Figure 10.2). Figure 10.2 also shows the difference between the adsorption curves of a finite cylinder and an infinite cylinder decreases, which decreases with the ratio L/R increasing as expected. In other words, the infinite cylinder model is likely to be a good approximation when L/R is sufficient large. The

reported absorption kinetics of acetaminophen (Figure 1 of ref 137) shows the times to reach half saturation are 25 and 50 minutes respectively for adsorption in cylindrical carbon granules treated with HNO_3 and NH_3 respectively. According to equation 10.16, the corresponding effective diffusion coefficients for cylindrical granules are 1.3×10^{-7} and 0.64×10^{-7} cm^2/s, which lie within the range of experimental values for consistent data [137].

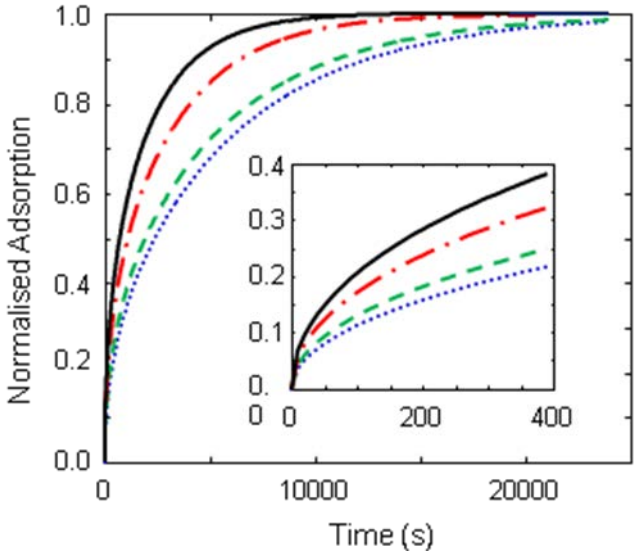

Figure 10.2 Simulated adsorption for spherical carbon granules with R = 0.488 mm and $D = 1.0\times10^{-7}$ cm^2/s (-), R = 1 mm and $D = 2.8\times10^{-7}$ cm^2/s (-.) respectively, and for a finite cylindrical carbon granule with R = 0.615 mm, L = 3.684 mm and $D = 1\times10^{-7}$ cm^2/s (--) and its infinite approximation with R = 0.615 mm, $L = \infty$ and $D = 1\times10^{-7}$ cm^2/s (··) [43].

From analysis of the bipartite expressions, the errors increase with time up to the joint point and decrease with time after the joint point. Comparison of the dimensionless time at the joint point, experimental time t = 2400 s, T = 0.6345 for infinite cylinder and T = 0.01768 for infinite planar sheet shows the error from the infinite planar sheet

calculation is negligible and the error for the finite cylinder mainly comes from the infinite cylinder calculation.

Equation 10.15 and equation 10.18 can be considered as functions of *Dt*, therefore, the calculated curves of these expressions can be stretched or compressed by adjusting the diffusion coefficient, i.e., a direct fit procedure to fit the calculated to the experimental curves. The advantage of a direct fit is that during the fit procedure the result is verified. The best fit procedure also minimises the standard deviation value for normalised adsorption:

$$\sigma = \sqrt{\frac{1}{m-1}\sum\left(\left(\frac{a_t}{a_{\max}}\right)_{\exp} - \left(\frac{a_t}{a_{\max}}\right)_{cal}\right)^2} \qquad 10.20$$

where *m* is the experimental point number and the summation is over all the experimental points.

10.4 Conclusion

We derived an accurate but simple expression for adsorption within cylindrical granules which can be used to determine the diffusion coefficient by direct fit of a calculated adsorption curve to an experimental one with an initial diffusion coefficient estimated by a one point method. We also obtained accurate but simple expressions for adsorption within an infinite planar sheet and an infinite cylinder, and formulae for one point methods to estimate diffusion coefficients.

Chapter 11 Effective Diffusion Coefficient Determination within Cylindrical Granules of Adsorbents Using a Direct Simulation Method

Analytical expressions for solute adsorption kinetics within porous carbon cylindrical granules of absorbents with a one point formula for effective diffusion coefficient determination are available based on the assumption that solute transport is the rate limiting step and that it follows Fick's Second Law. Here the first practical application of this theory is provided with an initial, estimated diffusion coefficient, refined by fitting calculated kinetic adsorption curves to experimental data determined for activated carbons. In an ideal experiment, experimental error (noise) is negligible, and no data refinement is needed. However, real experimental data are always more or less contaminated with noise. Where such noise is significant, a simulation method offers the best value for the effective diffusion coefficient. For this specific system, surface modification, pH and temperature effects on adsorption kinetics were analysed quantitatively as a basis of determining effective diffusion coefficients through the porous structure.

11.1 Introduction

Solute transport through a cylindrical matrix is of substantial importance. Many medicinal tablets are in a cylindrical form. Cylindrical carriers such as synthesized silica sol-gel, modified chitosans and hydroxyapatite have been used for drug encapsulation and controlled release [167–172]. Drug release from carriers is represented by drug release curves, e.g. mean cumulative release versus immersion

time. However, a drug release profile depends on the initial drug concentration in the carrier, and even a concentration normalised drug release curve depends on the dimension of the carrier. An effective diffusion coefficient, an intrinsic property of a carrier, is desired to characterise the drug release property of the carrier.

In a complementary area, solute adsorption from solution constitutes one of the most important practical applications of high surface area carbon. Drug species may be removed this way, e.g. for detoxification. The adsorption kinetics of the analgesic drug acetaminophen on to an adsorbing carbon surface has been reported in a series of studies [137, 163, 164, 173–175]. Investigations were extended to factors such as surface composition, pH value and temperature, affecting solute adsorption. In these studies a method to determine effective acetaminophen diffusion coefficients within cylindrical carbon granules was developed. The diffusion coefficient was expressed as a function of normalised adsorption and length to radius ratios. Values were determined from individual time and adsorption points. The effective diffusion coefficient of water in a polymeric cylinder was determined by fitting radial diffusion curves to experimental data [176]. However, analytical expressions to Fick's Second Law involve infinite series. Simple bipartite expressions for solutions to Fick's Second Law of diffusion through simple geometrical barriers have also been recently reported [33, 43]. Thus, the effective diffusion coefficient for glucose through a cylindrical collagen was determined by fitting a simulated concentration profile along the cylindrical axis to observed experimental data using a biosensor [30]. The release of the water-soluble antibiotics from a coated cylinder followed Fick's Second Law for a simple slab and effective diffusion coefficients were obtained by fitting the simulated to experimental release curves [177]. The above mentioned parameter for

acetaminophen at a membrane was determined by fitting simulated concentration gradients to experimental amperometric currents [36].

In the current study, the diffusion coefficient was determined based on the overall kinetics of uptake within cylindrical granules on the basis that diffusion through the pores, not adsorption, was the rate limiting process. This thereby provides an alternative practical approach to determining uptake kinetics driven by adsorption for cylindrical absorbent structures. Thus, the effective diffusion coefficient was used to quantitatively characterise adsorption kinetics, hereafter referring to uptake, and to analyse such adsorption property changes due to any carbon surface modification, solution pH or temperature.

11.2 Simulation and Best Fits

For adsorption at finite cylindrical granules, an expression was generated which was a function of the expressions of adsorption at an infinite cylinder and at an infinite planar sheet as [43]

$$f_{fc} = f_{is} + f_{ic} - f_{is} f_{ic} \qquad 11.1$$

For a simple simulation, knowledge of initial parameters is obligatory. The corresponding initial value for diffusion coefficients is then determined by a one point formula. Thus, if for a specific cylinder, equation 11.1 is plotted as a function of Dt adsorption is considered to reach half saturation, $a_t/a_{max} = 0.5$, when $Dt_{0.5} = \beta$, then the diffusion coefficient D can be estimated from time $t_{0.5}$ as:

$$D = \beta / t_{0.5} \qquad [\text{cm}^2/\text{s}] \qquad 11.2$$

where β is determined by the dimensions of the cylinder. In principle, any point of an adsorption curve can be used for a one point formula. The reason half saturation is used is for convenience and accuracy.

However, equation 11.1 can be considered to be a function of *t*, and calculated curves of this expression can be stretched or compressed by adjusting the diffusion coefficient *D*, i.e. a direct fit procedure can be used to fit a calculated adsorption curve to the experimental data. The best fit procedure minimises the standard deviation for a normalised adsorption:

$$\sigma = \sqrt{\frac{1}{m-1}\sum\left((\frac{a_t}{a_{\max}})_{\exp} - (\frac{a_t}{a_{\max}})_{cal} \right)^2} \qquad 11.2$$

where *m* is the experimental point number and the summation is over all the experimental points. The calculation here was carried out with Microsoft Excel solver.

The purpose of a best fit is to minimise the experimental errors, and a one parameter diffusion coefficient, here, was obtained from 19 or 21 experimental points. The large error at either the starting point or at the saturation value can be eliminated by further normalisation during curve fitting as:

$$\frac{a_t}{a_{\max}} = \frac{a_t / a_{\max} - a_b}{a_m - a_b} \qquad 11.6$$

where a_m and a_b are adjustable parameters and start from 1 and 0 respectively, which would need no adjustment.

We analysed the data of acetanilide (*ac*), aniline (*an*), acetaminophen (paracetamol) (*pa*) and phenol (*ph*) adsorption for D43/1 carbons at neutral (*nt*) and acidic (*ac*)

solutions and at three different temperatures (300, 310 and 320 K); the data was from literature – see [178] and the references therein. The adsorbent is activated carbon D43/1 from Carbo-Tech, Essen, Germany. This carbon was de-ashed according to the Korver procedure and is called D43/1-pure. The carbon was chemically modified with concentrated HNO_3, fuming H_2SO_4 and gaseous ammonia, and the resulting adsorbents are called D43/1-HNO_3, D43/1-H_2SO_4 and D43/1-NH_3, respectively.

Table 11.1 Phenol natural pH folder calculation results (the meanings of the collected parameters are presented in the text) [44].

Carbon	T (K)	D_e (10^7 cm^2/s)	σ	D_1 (10^7 cm^2/s)	σ	D_3 (10^7 cm^2/s)	σ
D43/1-pure	300	2.444	0.043	1.972	0.031	2.291	0.025
	310	2.353	0.022	2.569	0.018	2.783	0.016
	320	3.737	0.031	3.402	0.028	3.489	0.027
D43/1-H_2SO_4	300	2.353	0.019	2.296	0.018	2.202	0.018
	310	2.191	0.024	2.456	0.018	2.629	0.016
	320	3.530	0.036	3.255	0.035	3.251	0.027
D43/1-NH_3	300	1.629	0.026	1.593	0.026	1.809	0.020
	310	2.353	0.033	2.026	0.025	2.368	0.019
	320	2.647	0.035	2.368	0.031	2.905	0.023
D43/1-HNO_3	300	1.222	0.021	1.336	0.016	1.360	0.012
	310	1.925	0.027	2.216	0.018	2.079	0.016
	320	2.647	0.022	2.441	0.019	2.593	0.018

The procedure of the adsorption kinetic measurements is as follows [175]. To begin with, 125 ml 0.03 M adsorbate solution was prepared. Then, the adsorbent was placed into a container with a paddle agitator (60 rpm). Each point on the kinetic curve was determined by pipetting 1 ml of solution and measuring absorbance using a UV-VIS

spectrophotometer. After the absorbance measurement, the liquid sample in the pipette was placed back into the container. The sample preparation was the same for all the adsorption measurements. Each kinetic curve was measured at least twice. The temperature was controlled during the adsorption measurements. The error of the kinetic measurement is not greater than 0.03.

Table 11.2 Phenol acidic pH folder calculation results (the meanings of the collected parameters are presented in the text) [44].

Carbon	T (K)	D_e (10^7 cm^2/s)	σ	D_1 (10^7 cm^2/s)	σ	D_3 (10^7 cm^2/s)	σ
D43/1-pure	300	3.025	0.026	3.089	0.026	2.704	0.016
	310	2.191	0.033	2.663	0.016	2.803	0.015
	320	3.344	0.029	3.542	0.028	4.488	0.009
D43/1-H_2SO_4	300	1.765	0.030	1.590	0.026	1.805	0.023
	310	3.530	0.031	3.101	0.025	3.117	0.016
	320	4.236	0.037	3.791	0.034	4.377	0.027
D43/1-NH_3	300	3.025	0.027	2.773	0.013	2.939	0.012
	310	2.541	0.011	2.575	0.011	2.683	0.010
	320	3.530	0.024	3.363	0.023	4.009	0.011
D43/1-HNO_3	300	3.344	0.050	2.718	0.041	2.156	0.026
	310	2.541	0.039	2.208	0.033	1.868	0.025
	320	3.177	0.045	2.684	0.039	2.207	0.017

In this work the β value was calculated to be $\beta = 1.906\times10^{-4}$ cm^2 (Carbon D43/1: R = 0.0615 cm and L = 0.3687 cm). Some typical fitted results including initial values are listed in Tables 11.1 and 11.2 for phenol adsorption data. Agreement between simulated adsorption curves and experimental results is then subsequently improved by adjusting a_m and a_b. The D_e value at the second column was estimated with the one point formula and the third column is the corresponding standard deviation; the

fourth column is the D_1 value obtained with a one parameter (D_1) fit and the fifth column is the corresponding standard deviation; the sixth column is the D_3 value obtained with a three parameter (D_3, a_m and a_b) fit and the seventh column is the corresponding standard deviation. Two typical curve fits between simulated and experimental curves are shown in Figures 11.1 and 11.2 (for selected phenol adsorption data).

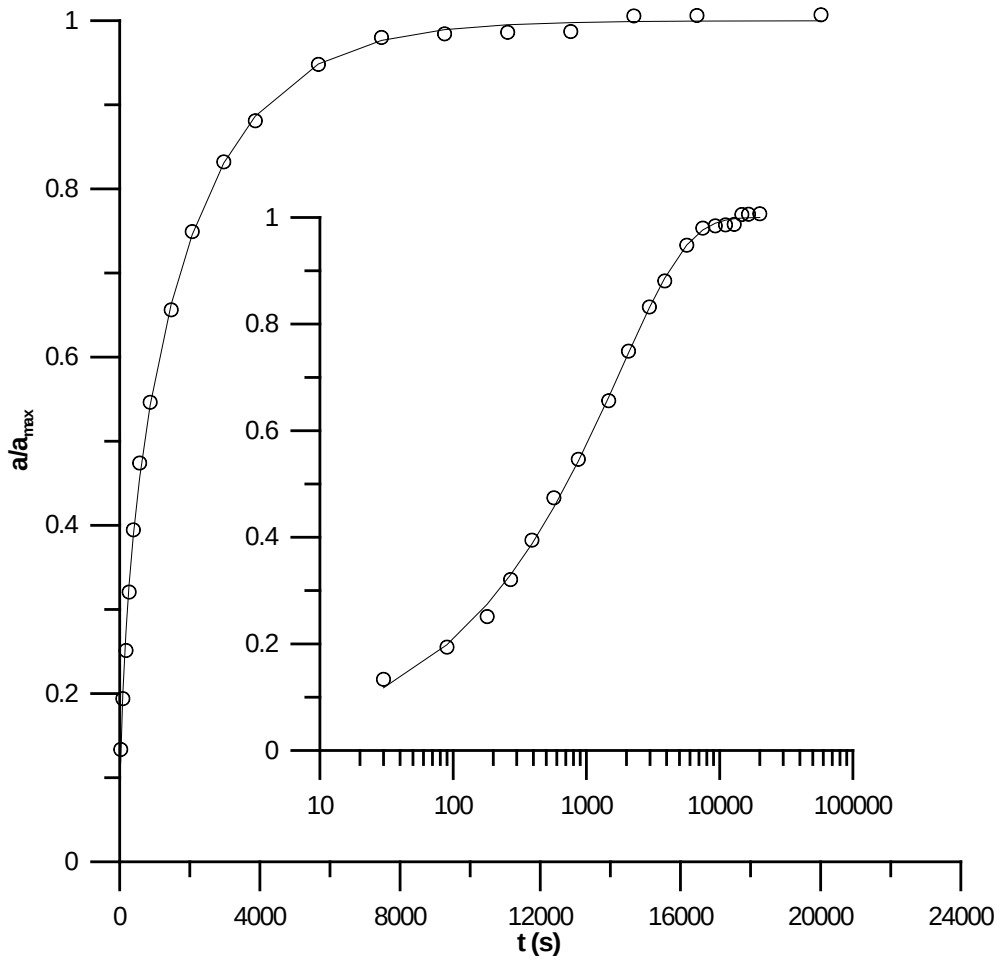

Figure 11.1 Experimental (points) and simulated (line) kinetics of adsorption curves for a finite cylindrical carbon granule with R=0.615 mm, L= 3.687 mm. Adsorption of phenol (acidic pH level) on D43/1-NH_3 at 310 K (Table 11.2). In order to provide the reader with some nuances of the analyzed plots they are also plotted in logarithmic scale (inset) [44].

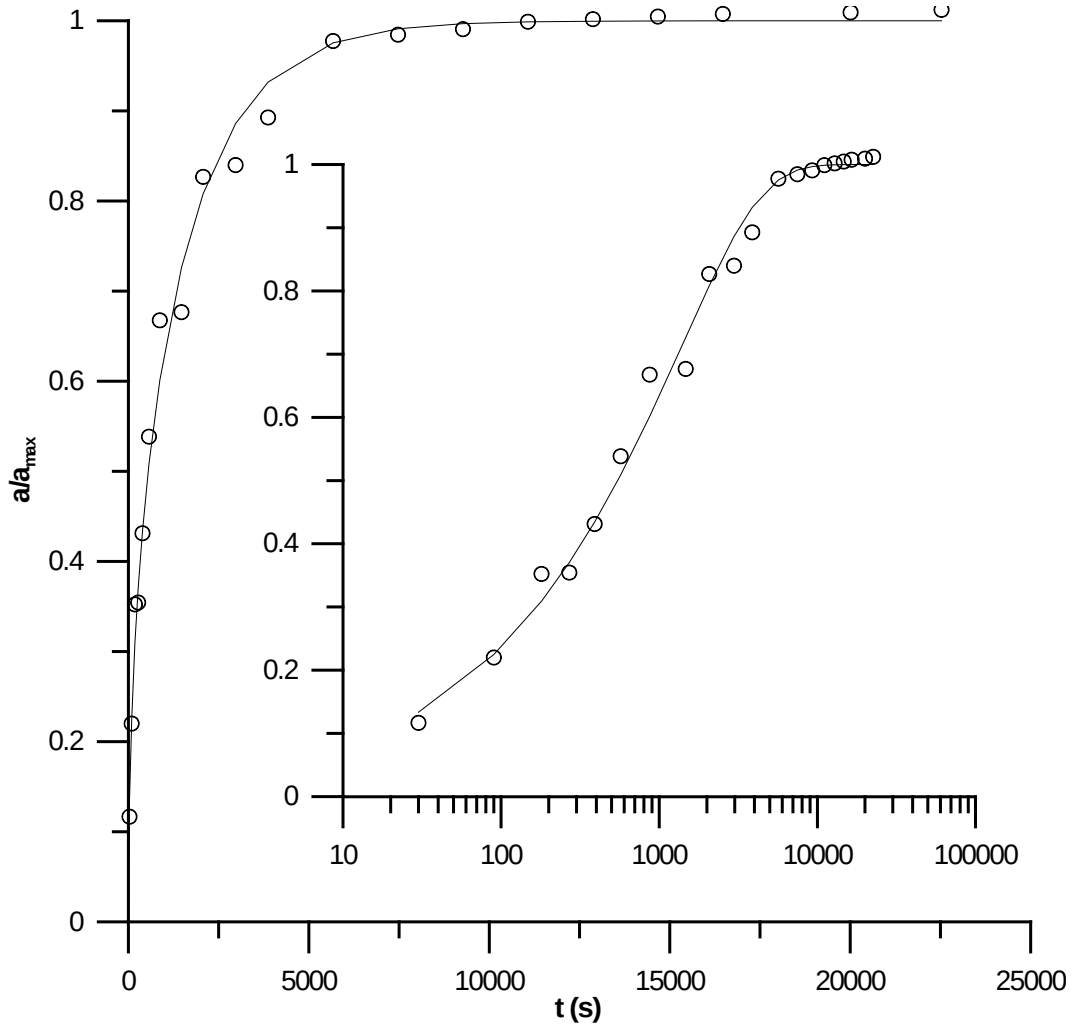

Figure 11.2 Experimental (points) and simulated (line) kinetics of adsorption curves for a finite cylindrical carbon granule with R=0.615 mm, L= 3.687 mm. Adsorption of phenol (neutral pH level) on D43/1-pure at 320 K (Table 11.1). In order to provide the reader with some nuances of the analyzed plots they are also plotted in logarithmic scale (inset) [44].

11.3 Results and Discussion

The advantage of the direct fit method for diffusion coefficient determination is that during the fitting procedure, it can be verified that the factor determining the adsorption kinetic process is the rate of solute transport through the pores which in turn follows Fick's Second Law (Figures 11.1 and 11.2). Figure 11.1 is one of the best

fits from all the results shown in Tables 11.1 and 11.2. It can be seen from Table 11.2 that D_e, D_1 and D_3 values, and standard deviation for D_e, D_1 and D_3 are very similar. This is also seen from Figure 11.1, where, notably, simulated and experimental adsorption overlaps at the half saturation point. It can also be seen from Figure 11.1 that the experimental errors are small and, therefore, the one point formula here is equivalent to the simulation method. As an extreme case, Figure 11.2 shows the worst fit from Tables 11.1 and 11.2. It can be seen from Table 11.1 that D_e, D_1 and D_3 values differ and that the standard deviation for D_e, D_1 and D_3 also decreases as expected with a three parameter fit. Compared with Figure 11.1, errors in four measurements in Figure 11.2 are clearly evident for the normalised adsorption values 0.66, 0.67, 0.83 and 0.88. In other words, curve fitting methods provided better precision than the single point method and become increasingly important with increased experimental errors. Average standard deviations (equation 11.5) calculated for all the studied systems decrease from phenol adsorbed at acidic pH up to acetanilide at the same pH in the sequence: *ph* ac (σ=0.0173) > *pa* nt (σ=0.0181) > *ph* nt (σ=0.0198) > *ac* nt (σ=0.0221) > *pa* ac (σ=0.0236) > *an* nt (σ=0.024) > *ac* ac (σ=0.032).

An analysis of bipartite expressions, equation 11.1, shows that errors increase with time up to the joint point and decrease with time after the joint point [43]. For most of the adsorption process, dimensionless time for an infinite planar sheet is less than the time at the joint point, 0.05326 [43], i.e., only equation 11.1a needs to be used. Therefore, the error for an infinite planar sheet calculation is negligible and the error for adsorption calculation of the finite cylinder mainly comes from adsorption calculation of the infinite cylinder.

Overall, the diffusion coefficient increases with temperature except for some special cases. The irregularities can be caused by the appearance of chemisorption [179]. Generally, diffusion coefficients are larger in acidic solutions than in neutral solutions, as shown by the comparison of Tables 11.1 and 11.2. We can also note that the diffusion coefficient decreases as molecular weight increases from aniline (MW93), phenol (MW94), acetanilide (MW135) and acetaminophen (MW151).

Finally, it is interesting to study how the diffusion coefficient depends upon the chemical composition of the carbon surface layer. This is possible since all the D43/1 carbons have almost the same pore size distributions [179] as was shown using the Density Function Theory (DFT) and Nguyen and Do Model (ND) [180]. Figure 11.3 shows some selected correlations. Since it was recently shown [178] that the energy of diffusion depends upon the carbon surface chemical composition we expect similar dependence for the diffusion coefficients calculated by the method from this study. It was shown that for studied systems the surface diffusion mechanism dominates [163, 181]. Miyabe and Takeuchi [182], considering the mechanism of surface diffusion, showed that this type of diffusion can be regarded as molecular diffusion restricted due to the adsorptive interaction between adsorbed molecules and the surface. One can see that for all studied adsorbates mainly carbon “basic” surface groups diminish diffusivity. Therefore, the interactions of diffusing molecules mainly with those groups are crucial (for some cases also the important role of surface “carbonyls” is seen). On the other hand, the interaction between aniline (being the most basic compound among studied ones) and strongly acidic surface groups influences the diffusion coefficients for this adsorbate.

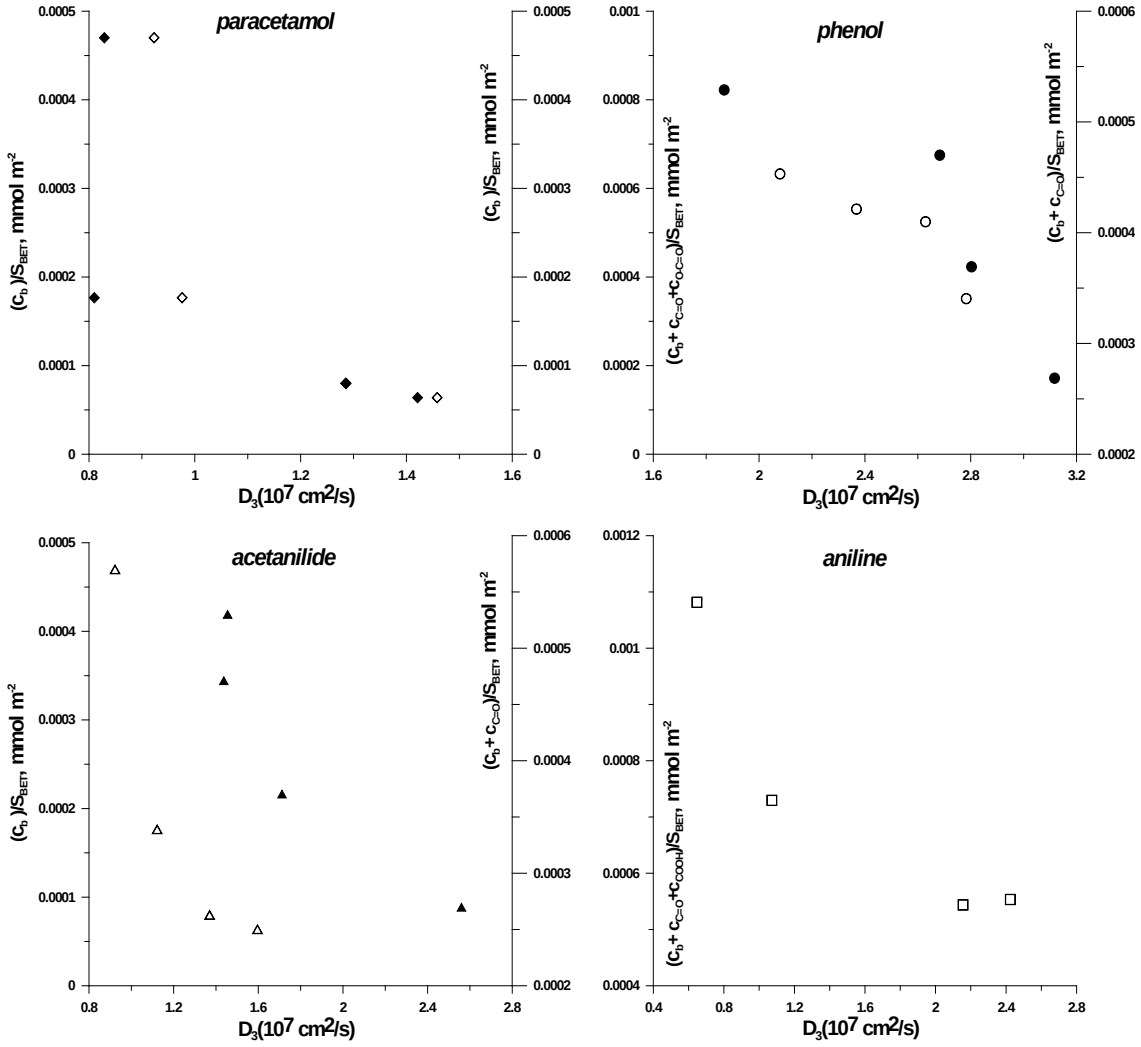

Figure 11.3 The dependence of the D_3 (calculated by the method described in this study) on the concentration of surface groups determined from the Boehm titration method (data for T = 320 K are shown). Open symbols are the data determined at the neutral pH value (7.0**)** (left *y* axis), close symbols for the acidic pH value (1.54) (right *y* axis) [44].

11.4 Conclusion

Effective diffusion coefficients *D* of acetanilide, aniline, acetaminophen and phenol adsorption within D43/1 carbons at neutral and acidic solutions and different temperatures (300, 310 and 320 K) were computed. The *D* value is larger in acidic

solution than that in neutral solution and increases with the temperature. The effective diffusion coefficient changes with surface modification and for studied systems the concentration of basic surface sites mainly determines its value.

We verified the expression for adsorption within cylindrical granules which were used to determine the effective diffusion coefficient by direct fit of a calculated adsorption curve to experimental data based on an initial diffusion coefficient estimated by a one point formula. This simple bipartite expression and simulation method for effective diffusion coefficient determination is generally applicable for mass transport in a cylindrical matrix, for example, designing a biodegradable polymeric carrier to provide controlled drug release.

Chapter 12 Conclusions and Continuing Work

In this chapter the contributing researches will be summarised. This thesis is primarily a progress report, and illustrates the current and ongoing researches.

12.1 Conclusions

The most commonly used quantity in diffusion studies is concentration, *c*. This is quantitatively linked to diffusion displacement $y = \int cdx / c_0 = f(t)$ where c_0 is the initial concentration and from that to time constant $t_c = f^{-1}(y)$ and diffusion rate $v = \partial y / \partial t$. For a semi-infinite diffusion system, these parameters are: $y = 2\sqrt{Dt/\pi}$, $t_c = \pi y^2 / 4D$ and $v = \sqrt{D/\pi t}$. Expressions for concentrations are different for different types of diffusion construct (geometrical shape, initial and boundary conditions) therefore expressions for diffusion displacement, diffusion time constant and diffusion rate are different. Use of the concentration gradient $\partial C / \partial x$, where $C = c/c_0$, is proposed at the diffusion driving force to analyse concentration change in the semi-infinite diffusion systems. This is an example for analysing biosensor behaviour using diffusion theory.

In Section 1.4, a one dimensional outer membrane mass transport limit model was used to analyse a biosensor. The current output of a biosensor is inversely proportional to the diffusion resistance to the surface L/D (L is the membrane thickness and D is diffusion coefficient) whereas the time constant is proportional to L^2/D. From this theoretical insight it was possible to use thinner, multi layered membrane structures instead of single thick layer membranes to achieve similar current responses but with much more rapid responses to glucose and lactate. If it is

assumed that both L and D are reduced to half their original values and the diffusion resistance keeps constant, then the time constant is reduced to half its original value. A multi-layered structure is used to reduce the diffusion coefficient because the interface between neighbouring layers contributes to the overall diffusion resistance but much less to the thickness. A fast sensor response is a key requirement for continuously tracking concentrations for external sample diffusion coefficient determinations.

Besides the conceptual understanding of diffusion phenomena, a series of accurate, simple, mathematical solutions to concentration (gradient) determination have been constructed. This has been applied to solute diffusion in simple geometrical matrices: planar sheets, cylinders and spheres under various initial and boundary conditions. Previous reported solutions were expressed in infinite mathematical series and therefore not easy to use. The key novelty of the expressions presented here is that they have very limited terms. Microsoft Excel is sufficient for this computation, which conveniently avoids finite element methods. These expressions have been used in my own work and to re-analyse the reported data and have advanced the calculations that can be applied. Work has included (where specified) the analysis of data from collaborators.

To measure glucose (lactate) concentrations in a cylindrical collagen gel, a collagen gel without substrate was immersed in a solution of the substrate. Substrate concentrations at the centre of the collagen gel were then tracked and simulated. The diffusion coefficient in collagen was thus determined by fitting the simulated concentration profiles to observed data (Chapter 2 and Chapter 3).

The expressions for concentration evolution in membranes are expressed in infinite series and improper simplification led to errors. The accurate but simple bipartite expressions have thus been constructed (Chapter 4).

Membrane covered planar electrode systems have previously been developed to measure electrochemical solute diffusion coefficients in the membrane. However, amperometric currents (concentration gradient) expressed in infinite series has limited applications of the model and led to errors (Chapter 6). Work with amperometric currents at membrane covered electrodes has simplified this and reduced errors (Chapter 5). This expression can be calculated with a calculator and gives the membrane covered planar electrode system a valid new application for *D* value determination. For this, solute diffusion coefficients in various polymeric membranes have been determined by fitting simulated to experimental current transients (Chapter 7 and Chapter 8).

A microfluidic system provides an efficient, economic way to study mass transport. Past expressions for mass transport in microfluidic system are again reported using infinite series, which delay experimental development. Expressions for concentrations and concentration gradients in a dual flow microfluidic system (Chapter 9) allowed measurement of the diffusion coefficient of ammonia in aqueous solution.

Drug release curves have been used to characterise drug release rates. However, these depend on the drug concentration, substrate size and geometrical shape. Expressions for drug release from cylindrical and spherical granules are presented in Chapter 10.

With these expressions, the acetaminophen diffusion coefficient has been determined from adsorption kinetics at porous carbon; the work was in collaboration with the Nicolaus Copernicus University, Poland (Chapter 11).

In summary, a series of expressions for solute transport in matrices of different shapes and phases under various initial and boundary conditions have been obtained and used to derive one-point methods for diffusion coefficient estimation. The expressions provide theoretical support for general mass transport studies.

12.2 Continuing Work

Various aspects of work are still continuing. In this section, this ongoing experimental work is completed and will need to be analysed mathematically.

Photonic crystal fibres (PCF) are usually used for optical purposes; however, these PCF fibres of transparent mechanical materials have been used to form a recessed electrode. O_2, hydrogen peroxide and acetaminophen diffusion coefficients in agarose gels and solutions with this recessed electrode have been determined. This is a new type of diffusion measurement platform usable for soft gels and aqueous samples.

Water vapour diffusion in packaging materials is a very important parameter for encapsulating medical devices *in vivo*. Collaborators have recorded water absorption in polyurethane and silicon rubber membranes. From the water absorption kinetics data, it is expected to determine diffusion coefficients and diffusion activation energies.

The effect of static compression on the mass transport property of tissue engineering scaffolds has attracted much interest. Single compressed and double compressed collagen gels (used to form collagen tissue mimics at the Tissue Engineering Centre, University College London) have allowed lactate diffusion coefficients under compressive change to be measured.

A group at the Institute of Chemistry, Chinese Academy of Sciences, Beijing, China, have worked for many years on controlled drug release. Diffusion coefficients have been measured by light refraction. However, a finite hydrogel block in an infinite reservoir has been used to approximate a finite hydrogel in a finite reservoir. Data on Ketoprofen release from Poly(acrylamid-co-acrylic acid) hydrogel is being used to analyse data with an improved model.

A membrane covered glucose biosensor will be studied to characterise the mass transport properties of specific covering materials. Ultimately, such parameters will allow the refinement of a model for glucose biosensors.

Characterisation of the mass transport property of the engineered scaffolds to be replaced is limited. As a living tissue, it is important to characterise its mass transport property. So, when the engineered tissue is implanted back into body, the engineered scaffold should match the rest of tissues for a proper recovery. The other point is that the types of tissues need to be grown in a bioreactor. For example, all natural tissues are heterogeneous. So, the next generation of tissue scaffolds should be 3D, heterogeneous. Study of natural cartilage is planned with the measurement of hydrogen peroxide and acetaminophen diffusion coefficients.

References

1. Crank J. The Mathematics of Diffusion, Clarendon Press, Oxford, 2nd edn., 1979

2. Abramowitz M, Stegun IA. Handbook of Mathematical Function. Dover Publications, Inc. New York. 1972.

3. Stucher M, Struk A, Altmeyer P, Herde M, Baumgrtl H, Lubers DW. J Physiol. 2002;538:985.

4. Heller A. Phys Chem Chem Phys. 2010;12:9972.

5. Jackson AR, Gu WY. Curr Rheumatol Rev. 2009;5:40.

6. Wheeler-Kingshott CAM, Barker GJ, Steens SCA, van Buchem MA. The Diffusion of Water, in ed. Tofts P. Quantitative MRI of the Brain, John Wiley & Sons, Ltd. 2003.

7. Mitchem L, Mio C, Snook RD. Anal Chim Acta. 2004;511:281.

8. Shnthirasingham C, Oyiliagu CE, Cao X, Gouin T, Wania F, Lee S, Pozo K, Harner T, Muir DCG. J Environ Monit. 2010;12:1650.

9. Cussler EL. Diffusion Mass Transfer in Fluid System. Cambridge University Press, Cambridge. 1989.

10. Barnes C. Phys. 1934;5:4.

11. Mills R, Woolf LA, Watts RO. AIChE J. 1968;14:671.

12. Dai H, Chen Q, Qin H, Guan Y, Shen D, Hua Y, Tang Y, Xu J. Macromolecules. 2006;39:6584.

13. Mahon PJ, Oldham KB. Anal Chem. 2005;77:6100.

14. Bowers RC, Wilson AM. J Am Chem Soc. 1958;80:2968.

15. Levich VG. Physicochemical Hydrodynamics, Prentice-Hall Inc. UK. 1962.

16. Gough DA, Leypoldt JK. Anal Chem. 1979;51:439.

17. Vadgama P, Desai M, Crump P. Electroanalysis. 1991;3:597.

18. Wilkins E, Atanasov P. Med Eng Phys. 1996;18:273.

19. Pearson J E, Gill A, Vadgama P. Ann Clin Biochem. 2000;37:119.

20. Wilson GS, Hu Y. Chem Rev. 2000;100:2693.

21. Wisniewski N, Reichert M. Colloids Surf B: Biointerf. 2000;18:197.

22. Clark LC, Lyons C. Ann NY Acad Sci. 1962;102:29.

23. Updike SJ, Hicks GP. Nature. 1967;214:986.

24. Shichiri M, Kawamori R, Yamasaki Y, Hakui N, Abe H. Lancet. 1982;20:1129.

25. Churchouse SJ, Battersby CM, Mullen WH, Vadgama PM. Biosensors. 1986;2: 325.

26. Pfeiffer EF. Diabetologia. 1987;30:51.

27. Bindra DS, Zhang Y, Wilson GS, Sternberg R, Thevenot DR, Moatti D, Reach G. Anal Chem. 1991;63:1692.

28. Chen CY, Tamia E, Ishihara K, Kosugi Y, Su YC, Nakabayashi N, Narube I. App Biochem Biotech. 1992;36:211.

29. Harrison DJ, Turner RFB, Baltes HP. Anal Chem. 1988;60:2002.

30. Rong Z, Cheema U, Vadgama P. Analyst. 2006;131:816.

31. Rong Z, Leitao E, Popplewell J, Alp B, Vadgama P. IEEE Sensors J. 2008;8:113.

32. Cheema U, Rong Z, Kirresh O, MacRobert AJ, Vadgama P, Brown RA. J Tissue Eng Regen Med. 2012;6:77.

33. Rong Z, Vadgama P. Biophys J. 2006;91:4690.

34. Rong Z, Vadgama P. J Electroanal Chem. 2008;614:166.

35. Rong Z, Vadgama P. Biomaterials. 2006;27:4266.

36. Rong Z, Rashid S, Vadgama P. Electroanalysis. 2006;18:1703.

37. Rong Z, Vadgama P. Electrochim Acta. 2009;54:4949.

38. Zorlutuna P, Rong Z, Vadgama P, Hasirci V. Acta Biomater. 2009;5:2451.

39. Chang H, Khan R, Rong Z, Sapelkin A, Vadgama P. Biofabrication. 2010;2:035002.

40. Kacanovska A, Rong Z, Schmidt M, Russell PJ, Vadgama P. Anal Bioanal Chem. 2010;398:1687.

41. Rong Z, Vadgama P. Int J Transport Phenomena. In revision.

42. Nair G, Garguili J, Shiju R, Rong Z, Shapiro E, Drikakis D, Vadgama P. ChemBioChem. 2006;7:1683.

43. Rong Z, Vadgama P. J Colloid Interf Sci. 2006;303:75.

44. Rong Z, Terzyk AP, Gauden PA, Vadgama P. J Colloid Interf Sci. 2007;313:449.

45. Leddy HA, Awad HA, Guilak F. J Biomed Mater Res B. 2004;30:397.

46. Awad HA, Wickham MQ, Leddy HA, Gimble JM, Guilak F. Biomater. 2004;25:3211.

47. Vicente AA, Dluhý M, Ferreira EC, Mota M, Teixeira FA. Biochem Eng J. 1998;2:35.

48. Bashkatov AN, Genina EA, Sinichkin YP, Kochubey VI, Lakodina NA, Tuchin VV. Biophys J. 2003;85:3310.

49. Kauri LM, Jung SK, Kennedy RT, Biochem Biophys Res Commun. 2003;304:371.

50. Churchouse SJ, Battersby CM, Mullen WH, Vadgama PM. Biosensors. 1986;2:325.

51. Longsworth LG. J Am Chem Soc. 1952;74:4155.

52. Longsworth LG. J Am Chem Soc. 1953;75:5705.

53. Dionne KE, Cain BM, Li RH, Bell WJ, Doherty EJ, Rein DH, Lysaght MJ, Gentile FT. Biomater. 1996;17:257.

54. Curcio E, Bartolo LD, Barbieri G, Rende M, Giorno L, Morelli S, Drioli E. J Biotech. 2005;117:309.

55. Phanthong C, Somasundrum M. J Electroanal Chem. 2003;558:1.

56. Chai Y., Mei LH, Lin DQ, Yao SJ. J Chem Eng Data. 2004;49:475.

57. Teixeira JA, Mota M, Venâncio A. Chem Eng J. 1994;56:B9.

58. Hannoun BJM, Stephanopoulos G. Biotechnol Bioeng. 1986;28:829.

59. Shaw M, Schy A. Biophys J. 1981;34:375.

60. Wu DQ, Zhang GL, Shen C, Zhao Q, Li H, Meng Q. World J Gastroenterol. 2005;11:1599.

61. Weng L, Liang S, Zhang L, Zhang X, Xu J. Macromol. 2005;38:5236.

62. Zhang T, Fang HHP. Environ Technol. 2005;26:155.

63. Taveira P, Mendes A, Costa C. J Membr Sci. 2003:221:123.

64. Rutherford SW, Do DD. Adsorpt. 1997;3:283.

65. Gough DA, Leypoldt JK. Anal Chem. 1980;52:1126.

66. Brown RA, Wiseman M, Chuo CB, Cheema U, Nazhat SN. Adv Funct Mater. 2005;15:1762.

67. Eastwood M, Porter R, Khan U, McGrouther G, Brown R. J Cell Physiol. 1996;166:33.

68. Carslaw HS, Jaeger JC. Conduction of Heat in Solids. Oxford University Press, Oxford, 2nd edn., 2005.

69. Özişik MN. Heat Conduction. John Wiley & Sons, New York. 1980.

70. Carsten HRF, McKerrow NW. Philos Mag. 1944;35:812.

71. Kim TJ, Jurng TH, Chung UH, Hong SI, Sens Actuators, B 2001;72:11.

72. Obradovic B, Carrier RL, Vunjak-Novakovic G, Freed LE, Biotechnol Bioeng. 1999;63:197.

73. Shram N, Netchiporouk L, Cespuglio R. Eur J Neurosci. 2002;16:461.

74. Okuda C, Sawa T, Harada M, Murakami T, Matsuda T, Tanaka Y. Am J Physiol. (Endocrinol Metab) 1992;26:E1035.

75. Fuse A. J Anesth. 1999;13:161.

76. Gutierrez G, Palizas F, Doglio G, Wainsztein N, Gallesio A, Pacin J, Dubin A, Schiavi E, Jorge M, Pusajo J, Klein F, Roman ES, Dorfman B, Shottlender J, Giniger R. Lancet. 1992;339:195.

77. Broder G, Weil MH. Science. 1964;143:1457.

78. Bakker J, de Lima AP. Crit Care. 2004;8:96.

79. Trzeciak S, Chansky ME, Dellinger RP, Hollenberg SM, Parrillo JE, Acad Emerg Med. 2006;15:S150.

80. Pittard AJ Ann Clin Biochem. 1999;36:401.

81. Pyne DB, Boston T, Martin DT, Logan A. Eur J Appl Physiol. 2000;82:112.

82. Pfitzinger P, Freedson PS, Int J Sports Med. 1998;19:349.

83. Yang L, Kissinger PT, Ohara T. Curr Sep. 1995;14:31.

84. Burmeister JJ, Palmer M, Gerhardt GA. Biosens Bioelectron. 2005;20:1772.

85. Kurita R, Hayashi K, Fan X, Yamamoto K, Kato T, Niwa O. Sens Actuators B. 2002;87:296.

86. Wu M, Lin Z, Li Y, Ren S. Sens Actuators B. 2000;66:269.

87. Marzouk SAM, Cosofret VV, Buck RP, Yang H, Cascio WE, Hassan SSM. Anal Chem. 1997;69:2646.

88. Pfeiffer D, Möller B, Klimes N, Szeponik J. Biosens Bioelectron. 1997;12:539.

89. Lafrance D, Lands LC, Burns DH. Vib Spectrosc. 2004;36:195.

90. Ellmerer M, Schaupp L, Trajanoski Z, Jobst G, Moser I, Urban G, Skrabal F, Wach P. Biosens Bioelectron. 1998;13:1007.

91. Guiseppi-Elie A, Brahim S, Slaughter G, Ward KR. IEEE Sensors J. 2005;5:345.

92. Ahmed S, Dack C, Farace G, Rigby G, Vadgama P. Anal Chim Acta. 2005;537:153.

93. Sotak CH. J Magn Reson. 1990;90:198.

94. Pfeuffer J, Lin JC, DelaBarre L, Ugurbil K, Garwood M. J Magn Reson. 2005;177:129.

95. Hazel JR, B. D. Sidell BD. Anal Biochem. 1987;166:335.

96. Kyröläinen M, Reddy SM, Vadgama PM. Anal Chim Acta. 1997;353:281.

97. Zhang X, Lin J, Cardoso L, Broderick M, Darley-Usmar V. Electroanalysis. 2002;14:697.

98. Hoare JP. The Electrochemistry of Oxygen, New York: Interscience Publishers, 1968.

99. Schneiderman G, Goldstick TK, J Appl Physiol Respirat Environ Exercise Physiol. 1978;45:145.

100. Jeong R, Hwang JY, Joo S, Chung TD, Park S, Kang SK, Lee W, Kim HC. Biosens Bioelectron. 2003;19:313.

101. Gredell JA, Turnquist PA, MacIver MB, Pearce RA. Br J Anaesth. 2004;93:810.

102. Goteti K, Masaki T, Kuji T, Leypoldt JK, Cheung AK, Kern SE. Pharm Res. 2006;23:718.

103. Akimoto T, Nagase Y. J Control Release 2003;88:243.

104. Daynes HA. Proc R Soc. 1920;*A*97:286.

105. Aguiar FA, Gallant AJ, Rosamond MC, Rhodes A, Wood D, Kataky R. Electrochem Commun. 2007;9:879.

106. Ito T, Audi AA, Dible GP. Anal Chem. 2006;78:7048.

107. Amatore C, Oleinick AI, Svir I. J Electroanal Chem. 2006:597:77.

108. Gavaghan DJ, Gillow K, Süli E, Langmuir 2002;22:10666.

109. Bond AM, Luscombe D, Oldham KB, Zoski CG. J Electroanal Chem. 1988;249:1.

110. Kralj B, Dryfe RAW. Phys Chem Chem Phys. 2001;3:3156.

111. Bowers RC, Wilson AM. J Am Chem Soc. 1958;80:2968.

112. Oglesby DM, Omang SH, Reilley CN. Anal Chem. 1965;37:1312.

113. Daum P, Lenhard JR, Rolison D, Murray RW. J Am Chem Soc. 1980;102:4649.

114. Abdelsalam ME, Denuault G, Daniele S. Anal Chim Acta. 2002;452:65.

115. Brown RJC, Milton MJT. IEEE Trans Instrum Meas. 2007;56:280.

116. Kao H, Chang CG. Acta Sci Nat Univ Nankin. 1964;8:401.

117. Kao H, Chang CG. Acta Sci Nat Univ Nankin. 1965;9:326.

118. Chovnyk NG, Vashchenko VV, Zh Fiz Khim. 1963;37:538.

119. Aoki K, Osteryoung J. J Electroanal Chem. 1981;122:19.

120. Shoup D, Szabo A. J Electroanal Chem. 1982;140:237.

121. Cottrell Z. Z Phys Chem. 1902;42:385.

122. Compañ V, Tiemblo P, García F, García JM, Guzmán J, Riande E. Biomater. 2005;26:3783.

123. Vadgama P, Desai M, Crump P, Electroanal. 1991;3:597.

124. Cook KE, Perlman CE, Seipelt R, Backer CL, Mavroudis C, Mockros LF. ASAIO J. 2005;51:404.

125. Garr-Peters JM, Ho CS. Crit. Rev. Biomed. Eng. 1987;14:289.

126. McBreen J, Nanis L, Beck W. J. Electrochem. Soc. 1966;113:1218.

127. Yen SK, Shih HC. J. Electrochem. Soc. 1988;135:1169.

128. Kimble MC, White RE, Tsou YM, Beaver RN. J Electrochem Soc. 1990;137:2510.

129. Tarnowski DJ, Bekos EJ, C. Korzeniewski C. Anal Chem. 1995;67:1546–1552.

130. Compañ V, Villar MA, Vallés E, Riande E. Polym. 1996;37:101.

131. Kim TJ, Jurng TH, Chung UH, Hong SI, Sens Actuators B. 2001;72:11.

132. Fang HHP, Shi X. J Membr Sci. 2005;264:161.

133. Silva Luz RDC, Damos FS, de Oliveira AB, Beck J, Kubota LT. Sens Actuators B. 2006;117:274.

134. Bard AJ, Faulkner LR. Electrochemical Methods. John Wiley & Sons, New York. 1980.

135. Taveira P, Mendes A, Costa C, J Membr Sci. 2003;221:123.

136. Falk B, Garramone S, Shivkumar S. Mater Lett. 2004;58:3261.

137. Terzyk AP. J Colloid Interf Sci. 2000;230:219.

138. Zhang J, Cai Z, Cong W, Su Z, Ouyang F. Sep Sci Technol. 2002;37:3039.

139. Cofan C, Radovan C. Sensors 2008;8:3592.

140. Christie I, Leeds S, Baker M, Keedy F, Vadgama P. Anal Chim Acta. 1993;272:145.

141. Li M, Jing L. Electrochim Acta. 2007;52:3250.

142. Lide DB, Frederikse HPR. CRC Handbook of Chemistry and Physics. CRC Press, London. 1993.

143. Wen W, Zhao H, Zhang S, Pires V. J Phys Chem C. 2008;112:3875.

144. Hahn CEW. Analyst. 1998;123:57R.

145. Winlove CP, Parker KH, Oxenham RKC. J Electroanal Chem. 1984;170:293.

146. Guzmán J, Iglesias MT, Riande E, Compañ V, Andrio A. Polym. 1997;38:5227.

147. Miner DJ, Rice JR, Riggin RM, Kissinger PT. Anal Chem. 1981;53:2258.

148. Razmi H, Harasi M. J Iran Chem Soc. 2008;5:296.

149. Itoh K, Kubo W, Fujiwara M, Watanabe H, Miyazaki S, Attwood D, Biol Pharm Bull. 2006;29:343.

150. Bond AM, Luscombe D, Oldham KB, Zoski CG. J Electroanal Chem. 1988;249:1.

151. Atencia J, Beebe DJ. Nature. 2005;437:648.

152. Costin CD, Synovec RE. Anal Chem. 2002;74:4558.

153. Costin CD, McBrady AD, McDonnell ME, Synovec RE. Anal Chem. 2004;76:2725.

154. McBrady AD, Synovec RE. J Chromatogr. 2006;1105:2.

155. Yang M, Yang J, Li CW. Zhao, J. Lab Chip**.** 2002;2:158.

156. Hatch A, Kamholz AE, Hawkins KR, Munson MS, Schiling EA, Weigl BH, Yager P. Nat Biotechnol. 2001;19:461.

157. Kamholz AE, Yager P. Biophys J. 2001;80:155.

158. Munson MS, Hawkins KR, Hasenbank MS, Yager P. Lab Chip. 2005;5:856.

159. Magennis SW, Graham EM, Jones AC. Angew Chem Int Ed. 2005;44:6512.

160. Schönfeld F, Hessel V, Hofmann C. Lab Chip**.** 2004;4:65.

161. Wu Z, Nguyen NT, Huang X. *J*. Micromech Microeng. 2004;14:604.

162. Nguyen NT, Wu Z. *J*. Micromech Microeng. 2005;15:R1.

163. Terzyk AP, Gauden PA. J Colloid Interf. Sci. 2002;249:256.

164. Terzyk AP, Rychlicki G, Biniak S, Lukaszewicz JP. J Colloid Interf. Sci. 2003;257:13.

165. Perry RH, Green DW, Maloney JO. Perry's Chemical Engineers' Handbook. Seventh Ed., McGraw – Hill, New York. 1997.

166. Timofiejev DP. Physisorption Kinetics Izd. AN. SSSR. 1962. [In Russian]

167. Radin S, Ducheyne P, Kamplain T, Tan BH. J Biomed Mater Res. 2001;57:313.

168. Kast CE, Valenta C, Leopold M, Bernkop-Schnürch A. J Control Release. 2002;81:347.

169. Langoth N, Kalbe J, Bernkop-Schnürch A. Int J Pharm. 2003;252:141.

170. Bernkop-Schnürch A, Guggi D, Pinter Y. J Control Release. 2004;94:177.

171. Hasegawa M, Sudo A, Komlev VS, Barinov SM, Uchida A. J Biomed Mater Res Part B. 2004;70:332.

172. Radin S, El-Bassyouni G, Vresilovic EJ, Schepers E, Ducheyne P. Biomater. 2005;26:1043.

173. Terzyk AP. J Colloid Interf Sci. 2002;247:507.

174. Terzyk AP. Adsorpt Sci Technol. 2000;18:477.

175. Terzyk AP, Gauden PA. Separat Sci Technol. 2001;36:513.

176. Smith RW, Booth J, Massingham G, Clough AS. Polym. 2004;45:4893.

177. Zhang X, McAuley KB, Goosen MFA. J Control Release. 1995;34:175.

178. Terzyk AP, J Colloid Interf. Sci. 2004;275:9.

179. Terzyk AP, J Colloid Interf Sci. 2003;268:301.

180. Nguyen C, Do DD. Langmuir 2000;16:1319.

181. Terzyk AP. J Colloid Interf Sci. 2004;272:59.

182. Miyabe K, Takeuchi S. J Phys Chem B. 1997;101:7773.

183. Lango T, Morland T, Brubakk AO. Undersea Hyperbaric Med. 1996;23: 247.

184. Campbell GS, Calissendorff C, Williams JH. Soil Sci Soc Am J. 1991;55:291.

185. Davies M, Tirovic M, Ye Z, Baker PH. Building Serv Eng Res Technol. 2004;25:175.

186. Wang W, Winlove CP, Michel CC. J Physiol. 2003;549:855.

187. Kondepati VR, Heise HM. Anal Bioanal Chem. 2007:388:545.

188. Rigby GP, Crump PW, Vadgama P. Analyst. 1996;121;871.

189. Shin JH, Schoenfisch MH. Analyst. 2006;131:609.

190. Koschwanez HE, Reichert WM. Biomater. 2007;28:3687.

191. Gifford R, Kehoe JJ, Barnes SL, Kornilayev BA, Alterman MA, Wilson GS. Biomater. 2006;27:2587.

192. Kaya T, Numai D, Nagamine K, Aoyagi S, Shiku H, Matsue T. Analyst. 2004;129:529.

193. Saito T, Wu CC, Shiku H, Yasukawa T, Yokoo M, Ito-Sasaki T, Abe H, Hoshi H, Matsue T. Analyst. 2006;131:1006.

194. Banaji M, Mallet A, Elwell CE, Nicholls P, Cooper C. PLoS Computational Biology 2008;4:e1000212.

195. Cochran DM, Fukumura D, Ancukiewicz M, Carmeliet P, Jain RK. Ann Biomed Eng. 2006;34:1247.

196. Jung SK, Gorski W, Aspinwall CA, Kauri LM, Kennedy RT. Anal Chem. 1999;71:3642.

Appendix List of Publications

1. Cheema, Umber; **Rong**, **Zimei**; Kirresh, Omar; Macrobert Alexander J; Vadgama, Pankaj; Brown, Robert A.
   Oxygen Diffusion through Collagen Scaffolds at Defined Densities: Implications for Cell Survival in Tissue Models.
   Journal of Tissue Engineering Regenerative Medicine, (**2012**) 6(1) 77 – 84.
2. Ekemen, Zeynep; Chang, Hong; Ahmad, Zeeshan; Bayram, Cem; **Rong, Zimei**; Denkbas, Emir Baki; Stride, Eleanor; Vadgama, Pankaj; Edirisinghe, Mohan.
   Application Actuated Fabrication of Biomaterials via Controlled Protein Bubble Generation and Manipulation.
   Biomacromolecules, (**2011**) 12(12) 4291 – 4300.
3. Kacanovska, Anna; **Rong**, **Zimei;** Schmidt, Markus; Russell, Philip St. J. Vadgama, Pankaj.
   Bio-sensing Using Recessed Gold Filled Capillary Amperometric Electrodes.
   Analytical and Bioanalytical Chemistry, (**2010**) 398 1687 – 1694.
4. Chang, Hong; Khan, Rachel; **Rong**, **Zimei;** Sapelkin, Andrei; Vadgama, Pankaj.
   Study of Albumin and Fibrinogen Membranes Formed by Interfacial Crosslinking Using Microfluidic Flow.
   Biofabrication, (**2010**) 2 035002 (10 pp).
5. Zorlutuna, Pinar; **Rong**, **Zimei**; Vadgama, Pankaj; Hasirci, Vasif.
   Influence of Nanopatterns on Endothelial Cell Adhesion: Enhanced Cell Retention under Shear Stress.
   Acta Biomaterialia, (**2009**) 5 2451 – 2459.
6. Sharifi, Shahriar; Mirzadeh, Hamid; Imani, Mohammad; **Rong**, **Zimei**;

Jamshidi, Ahmad; Shokrgozar, Mohammad Ali; Atai, Mohammad; Roohpour, Nima.

Injectable In Situ Forming Drug Delivery System Based on Poly(ε-Caprolactone Fumarate for Tamoxifen Citrate Delivery: Gelation Characteristics, In Vitro Drug Release and Anti-Cancer Evaluation.

Acta Biomaterialia, (**2009**) 5 1966 – 1978.

7. **Rong**, **Zimei**; Vadgama, Pankaj.

   An Electrochemical Method for Measurement of Mass Transport in Polymer Membranes Using Acetaminophen as a Model System.

   Electrochimica Acta, (**2009**) 54 4949 – 4953.

8. Whittaker, Robert; Booth, Richard; Dyson, Rosemary; Bailey, Clare; Chini, Louise Parsons; Naire, Shailesh; Payvandi, Sevil; **Rong**, **Zimei**; Woollard, Hannah; Cummings, Linda; Waters, Sarah; Mawasse, Lina; Chaudhuri, Julian; Ellis, Marianne; Michael, Vipin; Kuiper, Nikki; Cartmell, Sarah.

   Mathematical Modelling of Fibre-enhanced Perfusion inside a Tissue-engineering Bioreactor.

   Journal of Theoretical Biology, (**2009**) 256(4) 533–546.

9. Brown, Robert A; Cheema, Umber; Alp, Burcak; **Rong**, **Zimei**; Mudera, Vivek; MacRobert, Alexander J.

   *Perfusion and Tissue Engineering Scaffolds: Micro versus Nano Pores***.**

   Tissue Engineering, (**2008**) 14(5) 766–767.

10. **Rong, Zimei**; Vadgama, Pankaj.

    Bipartite Expressions for Amperometric Currents of Recessed Electrodes, Membrane Covered Planar Electrodes and Hanging Mercury Drop Electrodes.

Journal of Electroanalytical Chemistry (**2008**) 614(1–2) 166–170.

11. **Rong, Zimei**; Leitao, Eugenia; Popplewell, John; Alp, Burcak; Vadgama, Pankaj.

    Needle Enzyme Electrode for Lactate Measurement In Vivo.

    IEEE Sensors Journal, (**2008**) 8(1) 113–120.

12. Alp, Burcak; **Rong**, **Zimei**; Cheema, Umber; MacRobert, Alexander; Vadgama, Pankaj; Brown, Robert.

    Measurement of Glucose and Oxygen Concentration in Biomimetic Constructs.

    Tissue Engineering, (**2007**) 13(7) 1722–1722.

13. **Rong**, **Zimei**; Terzyk, Artur P.; Gauden, Piotr A.; Vadgama, Pankaj.

    Effective Diffusion Coefficient Determination within Cylindrical Granules of Adsorbents Using a Direct Simulation Method.

    Journal of Colloid and Interface Science, (**2007**) 313(2) 449–453.

14. **Rong, Zimei**; Vadgama, Pankaj.

    Bipartite Expressions for Diffusional Mass Transport in Bio-Membranes.

    Biophysical Journal, (**2006**) 91(12) 4690–4696.

15. Nair, Greeshma; Garguili, Joseph; Shiju, Ravindran; **Rong**, **Zimei**; Shapiro, Evgeniy; Drikakis, Dimitris; Vadgama, Pankaj.

    In Situ Fabrication of Crosslinked Protein Membranes Using Microfluidics.

    ChemBioChem, (**2006**) 7 1683–1689.

16. **Rong, Zimei**; Vadgama, Pankaj.

    Simple Expressions for Diffusion Coefficient Determination of Adsorption within Spherical and Cylindrical Absorbents Using Direct Simulation Method.

    Journal of Colloid and Interface Science, (**2006**) 303(1) 75–79.

17. **Rong**, **Zimei**; Rashid, Sarah; Vadgama, Pankaj.

A Bipartite Expression for the Transient Amperometric Current at a Membrane Covered Planar Electrode to Characterize Solute Diffusion through the Membrane.

Electroanalysis, (**2006**) 18(17) 1703–1709.

18. **Rong, Zimei**; Cheema, Umber; Vadgama, Pankaj.

Needle Enzyme Electrode Based Glucose Diffusive Transport Measurement in a Collagen Gel and Validation of a Simulation Model.

Analyst, (**2006**) 131(7) 816–821.

19. **Rong, Zimei**; Vadgama, Pankaj.

Dynamic Simulation Method to Characterise Oxygen Transport in Hydrogel Membranes.

Biomaterials, (**2006**) 27(23) 4266–4268.

20. Gargiuli, Joseph; Kyriacou, George; **Rong**, **Zimei**; Vadgama, Pankaj.

Use of Microfluidics for Stabilized Biosensors Interfaces and In Situ Membrane Formation.

Tissue Engineering, (**2006**) 12(4) 1122–1123.

21. **Rong, Zimei**; Vadgama, Pankaj.

Diffusion Coefficient Determination through Collagen Matrix Using Dynamic Computer Modelling.

Tissue Engineering, (**2006**) 12(4) 1025–1025.

22. Anna-Maria Spehar-Deleze, Salzitsa Anastasova, **Zimei Rong**, Dale Bickham, Hong Chang and Pankaj Vadgama.

General Platform for In Vivo Sensors for Oxygen, Glucose and Lactate Monitoring

In Dimitrios P Nikolelis (ed.) Portable Chemical Sensors: Weapons Against

Bioterrorism, NATO Science for Peace and Security Series: Chemistry and Biology, Springer Science + Business Media **2012**